KAUNAS UNIVERSITY OF TECHNOLOGY

SKIRMANTĖ ZADAVIČIŪTĖ

SYNTHESIS OF OXIDE AND SILICATE MATERIALS DENOTED BY SPECIFIC PROPERTIES

Doctoral Dissertation
Technological Sciences, Chemical Engineering (05T)

2018, Kaunas

This dissertation was prepared at the Department of Silicate Technology, Kaunas University of Technology, during the years 2014–2018.

Scientific supervisor:

Prof. Dr. Kęstutis Baltakys (Kaunas University of Technology, Technological Sciences, Chemical Engineering 05T).

Doctoral dissertation has been published in:
http://ktu.edu

Editor:

Armandas Rumšas (Publishing Office "Technologija")

ISBN 978-609-02-1455-8

The bibliographic information about the publication is available in the National Bibliographic Data Bank (NBDB) of the Martynas Mažvydas National Library of Lithuania.

KAUNO TECHNOLOGIJOS UNIVERSITETAS

SKIRMANTĖ ZADAVIČIŪTĖ

TIKSLINIŲ SAVYBIŲ OKSIDINIŲ IR SILIKATINIŲ MEDŽIAGŲ SINTEZĖ IR SAVYBĖS

Daktaro disertacija
Technologijos mokslai, chemijos inžinerija (05T)

2018, Kaunas

Disertacija rengta 2014-2018 metais Kauno technologijos universiteto Cheminės technologijos fakulteto Silikatų technologijos katedroje.

Mokslinis vadovas:

Prof. dr. Kęstutis BALTAKYS (Kauno technologijos universitetas, technologijos mokslai, chemijos inžinerija – 05T).

Interneto svetainės, kurioje skelbiama disertacija, adresas:
http://ktu.edu

Redagavo:

Armandas Rumšas (leidykla "Technologija")

ISBN 978-609-02-1455-8

Leidinio bibliografinė informacija pateikiama Lietuvos nacionalinės Martyno Mažvydo bibliotekos Nacionalinės bibliografijos duomenų banke (NBDB).

Table of Contents

Abbreviations

LDHs – layered double hydroxides
ex-LDHs – former layered double hydroxides
HTlc – hydrotalcite-like compounds
HT – hydrotalcite
Mg-Al LDHs – magnesium-aluminum layered double hydroxides
Mg-Al HT – magnesium-aluminum hydrotalcite
C-S-H – calcium silicate hydrate
Mg/Al – molar ratio of Mg and Al compounds
C/S – molar ratio of CaO and SiO_2
Me^{x+} – transition metals ions (Zn^{2+}, Co^{2+}, Cu^{2+}, Ni^{2+}, Mn^{2+}, Cr^{3+} or Fe^{3+})
CLDHs – calcined layered double hydroxides
CHT – calcined hydrotalcites
CHTM – calcined hydrotalcites of microwave
HA – humic acid
Ben – bentonite
Pal – palygorskite
MMO – mixed metal oxide
Gyr-200 – gyrolite calcined at 200 ºC
Gyr-1000 – gyrolite calcined at 1000 ºC
MHS – mechano-hydrothermal synthesis
MW – microwave synthesis
HS – hydrothermal synthesis
MW/HS – microwave and hydrothermal treatment
XRD – the X-ray powder diffraction
STA – simultaneous thermal analysis
DSC – differential scanning calorimetry
TG – thermogravimetry
FT-IR – Fourier transform infrared spectroscopy
SEM – scanning electron microscopy
AAS – atomic absorption spectrometry
S_{BET} – the specific surface area of the sample which was calculated by the BET equation
w/s – ratio of water versus solid
C_p – specific heat capacity

Introduction

Relevance of the Work

The emerging energy, transport and industrial sectors systematically and significantly contribute to air pollution emissions (OECD Environmental Outlook to 2050). With the objective to address these concerns, EU directives (No. 52017DC0675) recommend to alter production processes towards the direction of emission reduction by using advanced production and waste recycling technologies. Thus the creation of new generations of high selectivity and performance adsorbents and catalysts, as well as the search for new, inexpensive and simple methods for synthesizing this type of material has evolved into a major issue.

The various modifications of metal mixed oxides or their nano-sized compounds are perspective adsorbent/catalyst carriers. Due to the emerging new application areas, a growing number of different chemical composition compounds of layered double hydroxides (featuring the most common formula: $[M^{2+}_{1-x}M^{3+}_{x}(OH)_2]^2(A^{n-})_{x/n} \cdot mH_2O$, where M^{2+}, M^{3+} can be substituted by Mg^{2+}, Ca^{2+}, Fe^{2+}, Co^{2+}, Zn^{2+}, Cu^{2+} and Fe^{3+}, Al^{3+}, Bi^{3+}, In^{3+}, La^{3+}, Ga^{3+}, respectively, and A^{n-} is an exchangeable anion, including Cl^-, OH^-, CO_3^{2-}, SO_4^{2-} ar NO_3^-) are synthesized since they can incorporate various cations, inorganic or organic anions into their structure or form composite materials. among the most important compounds of this group there are hydrotalcite-type compounds, and the main mineral in this group is hydrotalcite ($Mg_6Al_2(OH)_{16}CO_3 \cdot 4H_2O$). Due to their specific structure, versatility in composition, morphology and particle size, hydrotalcite-type compounds have received much attention in potential applications such as catalysis, adsorption, biochemistry, or have been targeted as magnetic and optical functional materials.

In recent years, the interest in another compound, gyrolite ($NaCa_{16}Si_{24}O_{60}(OH)_8 \cdot 14H_2O$ or $Ca_{16}Si_{24}O_{60}(OH)_8 \cdot 14H_2O$) has grown up as well. This interest stems from the fact that gyrolite features a larger interlayer thickness of about 2.2 nm, and it can adsorb more new guests. Calcium silicate hydrate compounds including gyrolite can be used as a filler for the production of paper, rubber, plastics, and also as an adsorbent for organic and inorganic effluents.

It should be noted that the properties and structural features of multi-component materials determine the method and conditions of synthesis. The most common method used for the synthesis of metal mixed oxides is a multistep process including the preparation of raw materials, calcination-hydration, sol-gel, hydrothermal, regeneration or other aspects. Thus the involved production technologies are complex, expensive and time-consuming; they also suffer from other drawbacks, for instance, the production of large amounts of waste, the fixed solution medium ($7<pH<13.2$) must be maintained, it is difficult to control the structure and properties of the products) which can be eliminated by conducting the proposed hydrothermal/microwave synthesis. By selecting the optimal synthesis conditions (temperature, time and/or others), it is possible to control the dispersion of products, their crystal size and shape or the mineralogical composition.

It is known that thin mixed oxide/silicate oxide films can be formed by electrochemical precipitation, anodizing, formation of hydride and organic films and by physical vapour deposition techniques. Although chemical formation techniques

of thin films are economical, and as these films can be grown on a large surface, they do not exhibit high mechanical stability, are highly porous and do not form a barrier between the substrate and the environment. Physical vapor deposition methods enable to form thin films in a high vacuum, which results in good adhesion to the pallet, mechanical stability, hardness and higher environmental resistance of the relevant film. There are several physical methods for the formation of these films in the vapor phase: magnetron sputtering, pulsed laser deposition, ion plasma sputtering, electron beam evaporation, etc. It is expected that the structure as well as the physical and chemical properties of growing films will be controlled by using the synthetic targets denoted by specific properties or by changing the technological formation parameters of electron beam evaporation.

The aim of this work is to create an environmentally friendly periodic operation technology of oxide and silicate materials which would include hydrothermal and microwave synthesis of the initial compounds featuring specific properties and their application in adsorption or thin film formation.

In order to achieve the aim of the thesis, we have to fulfill these **objectives**:

1. To examine the influence of the composition of primary mixtures and hydrothermal/microwave synthesis parameters on the formation processes of hydrotalcite group compounds;
2. To evaluate the effect of mechanochemical and solid-state treatment on the mineralogical composition and structure stability of mixed metal oxides/hydroxides;
3. To determine the adsorption capacity of transition metals ions for the best samples of oxides and silicates;
4. To form thin mixed metal oxide films from targets which should possess specific properties by selecting the technological parameters of electron beam evaporation.

Scientific Novelty of the Research

It was proved that the crystallite size, the crystallinity, the crystal form and the mineralogical composition of the synthesized samples can be controlled by changing the conditions of microwave and hydrothermal treatment (isothermal curing duration (up to 48 h), milling duration (until 5 min) and intensity (650–950 rpm)). For the first time, simultaneous adsorption parameters of transition metal ions (Zn^{2+}, Cu^{2+}, Co^{2+}, Ni^{2+}, Mn^{2+}, Fe^{3+}, Cr^{3+}) by oxide and silicate samples was determined.

Practical Significance of the Scientific Research

The technology for the production of thin mixed metal oxide films by combining microwave/hydrothermal synthesis, their activation and electron beam evaporation methods was created. It was proved that it is possible to form mixed metal oxides with various thickness (from 4 nm to 23 nm) and to control their growth kinetics as well as their structural and morphological properties.

Approval and Publication of Research Results

The results of the research have been presented in 5 scientific publications included into the *Clarivate Analytics Web of Science* database: 3 of them published in *Journal of Thermal Analysis and Calorimetry*; 1 in *Desalination and Water Treatment* and 1 in *Materials Science* (Medžiagotyra). The results of the dissertation research

have been reported in 8 international conference proceedings: *Chemistry and Chemical Technology* (2015, Lithuania), *Advanced Materials and Technologies* (2015, Lithuania), *3rd Central and Eastern European Conference on Thermal Analysis and Calorimetry* (2015, Slovenia), *Chemistry and Chemical Technology* (2016, Lithuania), *BaltSilica* (2016, Lithuania), *Advanced Materials and Technologies* (2016, Lithuania), *XV Russian and International Conference on Thermal Analysis and Calorimetry* (2016, Russia), *Chemistry and Chemical Technology* (2017, Lithuania).

Structure and Content of the Dissertation

The dissertation consists of an introduction, relevant scholarly literature survey, the experimental part, the results and discussion part, conclusions and a list of references and publications on the dissertation topic. The list of references includes 189 bibliographic sources. The main results are discussed on 108 pages and illustrated in 11 tables and 35 figures.

During the doctoral studies, Skirmantė Zadavičiūtė participated in project *To Create a Silica Gel Waste Processing Technology which will Enable the Development of New Products* (No. SV9-0588/393) and KTU interdisciplinary project *The Environment Friendly Technology for Obtaining Thin Thermostable $Mg_xAl_yO_z$ Spinel Films* (No. MTEPI- P-15045).

Statements Presented for Defence

1. The structure of compounds possessing specific properties can be controlled by changing the parameters of both microwave and hydrothermal synthesis.
2. The mineralogical composition of targets denoted by specific properties and chemical composition of substrates determines the structural and morphological properties of thin mixed metal oxide films formed by applying the electron beam evaporation technology.

1. Literature Review

1.1 Classification, Structure, Synthesis and Properties of Layered Double Hydroxides

1.1.1 Classification and Structure Peculiarities of Layered Double Hydroxides

Layered double hydroxides belong to a general class which is called *anionic clay minerals*. It can be of either synthetic or natural origin. The LDHs are also known as hydrotalcite-like compounds (1). The LDHs clays can be represented by the general chemical formula $[M_{1-x}^{2+}M_x^{3+}(OH)_2]^{x+}(A^{n-})_{x/n}\cdot mH_2O$, where M^{2+}, M^{3+} can be substituted by Mg^{2+}, Ca^{2+}, Fe^{2+}, Co^{2+}, Zn^{2+}, Cu^{2+} and Fe^{3+}, Al^{3+}, Bi^{3+}, In^{3+}, La^{3+}, Ga^{3+}, respectively, and A^{n-} is an exchangeable anion including Cl^-, OH^-, CO_3^{2-}, SO_4^{2-}, NO_3^- (2). The anions occupy the interlayer region of these layered crystalline materials. Although a wide range of values of *x* is claimed to provide the LDHs structure, the pure phase of LDHs clays is usually obtained in a limited range, i.e. $0.2 \leq x \leq 0.33$ (2, 3). The parent material of layered double hydroxides is the naturally occurring mineral hydrotalcite having the formula $Mg_6Al_2(OH)_{16}CO_3\cdot 4H_2O$ (4).

The structure of LDHs can be explained by drawing an analogy with the structural features of the metal hydroxide layers in mineral brucite or simply as $Mg(OH)_2$ crystal structure. Brucite consists of hexagonal close packing of hydroxyl ions with alternate octahedral sites occupied by Mg^{2+} ions. Metal hydroxide sheets in brucite crystal are neutral in charge and stack one upon another by Van der Waal's interaction. The interlayer distance or the basal spacing in brucite has a value of about 0.48 nm. In LDHs, some of the divalent cations of these brucite-like sheets are isomorphously substituted by a trivalent cation and the mixed metal hydroxide layers, $[M_{1-x}^{2+}M_x^{3+}(OH)_2]^{x+}$, and in this form they acquire a net positive charge. This excess charge on the metal hydroxide layers is neutralized by the anions accumulated in the interlayer region. The interlayer region in LDHs also contains some water molecules for the stabilization of the crystal structure. The presence of anions and water molecules leads to an enlargement of the basal spacing from 0.48 nm in brucite to about 0.77 nm in Mg-Al LDHs. The layered double hydroxide and the brucite crystal structures are shown in Fig. 1.1 (5).

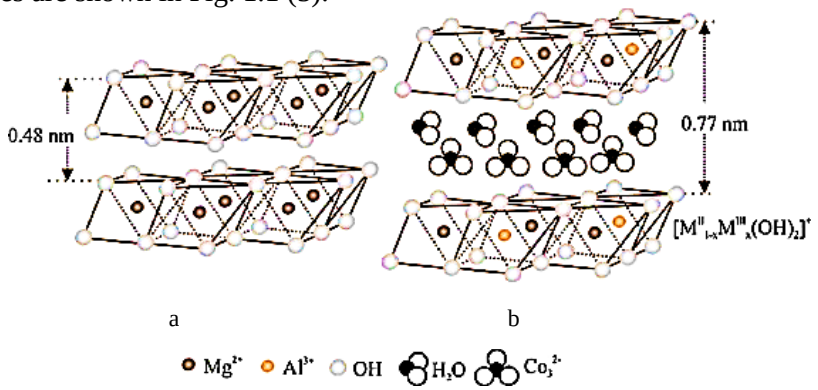

Fig. 1.1 The crystal structures of brucite (a) and layered double hydroxide (b) (5)

It should be noted that the changeable composition and a large amount of interfered ions of various elements in the crystal layered structure of LDHs is complicating the investigation of the structure and properties of these compounds. Therefore, not all the layered double hydroxide structures have been investigated and are definitely known. Yet, their classification is constantly evolving. Mills *et al*. divides LDHs found in nature into nine main groups of compounds (Table 1.1) (6):

Table 1.1 Nature layered double hydroxide compounds groups (7)

Group name	Mineral name	Mineral formula
Cualstibite	cualstibite	$Cu_2Al(OH)_6[Sb^{5+}(OH)_6]$
	omsite	$Ni_2Fe^{3+}(OH)_6[Sb(OH)_6]$
	zincalstibite	$Zn_2Al(OH)_6[Sb^{5+}(OH)_6]$
Fougèrite	fougèrite	$Fe^{2+}{}_4Fe^{3+}{}_2(OH)_{12}[CO_3]\cdot 3H_2O$
	mössbauerite	$Fe^{3+}{}_6O_4(OH)_8[CO_3]\cdot 3H_2O$
	trébeurdenite	$Fe^{2+}{}_2Fe^{3+}{}_4O_2(OH)_{10}CO_3\cdot 3H_2O$
Glaucocerinite	carrboydite	$[(Ni_{1-x}Al_x)(OH)_2][SO_4]_{x/2}\cdot nH_2O$
	glaucocerinite	$(Zn_{1-x}Al_x)(OH)_2(SO_4)_{x/2}\cdot nH_2O$
	hydrohonessite	$(Ni_{1-x}Fe^{3+}{}_x)(OH)_2[SO_4]_{x/2}\cdot nH_2O$
	mountkeithite	$[(Mg_{1-x}Fe^{3+}{}_x)(OH)_2][SO_4]_{x/2}\cdot nH_2O$
	zincaluminite	$Zn_6Al_6(SO_4)_2(OH)_{16}\cdot 5H_2O$
Hydrocalumite	hydrocalumite	$Ca_4Al_2(OH)_{12}(Cl,CO_3,OH)_2\cdot 4H_2O$
	kuzelite	$Ca_4Al_2(OH)_{12}[SO_4]\cdot 6H_2O$
Hydrotalcite	desautelsite	$Mg_6Mn^{3+}{}_2(OH)_{16}[CO_3]\cdot 4H_2O)$,
	droninoite	$Ni_6Fe^{2+}{}_3(OH)_{16}Cl_2\cdot 4H_2O$
	hydrotalcite	$Mg_6Al_2(OH)_{16}[CO_3]\cdot 4H_2O$
	iowaite	$Mg_6Fe^{3+}{}_2(OH)_{16}Cl_2\cdot 4H_2O$
	meixnerite	$Mg_6Al_2(OH)_{16}(OH)_2\cdot 4H_2O$
	pyroaurite	$Mg_6Fe^{3+}{}_2(OH)_{16}[CO_3]\cdot 4H_2O$
	reevesite	$Ni_6Fe^{3+}{}_2(OH)_{16}(CO_3)\cdot 4H_2O$
	stichtite	$Mg_6Cr^{3+}{}_2(OH)_{16}[CO_3]\cdot 4H_2O$
	takovite	$Ni_6Al_2(OH)_{16}[CO_3]\cdot 4H_2O$
	woodallite	$Mg_6Cr_2(OH)_{16}Cl_2\cdot 4H_2O$
	muskoxite	$Mg_7Fe_4O_{13}\cdot 10H_2O$
Quintinite	caresite	$Fe^{2+}{}_4Al_2(OH)_{12}[CO_3]\cdot 3H_2O$
	charmarite	$Mn^{2+}{}_4Al_2(OH)_{12}[CO_3]\cdot 3H_2O$
	chlormagaluminite	$Mg_4Al_2(OH)_{12}Cl_2\cdot 3H_2O$
	comblainite	$Ni_4Co_2(OH)_{12}[CO_3]\cdot 3H_2O$
	quintinite	$Mg_4Al_2(OH)_{12}[CO_3]\cdot 3H_2O$
	zaccagnaite	$Zn_4Al_2(OH)_{12}[CO_3]\cdot 3H_2O$
Wermlandite	karchevskyite	$Mg_{18}Al_9(OH)_{54}Sr_2(CO_3)_9(H_2O)_6(H_3O)_5$
	motukoreaite	$Mg_6Al_3(OH)_{18}[Na(H_2O)_6][SO_4]_2\cdot 6H_2O$
	natroglaucocerinite	$Zn_6Al_3(OH)_{18}[Na(H_2O)_6](SO_4)_2\cdot 6H_2O$
	nikischerite	$Fe^{2+}{}_6Al_3(OH)_{18}[Na(H_2O)_6][SO_4]_2\cdot 6H2O$
	shigaite	$Mn_6Al_3(OH)_{18}[Na(H_2O)_6][SO_4]_2\cdot 6H_2O$
	wermlandite	$Mg_7Al_2(OH)_{18}[Ca(H_2O)_6][SO_4]_2\cdot 6H_2O$
Woodwardite	honessite	$(Ni_{1-x}Fe^{3+}{}_x)(OH)_2[SO_4]_{x/2}\cdot nH_2O$
	woodwardite	$Cu_{1-x}Al_x(OH)_2[SO_4]_{x/2}\cdot nH_2O$

	zincowoodwardite	$Zn_{1-x}Al_x(OH)_2[SO_4]_{x/2}\cdot nH_2O$
Other compounds	brugnatellite	$Mg_6Fe^{3+}(CO_3)(OH)_{13}\cdot 4H_2O$
	coalingite	$Mg_{10}Fe^{3+}{}_2(OH)_{24}[CO_3]\cdot 2H_2O$

Due to emerging new application areas, a growing number of different chemical compounds of LDHs are being synthesized whose application depends on the selected synthesis method of these materials.

1.1.2 Synthesis Methods of Layered Double Hydroxide

During the last 20 years, numerous publications have been presented in relation with the synthesis and applications of LDHs compounds (8, 9). LDHs compounds have been synthesized by direct methods including co-precipitation (10), sol-gel (11), chimie douce (12), salt-oxide reaction, hydrothermal or microwave growth and electrochemical synthesis (13) (Fig. 1.2). Indirect methods include all the syntheses that use an LDHs as a precursor, for example, all anion exchange based methods such as direct anion exchange, anion exchange by acid attack with the elimination of the guest species in the interlayer region, and anion exchange by surfactant salt formation (Fig. 1.2) (13, 14). The non-anion exchange methods include the delamination-restacking method and LDHs reconstruction or regeneration method (15, 16) (Fig. 1.2).

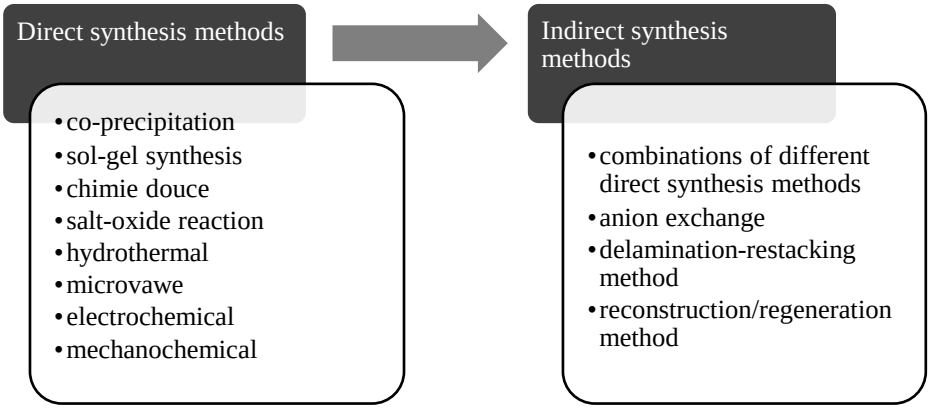

Fig. 1.2 The variety of methods of layered double hydroxide preparation (8)

The most common method used for the hydrotalcite type compound synthesis is co-precipitation, in which, a solution containing M^{2+} and M^{3+} metal cations in adequate proportions reacts with an alkaline solution (Table 1.2). This process starts with the preparation of an aqueous solution of magnesium and aluminum salts ($MgCl_2$ and $Al(NO_3)_3$), for example, as Table 1.2 shows, by keeping the molar ratio between them close to 3:1 or 2:1 (this ratio will define the degree of substitution of the trivalent cations in the $Mg(OH)_2$ layers). In neutral-acid pH, the solution is stable, and the Mg^{2+} and Al^{3+} cations remain dissolved (Table 1.2, b). Afterwards, the pH of the solution is carefully increased so that to induce the precipitation of the double hydroxide (usually,

$NaHCO_3$ or NH_4HCO_3 are frequently used to shift the pH as they also behave as the $(CO_3)^{2-}$ anions source (Table 1.2, c and d). By changing the pH, the temperature, or the stirring intensity, the nucleation-precipitation mechanism can be controlled, which results in the required particle sizes and shapes (Table 1.2, e). After finishing the reaction, the counter-cation used to increase the pH (in this case, Na^+ or NH^{4+}) remains in the obtained hydrotalcite suspension and must be withdrawn (usually by centrifugation, dialysis or ultra-filtration (Table 1.2, f)). Further hydrothermal treatment can be used with the objective to enhance the particles' crystallinity (Table 1.2, g and h) and to adjust the particle size distribution. In order to attain a dried powder, a spray-drier or liofilization must be applied to prevent particle agglomeration (Table 1.2, i). However, the method suffers from many drawbacks: the multistep synthesis route, the difficulty in obtaining high crystallinity compounds, a strong agglomeration of primary particles, poor morphology and particle size distribution as well as the production of large amounts of waste and others (17, 18, 19).

Table 1.2 Co-precipitation synthesis of Mg-Al LDHs (19)

Steps	Remarks
a) Solution of divalent cation salt (Ex.:$6MgCl_2$) + trivalent cation salt (e.g. $2AlCl_3$) ↓	Mg:Al=(3-2):1 (Excess of Mg^{2+} or Al^{3+} results hydrotalcite plus $Mg(OH)_2$ or $Al(OH)_3$ respectively)
b) $6Mg^{2+}+2Al^{3+}+18Cl^-+nH_2O$ ↓	pH≤7 (stable solution)
c) pH increase (e.g. $NaHCO_3$ addition)	CO_3^{2-} can be replaced by other anions (e.g. F^-, Cl^- or carboxylic organic anions)
d) $6Mg^{2+}+2Al^{3+}+18Cl^-+mNa^++m(CO_3^{2-})+mOH^-$ ↓	pH~10-12 (Metastable solution)
e) $Mg_6Al_2(OH)_{16}(CO_3)\cdot4H_2O+18NaCl$ ↓	pH~10-12 (Hydrotalcite suspension)
f) Purification (e.g. centrifugation) ↓	NaCl withdrawal
g) $Mg_6Al_2(OH)_{16}(CO_3)\cdot4H_2O$ (aqueous suspensions)	Low crystallinity particles
h) Hydrothermal treatment (e.g. autoclave) and controlled drying (e.g. liofilization or freeze drying) ↓	Improves the crystallinity, narrows the particle size distribution, prevents particle agglomeration
i) $Mg_6Al_2(OH)_{16}(CO_3)\cdot4H_2O$ (dried)	Dried hydrotalcite particles

Salomão *et al*. (19) reported successful preparation of synthetic Mg-Al LDHs hydrotalcite by employing the **co-precipitation** method from magnesium oxide (MgO) and aluminum hydroxide ($Al(OH)_3$) used as the starting materials. This method was developed with the objective to overcome two significant difficulties

caused by the co-precipitation method: the presence of counter cation impurities and the energy requirement of industrially sized co-precipitation which is relatively high compared with other industrial processes. Four potential reagents were chosen: caustic magnesia (MgO), magnesium hydroxide ($Mg(OH)_2$), calcined alumina (Al_2O_3) and aluminum hydroxide ($Al(OH)_3$). Experiments were carried out in order to determine the optimum amount of each reagent required for LDHs formation. Various ratios of reagents ranging from 10 wt% to 90 wt% of dry material were dry blended before thorough mixing with excess of water. The best results in terms of crystallinity and purity were obtained when using caustic magnesia (MgO) and aluminum hydroxide. Salomão *et al*. concluded that the LDHs were formed as a result of the hydration/dissolution/co-precipitation mechanism, in which, all the three processes took place almost simultaneously. It was found that the precipitation of Mg-Al LDHs from MgO and $Al(OH)_3$ was a highly temperature-dependent process (19, 20).

Panda *et al*. (21) reported an experiment of typical **co-precipitation** at constant pH. Synthesis and characterization of Mg-Al LDHs was conducted with three different molar ratios (2:1, 3:1 and 4:1) from mixed metal solutions containing magnesium nitrate hexahydrate ($Mg(NO_3)_2 \cdot 6H_2O$) and aluminum nitrate nonahydrate ($Al(NO_3)_3 \cdot 9H_2O$) dissolved in deionised water. The mixed metal solution was slowly combined with sodium carbonate solution with controlled addition of 1M sodium hydroxide solution used to maintain a constant pH of approximately 9, 10 or 11. Precipitation was carried out under an inert atmosphere. Panda *et al*. determined that in order to successfully prepare Mg-Al layered double hydroxides by employing the conventional co-precipitation technique, the synthesis parameters need to be carefully controlled while taking into account the reactivity of these precursors in the alkaline pH range generally involved for the precipitation of LDHs materials (21).

Smalenskaite *et al*. (22) synthesized Mg-Al layered double hydroxides by using **co-precipitation** and **sol-gel** preparation techniques. Via this novel aqueous sol-gel processing route, LDHs were obtained as a result of the decomposition (calcination) of the precursor gels at 650 °C followed by the rehydration of the intermediate crystalline MMO powders in water. The same synthesis methods were successfully applied for the production of cerium-substituted LDHs (Mg-Al-Ce) with the substitution rate from 0.05 mol% to 10 mol%. It was established that, in case of the Mg-Al-Ce, LDHs prepared by co-precipitation followed by calcination, the regeneration rate decreases with the increase of the cerium content whereas the conversion of the rehydrated sol-gel derived MMO into LDHs does not depend on the concentration of cerium and is close to 100% (22).

Budhysutanto *et al*. (23) investigated the effect of different pre-treatments (blending, ultrasound treatment and wet grinding) on the conversion rate of raw materials for the **hydrothermal synthesis** of hydrotalcite compounds. In this synthesis, solid reactants were used: magnesium oxide and aluminum trihydroxide whereas hydrotermal treatment was carried out at temperatures of 80 °C or 170 °C. It was determined that all pre-treatment methods resulted in a smaller particle size of raw materials – yet wet grinding had the strongest effect. Also, Budhysutanto *et al*. proposed a synthesis mechanism in which an amorphous brucite layer is formed at the surface of MgO particles. This amorphous layer slowly converts into crystalline

brucite with lower solubility. If the particle size of MgO is not small enough, MgO can be blinded by a thin layer of brucite. This process in particular hampers the conversion of brucite and $Al(OH)_3$ into hydrotalcite compounds at a prolonged exposure to water before the temperature is increased and the reaction takes place (Fig. 1.3) (23).

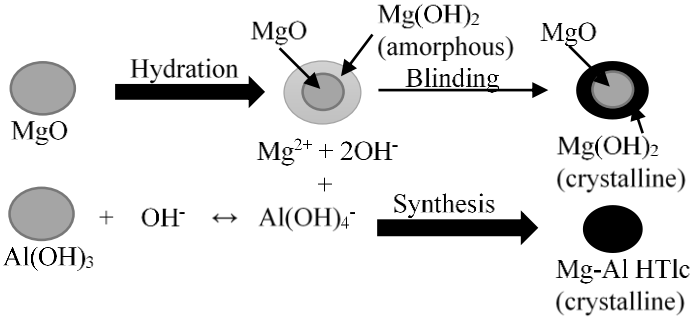

Fig. 1.3 Synthesis mechanism for the hydrothermal method by Budhysutanto *et al*. (23)

Liao *et al*. (24) announced that Mg-Al layered double hydroxides have been successfully synthesized by using a simple **hydrothermal** process. These LDHs were obtained from brucite and $Al(OH)_3$ when the hydrothermal reaction temperature ranged from 100 °C to 180 °C, and the reaction duration was 36 hours. The results showed that the cell parameters and Mg/Al molar ratios of the layered double hydroxide increase with the hydrothermal reaction temperature increasing from 140 °C to 180 °C (24).

Wang *et al*. (25) prepared magnesium-aluminum layered double hydroxides by employing **hydrothermal synthesis.** The Mg-Al LDHs were synthesized by using five types of solvents: pure water, water/ethanol, water/ethylene glycol, water/glycerin, and water/pentaerythritol. The salt solution ($Mg(NO_3)_2 \cdot 6H_2O$ and $Al(NO_3)_3 \cdot 9H_2O$ mixture) and other different solvent solutions were heated at 120 °C for 12 h. It was subsequently determined that the incorporation of polyhydric alcohol changes electrostatic interactions in the synthesis system, and consequently influences the diffusion of the constituent units as well as the formation and stacking of brucite layers (25).

Bankauskaite *et al*. (26) examined the formation of Mg-Al LDHs when Mg/Al ratio 3:1 was under **hydrothermal** conditions (the synthesis duration was 4, 24 and 72 h at 200 °C). The obtained results showed that the chemical nature of the initial Mg-containing components changes the formation mechanism of the synthesis products. It should be noted that $4MgCO_3 \cdot Mg(OH)_2 \cdot 5H_2O$ as a raw material is not recommended for the synthesis of hydrotalcite because – even after 24 h of isothermal curing at a temperature of 200 °C – hydrotalcite is not formed, and magnesium aluminum hydroxide hydrate is dominant in the synthesis products. Also, the initial magnesium-containing component is decomposed into magnesium carbonate and hydroxide. It was determined that hydrotalcite is formed as early as after 4 h of hydrothermal synthesis at a temperature of 200 °C when the Mg/Al molar ratio is

equal to 3:1 in the $Mg_5(CO_3)_4{\cdot}(OH)_2{\cdot}4H_2O$-γ-$Al_2O_3$/$Al(OH)_3$–$H_2O$ system. However, boehmite and magnesium carbonate are formed together with this compound (26).

Xu *et al*. (27) investigated the preparation of Mg-Al LDHs containing interlayer hydroxide anions from MgO and Al_2O_3 by applying the **hydrothermal** method. The above mentioned oxides were used to prepare aqueous suspensions with the molar ratios of 4. The suspensions were transferred to an autoclave with deionized water and thoroughly mixed by shaking. The obtained samples were hydrothermally treated for 5 or 10 days at 110 °C. The results of XRD analysis confirmed the presence of the target LDHs along with an impurity corresponding to brucite. It was established that pH was an important variable because higher purity solutions were obtained when this parameter was close to neutral. Moreover, the hydrothermal method is suitable for the preparation of large LDHs crystallites because hexagonal plate sheets with a lateral dimension of over 1 μm, typical of homogeneously precipitated MgAl-CO_3 LDHs, were found (27).

Fahami *et al*. (28) (29) performed synthesis of Mg-Al LDHs by employing two different methods. The obtained results demonstrated that Mg-Al LDHs were successfully synthesized via **hydrothermal** or **mechanochemical** treatment. The two methods formed a product with very similar structural characteristics. The formation and the structural features of Mg-Al-Cl LDHs were significantly influenced by different chlorine ion substitutions (0.12, 0.18, 0.3, and 0.42). It was thus determined that the product with a high crystallinity degree was obtained by using the hydrothermal method. Meanwhile, mechanochemistry as a facile and simple method can be applied for the mass production of Mg-Al-Cl LDHs with an acceptable crystalline phase (29).

Zhang *et al*. (30) synthesized Mg-Al layered double hydroxides by using the **mechano-hydrothermal** method. A two-step process was used (Fig. 1.4). In the first-step, a MgO and Al_2O_3 mixture was milled for 1 h under ambient conditions in air, the mill speed was kept constant at 450 rpm with a ball/mixture mass ratio of approximately 49. During the second step, the milled mixture of MgO and Al_2O_3 was placed in an autoclave with $NaNO_3$ solution at the selected temperature and duration. The use of this method allowed to achieve advantages of a lower reaction temperature and a shorter reaction time. Besides, the application of this process produced compounds with a higher crystallinity, dispersion and a more regular shape in comparison to the conventional mechanochemical and hydrothermal methods (30).

Also, the researchers employed this MHS method with the intention to synthesize Mg-Al-Fe LDHs from raw materials such as $Mg(OH)_2$, $Al(OH)_3$ and $Fe(NO_3)_3{\cdot}9H_2O$ or $Mg(NO_3)_2{\cdot}6H_2O$. They compared the conventional hydrothermal and mechanochemical methods with the combined mechano-hydrothermal method. The results showed that the pre-milling process played a key role in the LDHs formation during the subsequent hydrothermal treatment, and LDHs obtained by using the combined synthesis method exhibited better crystallinity and dispersion than the LDHs formed by employing mechanochemical synthesis (31).

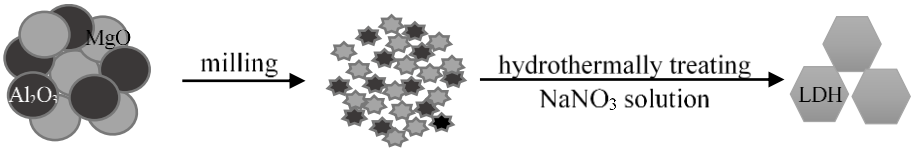

Fig. 1.4 Schematic representation of Mg-Al LDHs obtained via the mechano-hydrothermal synthesis method (30)

Microwaves can be used as a heating source during the synthesis of HTlc. Their interaction with materials produces dipole reorientation in dielectric materials (dielectric heating) and ionic conduction. In this way, there is a possibility to achieve uniform bulk heating of the materials – volumetrically distributed heating – by reducing thermal gradients (32).

Tao *et al*. (33) reported a rapid and cost-effective microwave strategy to fabricate nickel/cobalt double hydroxides. The scholars examined the effect of the reaction medium on the synthesis of LDHs when four different solvents (water, ethanol, isopropanol and tertbutanol) were used. Firstly, $Co(NO_3)_2 \cdot 6H2O$ and $Ni(NO_3)_2 \cdot 6H_2O$ were dissolved in 150 ml of ethanol and then transferred into a microwave reactor. The mixed solutions were well stirred and heated to the reflux state by using microwave radiation at a temperature of 78–80 °C when the microwave power of 200 W was employed for the reaction. Then, a mixture of ethanol and ammonia was slowly dropped into the mixed solution. After that, the microwave power was rapidly adjusted to 300 W and maintained at this level for 0.5 h. It was determined that the nanostructure and morphology of Ni-Co LDHs depended on the reaction medium. The sample prepared in the aqueous solution was established to be a mixture of $Ni(OH)_2$ and $Co(OH)_2$. Meanwhile, the Ni-Co LDHs produced in the organic solvent had a hydrotalcite-like structure. Moreover, the Ni-Co LDHs prepared in ethanol formed an ultrathin flower cluster structure with a three-dimensional morphology. The study demonstrated that the Ni-Co sample prepared in the ethanol solution featured the lowest density (33).

Prakruthi *et al*. (34) announced successful **microwave** synthesis of Mg-Al, Ni-Al, Cu-Al and Zn-Al layered double hydroxides. $Al(NO_3)_3 \cdot 9H_2O$ and $Mg(NO_3)_2 \cdot 3H_2O$ were dissolved in distilled water with the molar ratio of Mg/Al of 2:1. This solution was mixed with a mixture of $NaOH/Na_2CO_3$ (7:3) while vigorously stirring at ambient temperature with a controlled pH between 10 and 11. Subsequently, the resultant mixture was allowed to age at 80 °C for 30 min under microwave heating. The synthesis product was centrifuged and repeatedly washed with hot water until the centrifugate was neutral. Also, by using this method, other LDHs (Zn-Al, Ni-Al, Cu-Al) were also synthesized under microwave irradiation (34).

Kulyukhin *et al*. (35) determined the effect of different **microwave** synthesis conditions (at 80 °C by microwave heating under the power of 450 or 800 W for 3 or 10 min) on the formation of Mg-Al layered double hydroxides. The researchers found that the type of the heating source and time did not noticeably influence the structure of the formed Mg-Al LDHs. However, the use of microwave irradiation enabled not only the acceleration of the synthesis of layered double hydroxides but also the

preparation of compounds possessing high kinetic characteristics of U(VI) sorption (35).

Thus, most of the researchers investigating the field state that the final properties of products can be controlled by changing the synthesis conditions (36). However, the investigated data showed that, when the more common methods – such as co-precipitation, reconstruction or calcination rehydration – were applied, loose powders of irregular aggregates or products with impurities are usually formed (37). For this reason, other techniques – the post-synthesis treatments – were employed with the intention to modify the structural and surface properties of synthesized LDHs.

1.1.3 Post-Synthesis Treatment of Layered Double Hydroxides

The post-synthesis methods, such as calcination at elevated temperatures, delamination and restocking, grafting, intercalation by inorganic and organic species, structure reconstruction and mechanochemical treatment, are often used for the modification of layered double hydroxides (25, 38, 39).

An important feature of Mg-Al LDHs compounds is that, when they are calcined at moderate temperatures (up to 500 °C), these compounds form mixed, mostly amorphous, oxides, which can recover the layered structure after the exposure to water vapor or after the immersion in solutions containing the desirable anions, i.e., the memory effect (15, 34, 40–43). On the other hand, above 400 °C, these compounds crystallize to a MgO-like phase; meanwhile, at a higher temperature (>900 °C), MgO and $MgAl_2O_4$ spinel (mixed metal oxide) are detected (43–45). These mixed oxides are typically present over large specific surface areas thus affecting the thermal stability and synergic interactions between the different metal components (15, 34, 43–47).

Bastiani *et al*. (48) examined the influence of calcination conditions on the basic properties and catalytic performance of Mg-Al mixed oxides which were derived from a hydrotalcite sample (Al/(Al+Mg)=0.20). Various heating rates (1 or 10 K/min), calcination atmospheres (dry air, N_2, vacuum and dry air saturated with decarbonated water at 293 K) and time (2, 5, 10 and 15 h) of calcination at 723 K were evaluated. The results showed that the heating rate and the time of calcination at 723 K only play a minor role in terms of the basic properties and the catalytic performance of Mg-Al mixed oxides. It should be noted that the calcination atmosphere was the main parameter affecting the catalytic properties of Mg-Al mixed oxides; it was determined that calcination under dry air yielded the best results (48).

Bankauskaite *et al*. (49) published data on the application of modified hydrotalcites as precursors for the formation of (Na, K) Mg-Al spinel-type compounds. Synthesized pure samples and samples substituted with K^+ and Na^+ hydrotalcite were additionally calcined within the 800–1000 °C temperature range for 1–24 h in order to obtain nano-sized compounds. It was determined that after 1 h of calcination of the synthetic precursors at 850 °C, spinel-type compounds are formed only in the samples with alkali additives. Meanwhile, in the pure system, only traces of the above mentioned compounds were observed at 900 °C. It should be noted that the increase in the solid-state sintering temperature and duration led to the formation

of higher crystallinity (Na, K)$MgAl_2O_4$ spinel-type compounds, and their textural properties depended on the chemical composition of the precursors (49).

It is of interest that Basag *et al*. (50) announced that Co-Mg-Al mixed metal oxides were obtained from hydrotalcite-like precursors with various cobalt content and different Mg/Al ratios by calcination at 600, 700 and 800 °C temperatures. It was determined that MgO (periclase) was found in the samples which were calcined at temperatures of 600 °C and 700 °C. Meanwhile, phases with the spinel structure were identified together with periclase-like oxides in the $Co_5Mg_{62}Al_{33}$ and $Co_{10}Mg_{57}Al_{33}$ samples calcined at 800 °C. However, spinel-type compounds were not present in $Co_5Mg_{77}Al_{18}$ and $Co_{10}Mg_{72}Al_{18}$ samples. Also, it was established that the cation composition of hydrotalcite-like precursors and the calcination temperature strongly influenced the catalytic performance of the mixed metal oxides (50).

Komarnemi *et al*. (51) were the first to report the use of microwave radiation coupled with hydrothermal treatment (the so-called microwave-hydrothermal treatment). During the last decade, several research groups have been stuying the application of microwave radiation during the processing of HT. The use of microwaves as a source of heating during process of the aging of the slurry (which was obtained by co-precipitation) permitted to increase the crystallinity of the solids in short periods of time by modifying the properties of the as-prepared layered materials or after calcination (32, 52–54).

Benito *et al*. (32) studied how the microwave-hydrothermal synthesis affects the physical and chemical properties of the solids obtained by calcination of hydrotalcite. Mg-Al LDHs samples were calcined at a rate of 10 °C/min to 250, 550 and 1000 °C, and the compounds were intercalated with organic anions at 225 °C. The results obtained after the thermal treatment at the three selected temperatures (250, 550 and 1000 °C) were similar to those previously reported for Ni-Al and Zn-Ni-Al compounds (55) thus confirming that MWHS modified the properties of the thermally decomposed products. After the removal of crystallization water at 250 °C, the crystallinity of the solids decreased while the retention of the original lamellar structure and the size of the particles were more pronounced for the solids irradiated for longer times. Such differences were not observed among irradiated samples calcined at moderate (550 °C) temperatures as the poor crystallinity of the mixed oxide phase was obtained after dehydroxylation and decarbonation which made the analysis of the obtained results quite difficult to carry out. On the other hand, the crystallite size of MgO and $MgAl_2O_4$ phases segregated at 1000 °C decreased steadily as the irradiation time increased from 10 to 180 min (32).

Cross *et al*. (56) used two different calcination methods for $Cu_{1.4}Mg_{4.4}Al_{2.2}(CO_3)_{1.1}(OH)_{16}$. This material was calcined in a conventional furnace and in the microwave cavity at temperatures of 400, 500 and 750 °C. The obtained results show that microwave calcination results in enhanced crystallinity of the resultant oxides and in the spinel phase formed at a high temperature in comparison to the conventional calcination. It should be noted that magnesium and copper oxides were detected when hydrotalcite was calcinated at a temperature of 400–500 ºC. At a high temperature (>750 ºC), $MgAl_2O_4$ or Cu_2MgO_3 spinel type compounds dominated in the product (56).

Many LDHs materials show a unique phenomenon called **'the memory effect'**, which involves the regeneration of the layered crystalline structure from their calcined form when the latter is dispersed in an aqueous solution containing a suitable anion (5, 57, 58). This feature is often used to synthesize and modify LDHs with different types of intercalating anions. Typically, LDHs containing a carbonate anion are heated to a temperature in the range of 350–800 °C for several hours, and the resultant mixed metal oxide (to be more precise, a solid solution of the two metal oxides) is then dispersed in an aqueous solution of the desired anionic species (Fig. 1.5) (59, 60). The regeneration property shown by LDHs is extensively reported in numerous scholarly literature sources (61–63).

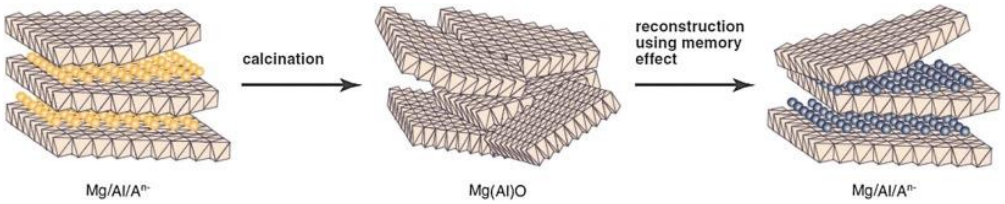

Fig. 1.5 The memory effect of Mg-Al layered double hydroxides (60)

The memory effect of hydrotalcite samples substituted with Na^+ or K^+ ions was examined in (64). Firstly, hydrotalcite samples were calcined within the 225–525 °C temperature range. It was determined that the crystal structure of hydrotalcite was already destroyed after 4 h of calcination at a temperature of 325 °C because only a small intensity of the diffraction peaks characteristic to magnesium carbonate and/or boehmite was observed. Meanwhile, at a temperature of 475 °C, after 4 h of calcination, MgO and Al_2O_3 compounds were formed. In the second part of the experiment, the influence of calcination conditions on the thermal stability of modified hydrotalcite samples was investigated. It was consequently observed that hydrothermally treated and subsequently calcined hydrotalcite samples only partially reconstructed the layered structure of the hydrotalcite because two or three times lower intensities of diffraction maximums typical to the latter compound were observed in all the rehydrated hydrotalcite samples. Meanwhile, the alkaline additives induced the memory effect of the hydrotalcite samples (64).

Lv *et al*. (65). carried out a 'memory effect' study of the removal of fluoride from aqueous solution by using calcined Mg-Al-CO_3 LDHs. It was investigated that layered double hydroxides calcined at different temperatures (200–800 ºC) regenerated their original layered structure in the examined anions. The researchers determined that LDHs transform to aluminum and magnesium oxides by the loss of interlayer anions within the temperature range of 200–500 ºC. Also, the interlayer carbonate of LDHs is decomposed completely when calcined at 500 ºC. When the calcination temperature is above 500 ºC, CLDHs are transformed into a spinel (a mixed metal oxide) which does not exhibit the property of reconstruction. This results in the observed decrease of the adsorption loading for anions. The obtained results show that LDHs calcined at 500 ºC are denoted by the highest capacity of removal of the fluoride ion because the discussed compound was found to reconstruct the intrinsic structure (65).

The regenerated Mg-Al LDHs phases upon the rehydration of the mixed oxides also displayed significant changes in the textural and morphological properties in comparison to their parent LDHs (15). As a matter of fact, the regenerated crystals showed a high tendency to the agglomeration with the formation of large conglomerates with a dramatic reduction of the surface area (66). The obtained Mg-Al, Mg-Zn-Al and Mg-Al-Ga hydrotalcite-like compounds upon reconstruction also displayed changes in both the composition and the morphology with a dramatic drop of the surface area. The explanation of this phenomenon was based on a dissolution-recrystallization mechanism of the reconstruction in contrast with the widely accepted topotactical character of regeneration (67, 68, 15).

Lin *et al*. (69) observed that calcined Mg-Al LDHs, Mg-Fe LDHs and Zn-Al LDHs exhibited a different memory effect phenomenon. The calcined Zn-Al LDHs demonstrated poor reconstruction of the ex-LDHs, whereas Mg-Al LDHs and Mg-Fe LDHs showed high-level recovery of the ex-LDsH (15, 70). Such results can be related to the poorly crystalline and highly reactive Mg(Al)O and Mg(Fe)O in comparison to the data for Zn(Al)O characterized by high crystallinity and poor reactivity. A well-crystallized (Ni,Al)O mixed oxide obtained by calcination of Ni-Al LDHs showed poor reactivity on rehydration and only a limited recovery of the layer structure (15, 71).

A number of remarks about the mechanism of regeneration of the calcined LDHs were proposed (15):

- The thermal treatment of the LDHs precursor with the removal of crystallization water at a low temperature determines the formation of a highly disordered phase. Its rehydration involves slow reconstruction of the layered structure with no changes in the composition and morphology in comparison to ex-LDHs. In this case, the so-called memory effect appears to be clear (15).
- When the LDHs precursor is mildly calcined with full decomposition, more or less crystalline mixed oxides with an increase in the surface area are obtained due to the crystal shuttering and to the formation of a maze of micro-cracks of the ex-LDHs crystals. The rehydration of poor crystallinity mixed oxides determines the rapid regeneration of the layered phase characterized by a dramatic change in the morphology and a decrease in the surface area. Such a decrease is related to the formation of highly compact aggregates of regenerated LDHs. In this case, direct synthesis appears to be the optimal mechanism of the recovery of the layered structure (15).
- At a high temperature of calcination, while using crystalline mixed oxide and in the context of partial changes in the local structure of M^{3+} and/or M^{2+} cations, the obtained result is comparable to the ex-LDHs. Partial regeneration of the layered phase takes place which is characterized by a different composition and morphology in comparison to the LDHs precursor. Also, in this case, the mechanism of the partial recovery of LDHs precursor involves direct synthesis (15).

Mechanochemical treatment is an efficient technique to alter the physical and chemical properties of solids and to synthesize several nanosized inorganic

compounds. In the course of milling, the powder is subjected to severe deformation, multiple fractures and cold weld, which results in the reduction of their particle size, a decrease in the degree of structure order, an increase in the surface area, and a formation of the amorphous phase (25). The structural alterations of milling materials can be effectively evaluated by crystallinity. Crystallinity is generally defined as the level of structure order or crystallite perfection. For layered structure solids, the crystallite size and/or layer stacking defects are the main factors affecting their crystallinity (25, 72).

It is worth noting that the role of calcination, hydrothermal and/or microwave post-synthesis treatments on the properties of LDHs is known (32, 43, 73) while the effects of the mechanochemical treatment conditions on their behavior can hardly be determined. To the best of our knowledge, only Wang *et al*. (25) prepared nanocrystalline Mg-Al layered double hydroxides via the hydrothermal method followed by mechanochemical treatment in order to evaluate the structural and textural changes upon grinding. Wang's team found that the latter processing (930 rpm; 9–330 min) had a significant effect on the structure and the physico-chemical properties of the obtained final products: during grinding at various treatment times, the crystallinity of LDHs gradually decreased, which led to the formation of an amorphous phase, while, at the same time, the original mesoporous structure was transformed to micro- and mesopores. Moreover, the continuous pore volume reduction was observed, whereas the surface area increased during the initial grinding stage and decreased in the final milling period (25).

It can thus be stated that these types of post-synthesis treatment provide a novel approach towards deliberate construction of materials structure as well as towards tailoring the physico-chemical properties of solids.

1.2 Classification, Structure and Synthesis of Calcium Silicate Hydrates Family Compound

1.2.1 Classification and Structure of Calcium Silicate Hydrates Family Compound

Recently, interest arose in another group of compounds, specifically, calcium silicate hydrates, which are used in many application areas, such as adsorption, production of plastics, rubber and other materials. These compounds are a highly multiplex system with over 30 stable phases (74). The general chemical formula of C-S-H is written as $xCaO \cdot ySiO_2 \cdot pH_2O$, where x, y, p are the numbers of moles (75). The first structural models of C-S-H were presented in 1952. Several models of C-S-H structure were proposed; they broadly portrayed it as a non-crystalline calcium oxide layer sandwiched by short and discrete silicate chains. The chains follow tetrahedral silica in a 'dreierketten' arrangement, in which, the smallest repeating unit is three tetrahedra, that is, one bridging and two pairing units (76, 77). Also, it was determined that the length of the silicate chain follows the formula $3n$-1 where n is an integer (75). The pairing tetrahedra share two oxygen atoms with the calcium oxide layer, whereas

the bridging tetrahedra share only one oxygen atom with the calcium oxide layer (Fig 1.6) (76, 78, 79).

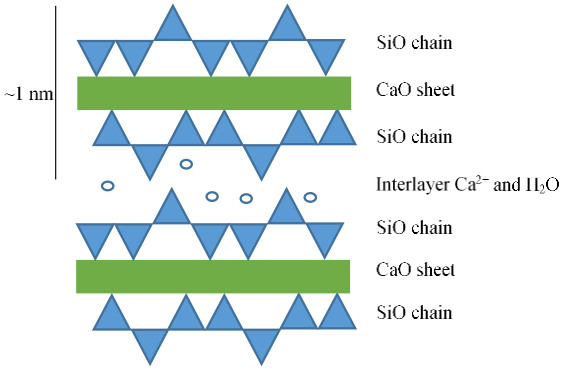

Fig. 1.6 The crystal structure of calcium silicate hydrate (76)

Taylor made important contributions to the study of the crystal structure of the lime-silica-water system (80). He examined the crystal properties of tobermorite-like C-S-H, C-S-H(I) and jennite-like C-SH, C-S-H(II). It was established that a tobermorite model in which the C/S ratio was raised above 0.83 by the omission of the bridging silica tetrahedra and their replacement with calcium ions in the interlayer. After that, Taylor continued to design the structure of C-S-H by proposing a model that is composed of structural components of jennite and 1.4 nm tobermorite. It was explained that the range in the C/S molar ratio was linearly proportional to the reciprocal value of the silicate chain length (81, 82) .

Kurczyk and Schwiete (83) observed C/S ratios between 1.80 and 1.92, when β-C_2S and C_3S were hydrated, and proposed a model based on tobermorite with calcium hydroxide and water in the interlayer to account for the higher C/S ratio. The silicate chain length was presumed to be infinite (76). Also, Stade *et al*. (84) proposed a model which is very similar to that of Kurczyk and Schwiete with the notable difference of allowing finite silicate chains (84). Richardson (85) proposed the generalized model from tobermorite/jennite or tobermorite/calcium hydroxide which is very similar to many of the previous models for the structure of C-S-H. However, this model did not fix the level of protonation of the silicate chain but its generality still allows for specific inconsistencies of other models to be compensated for (76).

Due to the nature of CSH formation and diversity, difficulties arise when attempting to study their structure and properties. It should be noted that not all the crystal structures of these compounds have been explored and are perfectly clear; therefore, their classification is constantly being improved. At present, the classification proposed by Taylor and Roy is the most widely recognized; it was supplemented by Kraus and Nolze in 1996 and by Richardson in 2008 (75). Calcium silicate hydrates are classified into the following groups: wollastonite, tobermorite, jenite, gyrolite, γ-Ca_2SiO_4 and other groups of C-S-H formed under hydrothermal synthesis conditions (Table 1.3).

Table 1.3 The classification of calcium silicate hydrates (75)

Group	Mineral	Molar rate of C/S	Formula of the mineral
Wollastonite	Nekoite	0.5	$Ca_3Si_6O_{15}\cdot 7H_2O$
	Okenite	0.56	$[Ca_8(Si_6O_{16})(Si_6O_{15})_2(H_2O)_6]^{4-}$ $[Ca_2(H_2O)_9\cdot 3H_2O]^{4+}$
	Pectolite	1.0	$Ca_2NaHSi_3O_9$
	Wollastonite 1A	1.0	$Ca_3Si_3O_9$
	Xonotlite	1.0	$Ca_6Si_6O_{17}(OH)_2$
	Foshagite	1.33	$Ca_4(Si_3O_9)(OH)_2$
	Hillebrandite	2.0	$Ca_2(SiO_3)(OH)_2$
Tobermorite	11 Å tobermorite	0.67	$Ca_4Si_6O_{15}(OH)_2\cdot 5H_2O$
	11 Å tobermorite	0.75	$Ca_{4.5}Si_6O_{16}(OH)\cdot 5H_2O$
	9 Å tobermorite	0.83	$Ca_5Si_6O_{16}(OH)_2$
	14Å tobermorite	0.83	$Ca_5Si_6O_{16}(OH)_2\cdot 7H_2O$
	Clinotobermorite	0.83	$Ca_5Si_6O_{17}\cdot 5H_2O$
	Clinotobermorite 9 Å	0.83	$Ca_5Si_6O_{16}(OH)_2$
	Oyelite	1.25	$Ca_{10}B_2Si_8O_{29}\cdot 12.5H_2O$
	C-S-H	≤1.5	$(SiO_3)_\infty$ and Si_2O_7 (?)
Jennite	Jennite	1.5	$Ca_9Si_6O_{18}(OH)_6\cdot 8H_2O$
	Metajennite	1.5	$Ca_9Si_6O_{18}(OH)_6\cdot 8H_2O$
Gyrolite	K-phase	0.44	$Ca_7Si_{16}O_{38}(OH)_2$
	Z-phase	0.56	$Ca_9Si_{16}O_{40}(OH)_2\cdot 14H_2O$
	Truscottite	0.58	$Ca_{14}Si_{24}O_{58}(OH)_8\cdot 2H_2O$
	Gyrolite	0.66	$Ca_{16}Si_{24}O_{60}(OH)_8\cdot 14H_2O$ $NaCa_{16}Si_{23}AlO_{60}(OH)_8\cdot 14H_2O$
	Reyerite	0.67	$Na_2Ca_{14}Si_{22}Al_2O_{58}(OH)_8\cdot 6H_2O$
	Reyerite	0.58	$Ca_{14}Si_{24}O_{58}(OH)_8\cdot 6(H_2O)$
γ-C_2S	Calcium chondrodite	2.5	$Ca_5[SiO_4]_2(OH)_2$
	Kilchoanite	1.5	$Ca_6(SiO_4)(Si_3O_{10})$
	C_8S_5	1.6	$Ca_8(SiO_4)_2(Si_3O_{10})$
	γ-C_2S hydrate	2.0	γ-Ca_2SiO_4
Other calcium silicate phases	Afwillite	1.5	$Ca_3(SiO_3OH)_2\cdot 2H_2O$
	α-C_2SH	2.0	$Ca_2(HSiO_4)(OH)$
	Cuspidine	2.0	$Ca_4(F_{1.5}(OH)_{0.5})Si_2O_7$
	Dellaite	2.0	$Ca_6(Si_2O_7)(SiO_4)(OH)_2$
	Jaffeite	3.0	$Ca_6[Si_2O_7](OH)_6$
	Killalaite	1.6	$Ca_{6.4}(H_{0.6}Si_2O_7)_2(OH)_2$
	Poldervaartite	2.0	$Ca(Ca_{0.67}Mn_{0.33})(HSiO_4)(OH)$
	Rosenhahnite	1.0	$Ca_3Si_3O_8(OH)_2$
	Suolunite	1.0	$CaSiO_{2.5}(OH)\cdot_{0.5}H_2O$
	Tilleyite	2.5	$Ca_5Si_2O_7(CO_3)_2$
	C_3S hydrate	3.0	$Ca_6(Si_2O_7)(OH)_6$

The interest in gyrolite has largely been growing in recent years compared to other calcium silicate hydrates occurring in the ternary system (CaO-SiO_2-H_2O). This interest arises from the fact that gyrolite, similarly to some other calcium silicate hydrates – tobermorite, xonotlite or C-S-H(I), is denoted by cation exchange capacity (86, 87). Gyrolite is a mineral with the most likely chemical formula $NaCa_{16}Si_{24}O_{60}(OH)_8 \cdot 14H_2O$ or $Ca_{16}Si_{24}O_{60}(OH)_8 \cdot 14H_2O$. It is known that the above mentioned compounds can be synthesized by hydrothermal treatment from a mixture of CaO and SiO_2 (87).

1.2.2 Synthesis of a Calcium Silicate Hydrates Family Compound: Gyrolite

For the first time, gyrolite was synthesized by Flint *et al*. (88). These authors determined that this synthesis route is an extremely complex and time-consuming process because after 6–42 days of hydrothermal synthesis at a temperature of 150–350 °C, when C/S molar ratios varied from 0.5 to 0.66, only gyrolite was formed (88). After that, Kalousek and Nelson (89) determined that gyrolite can be prepared by interacting dicalcium silicate with SiO_2 in aqueous suspension under hydrothermal conditions. It was found that the natural gyrolite and the synthetic gyrolite behave analogously if hydrothermal synthesis is performed at a temperature of 200–300 °C. Above this temperature, both compounds decompose into stable phases: truscottite and xonotlite (89). Okada *et al*. (90, 91) prepared gyrolite by using lime and amorphous silica as the starting materials. Hydrothermal synthesis was carried out at 200 °C for different numbers (0.5–128) of hours when C/S molar ratios were 0.50 and 0.66 (90, 91).

Also, the influence of different SiO_2 modifications during the crystallization process of gyrolite was examined. The obtained results showed that gyrolite did not form even after a week in the mixtures of CaO and amorphous SiO_2 at 150 °C under saturated steam pressure. A positive effect on the synthesis was observed when the temperature was increased because, after 32 h and 72 h of treatment at 200 °C and 175 °C, respectively, pure gyrolite was produced. It should be underlined that, in the mixtures with quartz, the mechanism of this compound formation was quite different. Due to a low quartz solubility rate within the 150–200 °C temperature range, neither the Z-phase nor gyrolite formed even after 72 h of hydrothermal curing (92).

Shaw *et al*. (93) synthesized gyrolite within the 190–240 °C temperature interval. These authors investigated the mechanical, kinetic and energetic processes which occured during the formation of gyrolite. Moreover, they determined that the formation of this compound in the pure calcic system involves a three-stage process: an amorphous gel → a C-S-H gel → the Z-phase → gyrolite (93).

Baltakys and Siauciunas (94) determined that the stirring of suspensions had a positive effect on the formation of gyrolite because the crystallization of this compound was accelerated, and pure gyrolite was obtained after 16 h of isothermal curing at a temperature of 200 °C. It should be noted that stirring affects the sequence of the formed intermediate compounds: gyrolite crystallized together with the Z-phase (94).

Also, Baltakys *et al*. (89) determined the influence of hydrothermal synthesis conditions on the gyrolite-specific surface area, the dominant pore size and their differential distribution by the radius. The hydrothermal synthesis of gyrolite was carried out at a temperature of 200 °C while employing different duration (32, 48, 72, 120, 168 h) when the molar ratio of C/S was equal to 0.66. It was established that a stable gyrolite crystal lattice was formed only after 120 h of isothermal curing. The authors found that the structure of gyrolite and the shape of the dominating pores (from the pores between parallel plates to the cylindrical pores) changed when the duration of hydrothermal synthesis was prolonged (89).

The influence of the gypsum additive on the gyrolite formation process was examined as well (95). It was determined that, at the beginning of synthesis, sulfate ions stimulated the Z-phase formation with a low-base mixture (C/S=0.66). After 72 h of hydrothermal treatment, gyrolite was the final product in both mixtures: with sulphate ions as well as without them. The results showed that the persistence of the intermediate compounds in the synthesis of gyrolite depends on the methods of calculating the gypsum additive. The crystallization process of gyrolite was more intensive when the initial mixture composition according to the molar ratios was calculated (95).

Moreover, Różycka *et al*. (96) examined a single phase gyrolite-cation exchanger which was successfully synthesized in the CaO-SiO_2-Na_2O-H_2O system. It was the first successful attempt to synthesize the single-phase gyrolite by using quartz as a siliceous material. The authors found that the content of NaOH was a crucial factor for gyrolite crystallization. The optimum amount of NaOH varied within a narrow range, i.e., between 0.75% and 1.00%. It should be noted that the decrement or increment in the quantity of NaOH did not allow to obtain gyrolite in its pure form, and that unreacted quartz was observed in the final products (96).

Eisinas (97) determined that gyrolite remains stable when the hydrothermal synthesis duration varies from 32 to 168 hours at a temperature of 200 °C. In Eisinas' research, it was observed that the crystallite size increased while the S_{BET} value changed from 82.07 m^2/g to 46.00 m^2/g. Furthermore, it was determined that within 8 h of isothermal curing by entering the synthesis products' structure, ZnO induces both Z-phase (4 h) and gyrolite (24 h) formation. Meanwhile, the addition of CuO accelerates the process because, within 8 h of synthesis, the recrystallization of the formed Z-phase to both gyrolite gel (16 h) and gyrolite (48 h) proceeds faster in comparison with pure mixtures (97).

Iljina (98) confirmed previous results. The scholar synthesized gyrolite after 32, 48, 72, 120 and 168 h at a temperature of 200 °C in CaO and $SiO_2 \cdot nH_2O$ mixture (C/S=0.66). The obtained results showed that as early as after 32 h of isothermal curing, the main synthesis product – gyrolite – was formed. Also, the crystallinity of gyrolite increased by prolonging the isothermal curing duration from 32 to 168 h, and no other compounds were identified. It should be noted that in higher basicity mixtures (C/S=0.83 and C/S=1.0), calcium silicate hydrates compounds with a smaller CaO/SiO_2 ratio were formed. Consequently, in the mixture with a smaller ratio (C/S=0.55 and C/S=0.66), gyrolite was the main compound, and, when the C/S molar ratio was increased from 0.83 to 1.0, it gradually recrystallized into 1.13 nm

tobermorite and xonotlite in pure mixtures (98). In further research, Iljina *et al*. (86) determined the influence of the hydrothermal synthesis duration at a temperature of 200 °C on the crystallinity and stability of gyrolite. Gyrolite was being synthesized for 120, 168, 336, and 504 h at 200°C from a molar ratio of CaO/SiO_2 of 0.66. It was established that gyrolite formed after 120–168 h of hydrothermal treatment. Meanwhile, after 336–504 h of treatment, gyrolite became metastable, and a new compound of calcium silicate hydrate – truscottite – was formed (86).

Thus the data of other authors showed that gyrolite can be successfully synthesized by using CaO and various forms of SiO_2 when the molar ratio of C/S is equal to 0.66 in aqueous suspension at temperatures of about 200 °C.

1.3 Application of Layered Double Hydroxides and Calcium Silicate Hydrates Family Compounds or Their Oxides in the Adsorption of the Ions of Transition Metals

Recently, due to the increasingly stringent environmental legislation, it is recommended to change the manufacture process by reducing the amounts of contaminants while using advanced recuperative waste removal technologies (99). The metals released into the environment pose a significant threat to the aquatic environment and human beings (100, 101). Pb, Cd, Fe, Mn, Cu, Zn, Cr and Ni are especially common metals that tend to accumulate in living organisms, which causes numerous diseases and disorders. These metals are often found in the surface water, groundwater and soil (102). The removal of heavy metals from wastewater is of crucial importance due to their high toxicity, solubility in the presence of water, non-biodegradability and persistent nature. It should be noted that it is necessary to treat metal-contaminated effluents prior to water discharge to the environment. For this reason, various techniques have been employed for removing dissolved heavy metals, including chemical precipitation, ion exchange and electrochemical removal (103, 104, 105). However, these methods are denoted by essential disadvantages: incomplete removal, high energy requirements or the production of toxic sludge (103, 105). There are two major strategies to improve the quality of the water systems as well as achieve prevention of soil contamination: removal of heavy metals and their irreversible immobilization (105). Currently, numerous approaches have been investigated while striving for the development of cheaper and more efficient technologies with the objective of not only decreasing the amount of the produced wastewater but also of improving the quality of the treated effluent (105). The effective removal/immobilization of metal ions from aqueous solutions can be achieved by applying adsorption (106, 107). In terms of these methods, the adsorption technique is considered to be the most attractive process because of its simplicity, convenience and high removal efficiency (107– 111). The search for low-cost adsorbents denoted by metal-binding capacities has been the focus of extensive research. The adsorbents may be of mineral, organic or biological origin, zeolites, industrial by-products, agricultural waste and polymeric materials (105, 112). However, in order to improve their adsorption capacity and enhance the separation rate, the design and exploration of novel adsorbents is still necessary.

Adsorption by layered double hydroxides family compounds (hydrotalcite) or their oxides

In recent years, layered double hudroxides received significant attention in environmental remediation due to their low cost, high surface area, highly tunable interior architecture, non-toxicity and exchangeable anionic features (113-115). Based on the preparation method or on post-synthesis treatment, adsorbents of LDHs can be used in a variety of different ways (Fig. 1.7) (116).

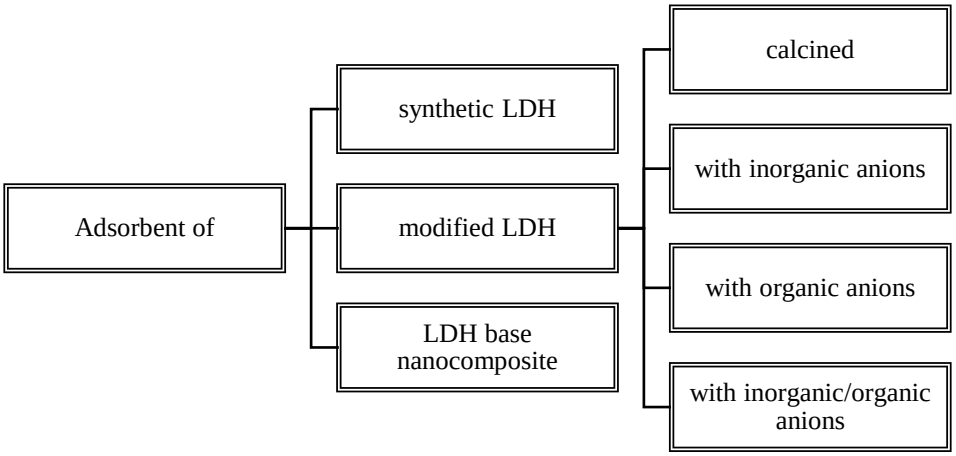

Fig. 1.7 Various types of layered double hydroxides as adsorbents (117–121)

Kameda *et al*. (122) investigated heavy metal ions (Cd^{2+} and Cu^{2+}) adsorption on modified Mg-Al layered double hydroxide with organic acid anions (citrate, malate and tartrate). The scholars determined that the researched LDHs intercalated high amounts of Cu^{2+} or Cd^{2+} ions from the aqueous solution at pH 5.0. The obtained results indicate that the organic acid anion intercalated Mg-Al LDHs can be applied for wastewater treatment, but the different stabilities of the anion-metal complexes result in the different uptake capacities of Cu^{2+} and Cd^{2+} (122).

Zang *et al*. (123) examined the removal of Cu(II) ions by using synthetic hydrotalcite-like compounds (Mg/Al molar ratio of 2:1; synthesis method – co-precipitation). It was established that the Mg-Al HTlc showed good sorption capacity for Cu(II) from $CuSO_4$ solution, which indicates that the use of hydrotalcite-like compounds as promising inorganic sorbents for the removal of heavy metal ions from water is possible. Moreover, it was determined that the sorption kinetics and the sorption isotherm of Cu(II) on the HTlc obeyed the pseudo-second order kinetic model and the Langmuir equation, respectively. It should be noted that the removal of Cu(II) ions by hydrotalcite-like compounds was strongly dependent on the initial pH of the bulk solution, and it was relatively small in the initial pH range of 4–5 whereas it reached about 100% when the initial pH was higher than 7 (123).

Li *et al*. (124) explored single sorption of copper ions into a Mg-Al hydrotalcite-like compound modified with dodecylsulfate and ethylenediaminetetraacetate ions.

They discovered that modification can decrease the specific surface area of the Mg-Al HTlc – yet it can still promote the sorption of Cu^{2+} ions. Pseudo-second order equations were fitted to the kinetic data, and the rate constant was calculated (k_2=0.015 g/mg·min). The results of the initial pH agreed with the previously obtained data because a higher pH of the initial solution significantly increased the sorption of Cu^{2+} (124).

Also, the effect of calcination (at 300, 400, 500 and 600 °C for 4 h) and adsorption temperatures (at 20, 30, 40, 50 and 60 °C when the initial pH equals 5.5) on the Cr(VI) removal out of the calcined Mg/Al hydrotalcite was investigated. The results showed that MMO500 was a promising adsorbent in Cr(VI) pollution control because this sample featured the largest adsorption capacity of 94.64 mg/g for Cr(VI) when the concentration of chromium ions was 100 mg/l at 50 °C. However, it should be taken into consideration that the equilibrium capacity decreased to 82.06 mg/g at 600 °C. This equilibrium was achieved within a short time frame at a temperature below 300 °C but the time was extended at temperatures between 400 to 600 °C. It should be noted that the largest adsorption capacity of samples depended on calcination and adsorption temperatures (41). Meanwhile, Liu *et al*. (125) investigated chromium ions adsorption on calcined Mg/Al hydrotalcites (Mg/Al molar ratio of 3.0; calcined at 500 °C for 5 h) by using two different calcination methods: hydrothermal and microwave. The obtained results showed that microwave calcination resulted in the enhanced crystallinity and specific surface area of Mg/Al bimetallic oxides if compared to the conventional calcination. Adsorption experiments were carried out at temperatures of 20, 40 and 60 °C when Cr(VI) solution was at its initial concentration of 30–150 mg/l with 20 mg/l increments at pH=5.5; the reactions took 3 h. It was determined that CHTM exhibited a higher adsorption capacity than CHT, and the maximum adsorption capacity of Cr(VI) of CHTM was 111.8 mg/g under trial conditions. A likely cause of this phenomenon is that CHTM had a bigger pore size, higher special surface areas as well as pore volumes than those of CHT. Liu *et al*. believe that Mg-Al bimetallic oxides derived from hydrotalcite as adsorbents removed the contamination in the wastewater through 'the memory effect' (i.e. the structure reconstruction). The layered crystal structure was easily regenerated during the adsorption process (125).

Sun *et al*. (126) examined Cu^{2+}, Zn^{2+} and Ni^{2+} ion adsorption on calcined Mg-Al hydrotalcite (at 450 °C for 2 h) from the aqueous solution at different temperatures (25, 35, 50 °C). The obtained results showed that the adsorption of Cu^{2+}, Zn^{2+} and Ni^{2+} showed similar tendencies, which suggests potentially homologous adsorption processes. The uptake of Cu^{2+}, Zn^{2+} or Ni^{2+} was rapid for the first 20, 50 and 50 min, respectively. Afterwards, it slowed down and gradually got close to saturation. The adsorption rate of CHT for Cu^{2+} was the highest (from $7.27 \cdot 10^{-4}$ g/mg·min to $15.85 \cdot 10^{-4}$ g/mg·min), whereas Zn^{2+} was determined to possess the maximum adsorption ability (from 302.8 mg/g to 408.4 mg/g) when the concentration of heavy metals was 200 mg/l, the volume of the solution was 100 ml, the sorbent dosage was 0.5 g/l, and the adsorption temperature increased from 25 °C to 50 °C. Furthermore, the adsorption capacity of CHT increased with the rising temperature, which demonstrated that a higher temperature was beneficial for enhancing the adsorption

efficiency. What is more, Sun *et al*. proposed an adsorption mechanism (Fig. 1.8). This process includes two steps: potentially toxic metal ions in the aqueous solution form hydroxide precipitates on the surfaces of adsorbents with high alkalinity whereas CHT experiences rehydration thus, together with hydroxide precipitates, forming new hydrotalcite compounds. Simultaneously, a part of Mg was substituted by Cu, Zn or Ni (126).

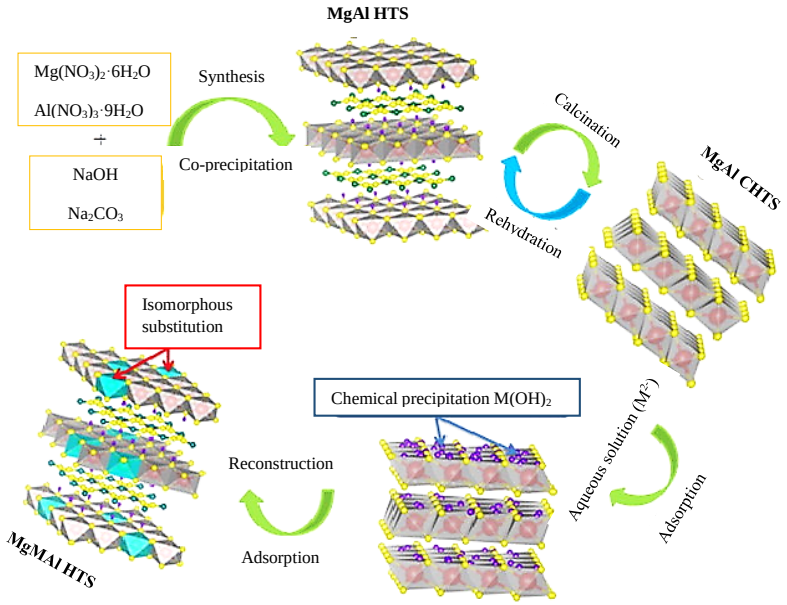

Fig. 1.8 Probable adsorptive mechanism between the heavy metal ion and calcined Mg-Al hydrotalcite (126)

González *et al*. (127) determined the synthetic layered double hydroxide-humate hybrid adsorption capacities for the removal of Cu^{2+}, Pb^{2+} and Cd^{2+} from aqueous solutions. Also, the sorption capacities of humic acid (HA), LDHs-Cl and LDHs-HA were compared under the same experimental conditions. The results showed that copper was completely (100%) removed by LDHs-Cl and LDHs-H, both sorbents being more effective than HA. Moreover, LDHs-Cl and LDHs-HA were able to produce almost complete removal of Pb^{2+} ions (87% and 95%, respectively), while HA showed lower sorption values (79%). Finally, HA produced the highest Cd^{2+} removal levels (64%) followed by LDHs-HA and LDHs-Cl at 56% and 37%, respectively. The buffering capacity of LDHs-Cl produced the highest pH values (from 8.2 to 9.3), while the least important pH change (from 6.8 to 5) was achieved for HA (127). After that, González *et al*. investigated Cu^{2+}, Pb^{2+} and Cd^{2+} ion exchange mechanisms from layered double hydroxides containing different amounts of humate anions (LDHs-HA50 and LDHs-HA100) and intercalated by chloride anions (LDHs-Cl). The results showed that the maximum uptake of Cu^{2+} on LDHs-HA100, LDHs-HA50 and LDHs-Cl was equal to 0.76, 1.02 and 1.95 mmol/g,

respectively. The amounts of sorbed Pb^{2+} were 0.48, 0.25 and 0.61 mmol/g, whereas, for Cd^{2+}, it was equal to 0.35, 0.18 and 1.03 mmol/g on LDHs-HA100, LDHs-HA50 and LDHs-Cl, respectively. In all the cases, the removal of the three metals was higher on LDHs-Cl. This result was quite unexpected given that humate functional groups have a high affinity for metal cations. The final pH=8.2–9 values achieved after sorption processes on LDHs-Cl suggest that the main mechanism of the uptake of metals probably occurred through their precipitation as metal hydroxides. Kinetic studies were carried out, and the results confirmed that all the sorption processes were in agreement with the pseudo-second kinetic order (128).

Chen *et al*. (129) studied the modified bentonite adsorption properties of hydrotalcite-like compounds for Pb^{2+} and Cu^{2+} ions. The kinetic study revealed that the experimental data satisfies the pseudo-second order model. It was also determined that the adsorption process attains the balance within the first 20 min for Pb^{2+} and within 60 min for Cu^{2+} ions. The highest removal capacity was found to be 384.6 mg/g and 156.3 mg/g for Pb^{2+} and Cu^{2+} at about pH=6.5, respectively. This research demonstrated that HTlc-Ben could be considered as a promising adsorbent for the removal of toxic substances (129).

Yang *et al*. (130) investigated Mg-Al layered double hydroxides modified clay adsorbents while seeking efficient removal of Pb^{2+}, Cu^{2+} and Ni^{2+} from water. The results of various initial pHs (ranging from 2.5 to 5.0) showed that the adsorption capacity for Pb^{2+} on Pal-Mg-Al LDHs increased significantly from 28.8 mg/g to 99.3 mg/g as pH approached 3.0, whereas it gently increased from 14.7 mg/g to 35.1 mg/g for Cu^{2+} and from 7.5 mg/g to 10.6 mg/g for Ni^{2+}. The maximum adsorption capacities of Pal-CLDHs for Pb^{2+}, Cu^{2+} and Ni^{2+} were achieved at pH=5.0, which were 99.8 mg/g, 64.0 mg/g and 41.8 mg/g, respectively. However, the adsorption capacity of Ni^{2+} on Pal-CLDHs was found to be approximately 3 times higher than that for Pal-Mg-Al LDHs. It was determined that the adsorption capacities of the three metal cations on Mg-Al layered double hydroxides modified palygorskite were higher than those of palygorskite and Mg-Al layered double hydroxides at the initial metal ion concentration level of 100 mg/l and at the initial pH=5.0. Also, the adsorption of Pb^{2+}, Cu^{2+} and Ni^{2+} on Pal-CLDHs showed that calcination could improve the adsorption performance (130).

Peligro *et al*. (131) explored heavy metal (Cu^{2+}, Pb^{2+} and Zn^{2+}) sorption capacity by *in situ* formation of layered double hydroxides as a function of the sorbent mass (m_{LDHs}). It was determined that the removal of Cu^{2+} and Zn^{2+} increased with increasing m_{LDHs} and reached the maximum value of 99% and 40%, respectively. On the other hand, the maximum Pb^{2+} removal percentage (40%) was obtained at the lowest m_{LDHs}, and then it diminished with the increasing m_{LDHs} to 25%. Finally, the pH of the dispersion continuously increased while increasing m_{LDHs} up to 5.5 at m_{LDHs}=1.2 g. Therefore, although Cu^{2+} was eliminated with high efficiency in all the cases, Pb^{2+} and Zn^{2+} removal requires fine tuning of the removal process in order to achieve high efficiency (131).

The above outlined studies illustrated that layered double hydroxides can be effectively used for the adsorption of various heavy metal ions. Their versatility, easily

tailored properties make them very attractive in the production of new adsorbents. As a result, the discussed substances can be applied for wastewater treatment.

Adsorption by a Calcium Silicate Hydrates Family Compound: Gyrolite

To date, another large group of compounds, specifically, calcium silicate hydrates, has been receiving significant attention in academic attempts to resolve environmental problems. These compounds are mesoporous materials which have a high surface area and a great pore volume, which was beneficial for their broad application in drug delivery, bone tissue engineering, and adsorption for heavy metal ions (132, 133). In comparison with other calcium silicate hydrates, gyrolite has a larger interlayer thickness of about 2.2 nm; therefore, it can adsorb more new guests (134).

Bankauskaite *et al*. (135) examined the sorption of copper ions by synthetic pure gyrolite (C/S=0.66, 96 h, 200 °C) in alkaline solutions when the initial concentration of Cu^{2+} ions ranged from 1 g/dm^3 to 20 g/dm^3 after 360 min of sorption at 25 °C. It was determined that the cation exchange capacity of gyrolite depended on the concentration of copper ions because a fivefold increase in the concentration (from 1.0 to 5.0 g/dm^3) of the primary solutions reduced the duration of the ion exchange reaction when shifting from 15 min to 5 min. Also, in the solutions with higher initial concentrations of Cu^{2+} ions (10.0 and 20.0 g/dm^3), the sorption proceeded more intensively, and all the copper ions were adsorbed within 1 min. It should be noted that the cation exchange reactions were reversible in the alkaline solution because almost 90% of copper ions was adsorbed in a physical process, while the remaining part of the cation was bound by a chemical reaction (135). However, Kasperaviciute's work (136) also showed that in an acidic medium gyrolite can adsorb only 41.48% of Cu^{2+} ions (136).

Baltakys *et al*. (137) established gyrolite adsorption capacities for cadmium ions. The results showed that the cation exchange reaction proceeded intensively during the first minute of the adsorption process because 87.54 mg cadmium ions/g entered into the structure of gyrolite when the initial concentration was 1 g cadmium ions/dm^3. After 120 min, almost all the cadmium ions were incorporated into the crystal structure of gyrolite (96.96 mg cadmium ions/g). Furthermore, Baltakys *et al*. determined that gyrolite acted as a chemisorbent but not like the usual adsorbent (137).

Also, Baltakys *et al*. (138) investigated the removal of Zn(II), Cu(II) and Cd(II) ions from alkaline and acidic solutions by using gyrolite. It was established that the adsorption reactions were more intensive in the alkaline solution (pH=10.61) because, after 30 min, almost all (98–99%) Cu^{2+}, Zn^{2+} and Cd^{2+} ions had been adsorbed. Meanwhile, the ion exchange equilibrium was reached only after 3 min in the acidic solution (pH=5.86). It was discovered that the cation exchange reactions were dependent on the pH of the solution. 20% of heavy metal ions participate in the ion exchange reaction whereas 80% of ions are present in gyrolite by chemosorption when pH=10.61. In the acidic solution, the cation exchange mechanism differs because all the heavy metal ions participate only in the ion exchange reaction (138).

Meanwhile, Iljina *et al*. (134) investigated the influence of the solution's pH on the gyrolite adsorption capacity for Zn^{2+} ions. It was discovered that the adsorption

process in the alkaline solution proceeded faster and more efficiently than in acidic environments because, after 30 s, 95% of Zn^{2+} ions (28.50 mg Zn^{2+}/g) were intercalated into the gyrolite structure, whereas in the acidic medium only 68% of Zn^{2+} ions (20.43 mg Zn^{2+}/g) were intercalated when the concentration of zinc ions was 0.3 g/dm^3. It was estimated that the substitution reaction was found to be typical for gyrolite in the alkaline solution because 82% of zinc ions participated in the ion exchange reaction, and the other part of these ions was present in gyrolite as a result of the addition interaction. The obtained results in the acidic solution agreed with the previously received data because all the zinc ions participated only in the ion exchange reaction (134). Iljina *et al*. (139) also determined the adsorption of Zn^{2+} ion in alkaline solutions by using a different synthetic gyrolite (for 32, 48, 72, 120, and 168 h at 200 ºC when C/S=0.66) as an adsorbent. It was consequently established that by prolonging the duration of synthesis from 32 to 168 h, the adsorption capacity of gyrolite decreased from 99% (29.92 mg Zn^{2+}/g) to 93% (27.91 mg Zn^{2+}/g), respectively. It was also established that the adsorption reactions were not reversible processes, and that they followed the pseudo-second-order model (139). Bankauskaite (140) examined that synthetic gyrolite (200 °C, 48 h) is denoted by higher adsorption capacities of zinc ions (21.75 mg Zn^{2+}/g). It was established that after 60 min, 12.48 mg Zn^{2+}/g was intercalated into the adsorbent crystal structure when the concentration of zinc ions was 0.25 g/dm^3 (140).

To sum up, the data presented in the researched scholarly literature showed that synthetic gyrolite can successfully remove various heavy metal ions from aqueous solutions, and most of the ions are immobilized into the structure of this compound.

****

The studies we cover in our research illustrated that, despite the significant progress achieved in terms of the preparation of layered double hydroxides, most of the applications of these materials are still restricted due to the formed LDHs which are usually loose powders of irregular aggregates. Besides, most of the synthesis methods are indirect, complicated and expensive. While substantial preliminary work has already been done in the framework of the preparation of another large group of compounds, specifically, calcium silicate hydrates, to date, only hydrothermal treatment has been used for the synthesis of these materials. For this reason, the application of more advanced techniques in the preparation of both groups of compounds is required in order to produce specific materials with the necessary physical and chemical properties. The data of the researched literature showed that this goal can be achieved by employing hydrothermal or microwave synthesis. However, the information about the application of direct microwave or hydrothermal treatment for the preparation of LDHs or C-S-H from solid initial materials is limited. It is worth noting that the structural and surface properties of LDHs can also be modified by using the post-synthesis methods (calcination, mechanochemical treatment and others). Nevertheless, detailed knowledge on the control of solid-state and mechanochemical activation parameters is still badly lacking, especially regarding the studies of Mg-Al LDHs. Still, it is known that two large groups of compounds, i.e., layered double hydroxides and calcium silicate hydrates, can be effectively used as adsorbents for the uptake of various heavy metal ions; however,

the scholarly literature data on the single and simultaneous adsorption of heavy metals ions by directly synthesized hydrotalcite and gyrolite are scarce. Thus it is necessary and highly topical to explore the sorption properties of hydrotalcite and gyrolite because of their crucial importance in search of low-cost and effective adsorbents.

2. Materials and Methods

2.1 Materials

The following reagents were used as the starting materials:

$MgCO_3$ (*Eurochemicals*, Slovakia, purity 99%) having a specific surface area S_a=1135 m^2/kg.

γ-Al_2O_3, which has been produced by burning aluminum hydroxide (*Stanchem*, Poland, purity 99%) at 475 °C for 5 hours and ground to the specific surface area S_a=3641 cm^2/kg.

CaO, which has been produced by burning calcium hydroxide (*Stanchem*, Poland, purity 97%) at 950 °C for 30 minutes and ground to the specific surface area S_a=1234 m^2/kg with the quantity of free CaO equal to 98.83%.

Finely ground $SiO_2 \cdot nH_2O$ (*Reaktiv*, Russia, purity 98%) having a specific surface area S_a=1804 m^2/kg with loss of ignition equaling 7.84%.

$Ni(NO_3)_2$ solution (c=0.25 g Ni^{2+}/dm^3) which was prepared by dissolving $Ni(NO_3)_2 \cdot 6H_2O$ (*Chempur*, Poland, purity 98%) in distilled water.

$Mn(NO_3)_2$ solution (c=0.25 g Mn^{2+}/dm^3) which was prepared by dissolving $Mn(NO_3)_2 \cdot 4H_2O$ (*Chempur*, Poland, purity 99%) in distilled water.

$Zn(NO_3)_2$ solution (c=0.25 g Zn^{2+}/dm^3) which was prepared by dissolving $Zn(NO_3)_2 \cdot 6H_2O$ (*Poch*, Poland, purity 99%) in distilled water.

$Co(NO_3)_2$ solution (c=0.25 g Co^{2+}/dm^3) which was prepared by dissolving $Co(NO_3)_2 \cdot 6H_2O$ (*Chempur*, Poland, purity 99%) in distilled water.

$Cu(NO_3)_2$ solution (c=0.25 g Cu^{2+}/dm^3) which was prepared by dissolving $Cu(NO_3)_2 \cdot 6H_2O$ (*Poch*, Poland, purity 98%) in distilled water.

$Fe(NO_3)_3$ solution (c=0.25 g Fe^{3+}/dm^3) which was prepared by dissolving $Fe(NO_3)_3 \cdot 6H_2O$ (*Chempur*, Poland, purity 99%) in distilled water.

$Cr(NO_3)_3$ solution (c=0.25 g Cr^{3+}/dm^3) which was prepared by dissolving $Cr(NO_3)_3 \cdot 9H_2O$ (*Sigma-Aldrich Chemie GmbH*, Germany, purity 99%) in distilled water.

Other pure chemical reagents (acetone, HCl).

2.2 Methods

This materials of this chapter have previously been published as: Bankauskaitė Agnė; Eisinas Anatolijus; Baltakys Kęstutis; Zadavičiūtė Skirmantė. A Study on the Intercalation of Heavy Metal Ions in a Wastewater by Synthetic Layered Inorganic Adsorbents. In: *Desalination and Water Treatment*. Philadelphia, PA: Taylor & Francis. 2015 (56), pp. 1576–1586, ISSN 1944-3994.

Zadavičiūtė Skirmantė; Baltakys Kęstutis; Eisinas Anatolijus; Bankauskaitė Agnė. Simultaneous Adsorption at 25 °C and the Peculiarities of Gyrolite Substituted with Heavy Metals. In: *Journal of Thermal Analysis and Calorimetry*. Dordrecht: Springer. 2017 (127), 335–343, ISSN 1388-6150.

Zadavičiūtė Skirmantė; Bankauskaitė Agnė; Baltakys Kęstutis; Eisinas Anatolijus. The Study of Cp Determination of Hydrotalcite Intercalated with Heavy Metal Ions. In: *Journal of Thermal Analysis and Calorimetry*. Dordrecht: Springer. 2018 (131), 521–527, ISSN 1388-6150.

Formation of Compounds Having Specific Properties in the CaO-SiO_2-H_2O System

In order to select the most suitable synthesis method for the formation of gyrolite, the samples were prepared via:

1) *hydrothermal treatment*: 8.79 g of CaO and 6.21 g of SiO_2 corresponding to the molar ratio of CaO/SiO_2=0.66 were dissolved in 150 ml of deionized water. The mixtures were transferred to a 250 ml *Lampart* autoclave for hydrothermal treatment in unstirred suspensions at 200 °C for 48 h. These conditions of synthesis were chosen to match the previously published data (92). After isothermal curing, the products were filtered, rinsed with acetone to prevent the carbonization of materials, dried at 50±5 °C and processed through a sieve with a 80-μm mesh.

2) *microwave treatment*: 0.88 g of CaO and 0.62 g of SiO_3, corresponding to the molar ratio of CaO/SiO_2=0.66, were dissolved in 15 ml of deionized water. The mixtures were transferred to a 30 ml *Monowave 300* microwave autoclave with 850 W power in stirred suspensions at 200 °C for 3 h. After isothermal curing, the products were filtered, rinsed with acetone in order to prevent the carbonization of materials, dried at 50±5 °C, and processed through a sieve with a 80-μm mesh.

The recommended optimal duration of one cycle for microwave treatment of 3 h was not suitable for the formation of calcium silicate hydrate when the molar ratio (C/S) of the primary mixture was equal to 0.66. The XRD results showed that, after conducting the above mentioned synthesis in the CaO-SiO_2-H_2O suspensions, only C-S-H (I) (ICDD File No. 34-0002; *d*-spacing equaling 0.125, 0.305, 0.183 nm) was dominating in the synthesis products (Fig. 2.1, a).

Meanwhile, after performing hydrothermal treatment (200 °C, 48 h), the main synthesis product – gyrolite (ICDD File No. 42-1452; *d*-spacing equaling 2.237, 1.126, 0.837 nm) – was formed, and no other compounds were observed in the system (Fig. 2.1, b). The present results were in good agreement with the data obtained by Baltakys *et al*. (137).

The results of simultaneous thermal analysis showed that, in the DSC curve, two thermal effects were identified: the endothermic effect at 145–151 °C which is typical of water dehydration, and the exothermic effect at 836–853 °C which characterizes the formation of wollastonite (Fig. 2.2, curves 2).

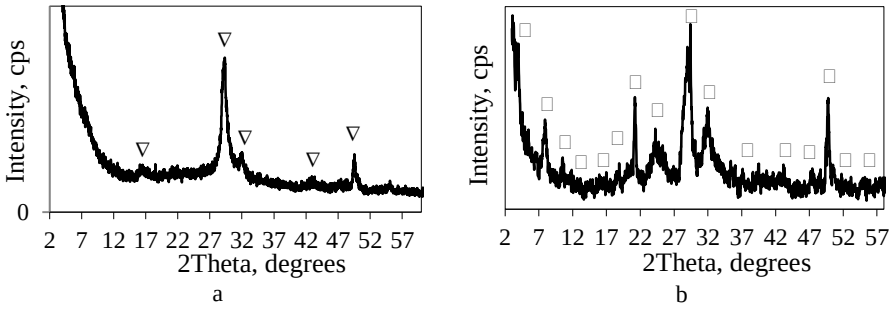

Fig. 2.1 X-ray diffraction patterns of microwave (a) and hydrothermal (b) synthesis products. Indices: ∇ represents C-S-H(I), □ denotes gyrolite

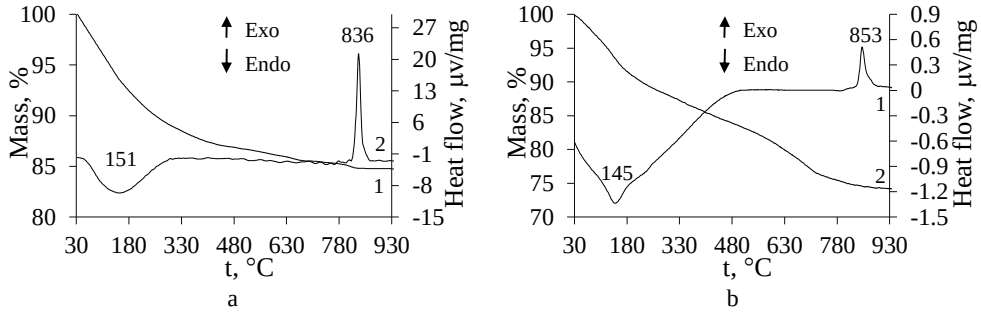

Fig. 2.2 STA curves (1 represents *TG*, 2 stands for *DSC*) of microwave (a) and hydrothermal (b) synthesis products

Formation of Compounds Possessing Specific Properties in the $MgCO_3$-Al_2O_3-H_2O System

The samples were prepared via the *hydrothermal method*: 4.98 g or 6.14 g of $MgCO_3$ and 3.02 g or 1.86 g of γ-Al_2O_3 corresponding to the molar ratio of the primary mixtures Mg/Al which were equal to 1 and 2 were dissolved in 80 ml of deionized water. The mixtures were transferred to a 160 ml *Parr Instrument* autoclave for hydrothermal treatment in stirred suspensions at 200 °C for 1 and 3 h. After isothermal curing, the products were filtered, rinsed with acetone in order to prevent the carbonization of materials, dried at 50±5 °C, and processed through a sieve with a 80-μm mesh.

The samples were prepared via the *microwave method*: 0.93 g or 1.15 g of $MgCO_3$ and 1.15 g or 0.35 g of γ-Al_2O_3 corresponding to the molar ratio of primary mixtures Mg/Al which were equal to 1 and 2 were dissolved in 15 ml of deionized water. The mixtures were transferred to a 30 ml *Monowave 300*" microwave autoclave with 850 W power. After isothermal curing, the products were filtered, rinsed with acetone to prevent carbonization of materials, dried at 50 ± 5 °C, and put through a sieve with a 80-μm mesh.

The determination of free CaO (141)

1 g of the sample was weighed and placed into a 250 cm^3 conical flask, poured with 150 cm^3 of distilled water, and 5 – 10 ps. of glass beads were added. The slurry was heated for 5 minutes. After that, the suspension was cooled down, the inner wall of the flask sprayed with distilled water and 2 – 3 drops of phenolphthalein indicator were added. Finally, the suspension was titrated with 1N HCl until the pink colour disappeared. The amount of free CaO (*X*) in the sample was calculated by using equation:

$$X = \frac{V \cdot N \cdot 28.04 \cdot 100}{G \cdot 1000}, \qquad (2.1)$$

Where *N* is normality of HCl; *V* is volume of titrated HCl, cm^3; 28.04 is CaO equivalent, g; *G* is initial mass of sample, g.

Thermal stability of Synthesis Products

The thermal stability of synthesis products was estimated in a high-temperature furnace "SNOL 8.2/1100" (temperature up to 1100 °C) at 575 and 1000 °C temperature for 1 h.

The Mechanochemical Treatment of Mg-Al hydroxides

The mechanochemical treatment of synthesis products was performed by using laboratory vibrating disc mill "Fritsch Pulverisette 9" consisting of a 250 ml hardened steel container with 2 rings and 1 disk. The vibrating frequencies of the grinding sets ranged from 650 to 950 rpm, while 0.5, 1, 3 and 5 min of grinding durations were chosen.

Reconstruction of Mg-Al hydroxides (64)

After mechanochemical treatment, the resulting solid materials were then rehydrated for 1 h in a distilled water at room temperature, i. e. 1 g of sample was added to 100 ml of distilled water in a 250 ml conical flasks (64).

Granulometric analysis

Granulometric analysis of samples was determined using a "L3P Sonic Sifter" fractional equipment. Sifting – separation device performance is based on the principle of vibrating air pole (dry separation), i. e. vertical pulse or shock wave every four seconds are transferred to sieves (425, 212, 106, 80, 63 μm), in which easily together joined or agglomerated particles are dispersed, when the duration of sieve analysis was equal to 4 min by applying 60 Hz current.

Adsorption Experiments and Kinetic Models

Single adsorption experiments

Adsorption experiments were carried out at a temperature of 25 °C in the thermostatic absorber *Grant SUB14* at different time periods (0.5, 1, 2, 3, 5, 10, 15 and 60 min). A series of suspensions in conical flasks were prepared, each containing 1 g of gyrolite or calcined hydrotalcite (575 °C, 4 h) and 100 ml of 0.25 g·Me^{x+}/dm^3 aqueous solutions (where Me^{x+} denotes Ni^{2+}, Mn^{2+}, Fe^{3+}, Co^{2+}, Zn^{2+} ions, respectively). The percentage of the adsorbed ions was determined on the basis of the variations in the concentration of the cations both in the solution and in gyrolite or hydrotalcite. The saturated adsorbents were rinsed with distilled water, dried at 50±5 °C, and dissolved in HCl (1:1).

Simultaneous adsorption experiments

Hydrotalcite adsorption experiments were carried out at temperatures of 25, 35 and 45 °C in a thermostatic absorber *Grant SUB14* with different time periods (0.5, 1, 3, 5, 10, 15 and 30 min). The amount of 1 g of hydrotalcite was added to a 100 ml mixture of transition metal ions solution containing 0.25 g Me^{x+}/dm^3 (where Me^{x+} denotes Co^{2+}, Cu^{2+}, Cr^{3+} ions, respectively). The percentage of adsorbed ions was determined on the basis of the variations in the concentration of the cations both in the solution and in hydrotalcite. The saturated adsorbents were rinsed with distilled water, dried at 50±5 °C, and dissolved in HCl (1:1). It was determined that, after 60 min, the amount of the transition metal ions leached from hydrotalcite to the aqueous medium was below the detection limit.

Gyrolite adsorption experiments were carried out at a temperature of 25 °C in a thermostatic absorber *Grant SUB14* for various time periods (0.5, 1, 2, 3, 5, 10, 15 and 60 min). The amount of 1 g of gyrolite was added to a 100 ml of mixture of

transition metal ion solutions containing 0.25 g Me^{x+}/dm^3 (where Me^{x+} denotes Ni^{2+}, Zn^{2+}, Co^{2+}, Mn^{2+}, Cu^{2+}, Fe^{3+} ions, respectively). The percentage of the adsorbed ions was determined on the basis of the variations in the concentration of the cations both in the solution and in gyrolite. The saturated adsorbents were rinsed with distilled water, dried at 50±5 °C, and dissolved in HCl (1:1). It was determined that, after 60 min, the amount of transition metal ions leached from gyrolite to the aqueous medium was below the detection limit.

The pH value was measured with a *Hanna Instrument Hi 9321 microprocessor pH meter*.

In order to determine the kinetic parameters of adsorption reactions, the kinetic models have been developed and fitted for the adsorption process. The *first order adsorption kinetics* model was chosen in analogy to the Largergren model (142–144) which can be represented by the equation:

$$\frac{dq_\tau}{d\tau} = k_1(q_e - q_\tau), \tag{2.2}$$

where: q_e and q_τ are the amounts of adsorbed ions at equilibrium and at time τ_e, respectively (mg/g), and k_1 is the rate constant of pseudo-first order adsorption (min^{-1}). After integration and after applying the boundary conditions $\tau=0$ to $\tau=\tau_e$ and $q_\tau=0$ to $q_\tau=q_e$, the integrated form becomes:

$$\log(q_e - q_\tau) = \log q_e - \frac{k_1}{2.303}\tau \tag{2.3}$$

The *pseudo second order adsorption kinetic* model was also chosen in analogy to the models discussed in (143–145); it can be expressed as:

$$\frac{dq_\tau}{d\tau} = k_2(q_e - q_\tau)^2, \tag{2.4}$$

where k_2 is the rate constant of the pseudo-second order adsorption (g/mg·min). For the boundary conditions $\tau=0$ to $\tau=\tau_e$ and $q_\tau=0$ to $q_\tau=q_e$, the integrated form of the equation is expressed as follows (which is the integrated rate law for the pseudo-second order reaction):

$$\frac{\tau}{q_\tau} = \frac{1}{k_2 q_e^2} + \frac{1}{q_e}\tau, \tag{2.5}$$

Atomic Absorption Spectrometry

The concentration of Co^{2+}, Fe^{3+}, Zn^{2+}, Mn^{2+}, Ni^{2+}, Cu^{2+}, Cr^{3+} and Ca^{2+} ions was determined by using a *Perkin Elmer Analyst 400* atomic absorption spectrometer with the following parameters: Zn^{2+} wavelength=213.86 nm; Co^{2+} wavelength=240.73 nm; Ni^{2+} wavelength=232 nm; Mn^{2+} wavelength=279.48 nm; Cu^{2+} wavelength=324.75 nm; Fe^{3+} wavelength=248.33 nm; Ca^{2+} wavelength=422.67 nm; Cr^{3+} wavelength=357.87 nm; the hollow cathode lamp current (I)=30 mA; the type of the flame was C_2H_2–air; the oxidant air was provided at a rate=10 l/min; acetylene=2.5 l/min. All the tests were repeated three times. The calibration curves are presented in Fig. 2.3 and Fig. 2.4.

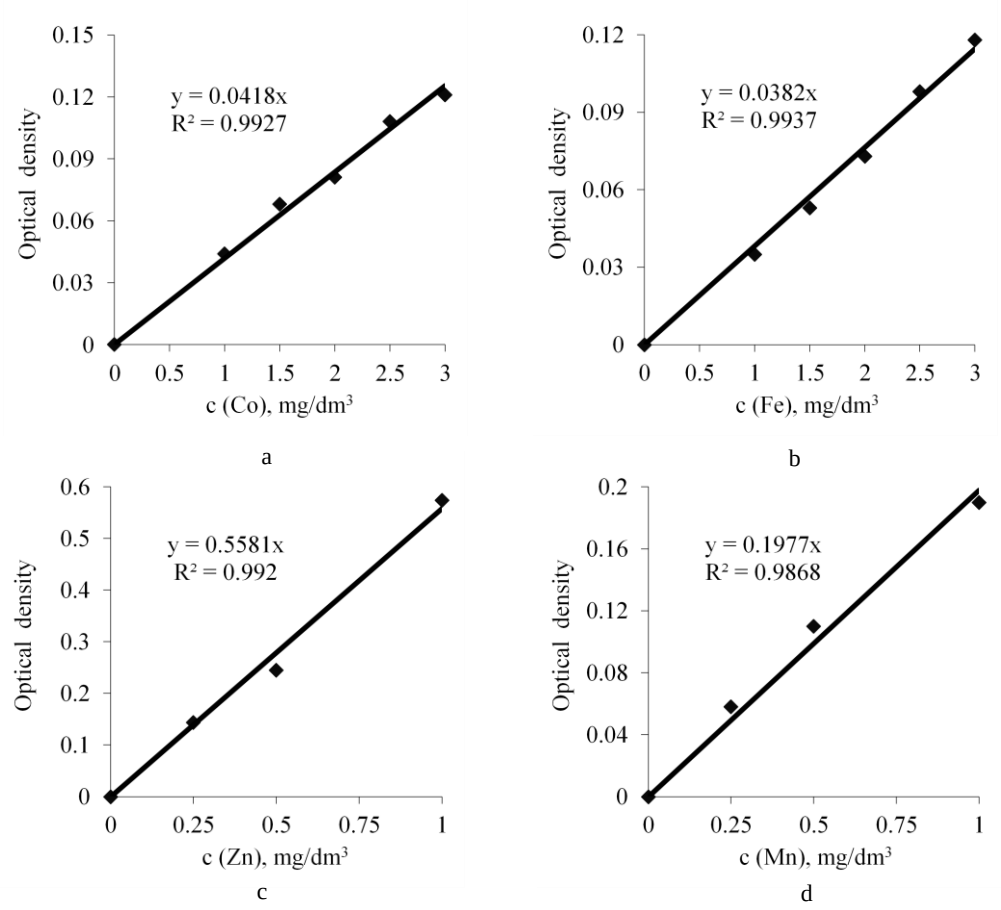

Fig. 2.3 Calibration curves for the calculation of Co^{2+} (a), Fe^{3+} (b), Zn^{2+} (c) and Mn^{2+} (d) ions concentration

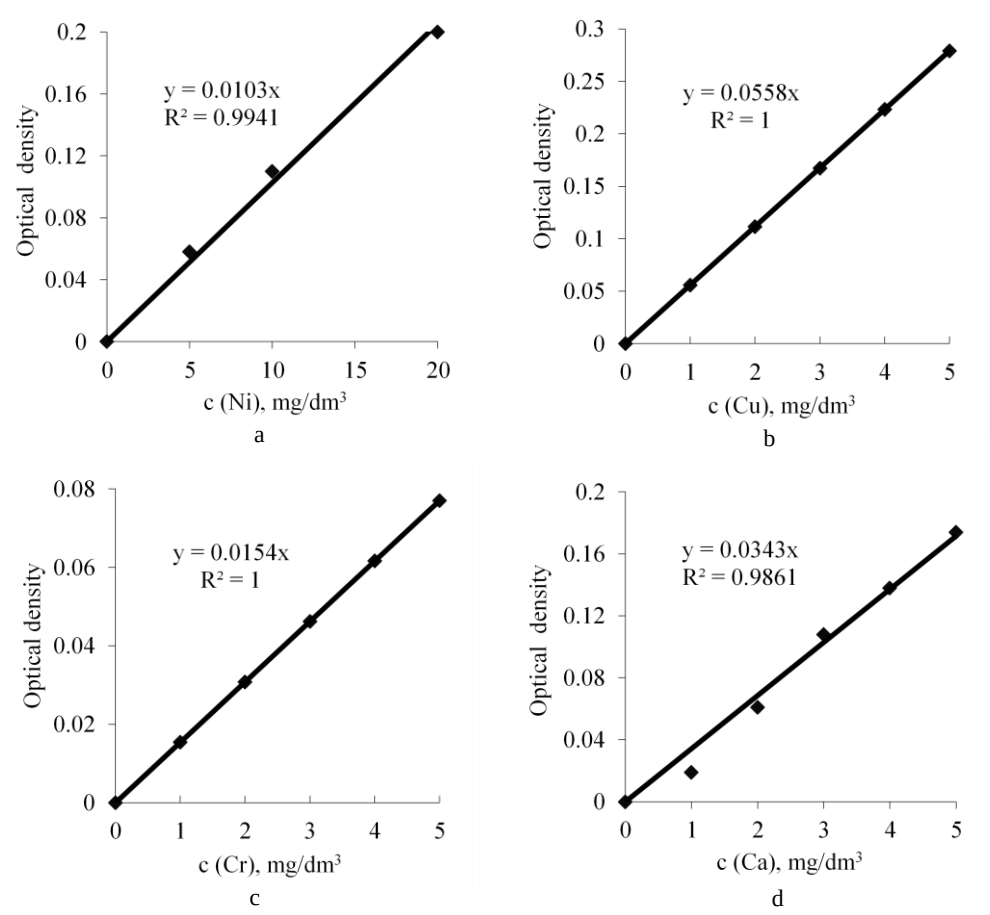

Fig. 2.4 Calibration curves for the calculation of Ni^{2+} (a), Cu^{2+} (b) Cr^{3+} (c) and Ca^{2+} (d) ion concentration

X-Ray Powder Diffraction (XRD)

The XRD analysis of the samples was performed on a *Bruker D8 Advance* diffractometer operating at the tube voltage of 40 kV and at a tube current of 40 mA. The X-ray beam was filtered with the *Ni 0.02 mm* filter upon the selection of the CuKα wavelength. The diffraction patterns were recorded in *Bragg-Brentano* geometry by using a fast counting detector *Bruker LynxEye* based on the silicon strip technology. The specimens were scanned over the range of 3–70 ° (2 θ) at a scanning speed of 6°/min while using a coupled two theta/theta scan type. XRD software *Diffrac.Eva* was used for the calculation of the crystallite size and the intensities of the main diffraction peak for the synthesis products. Scherrer's equation was used for the calculation of the crystallite size (D_{hkl}):

$$D_{hkl} = \frac{k \cdot \lambda}{B_{hkl} \cdot \cos\theta} \quad (2.6)$$

where: λ is the wavelength of CuKα radiation, θ is Bragg's diffraction angle, B_{hkl} is the full width at half maximum intensity, and k is a constant (the value used in this study was 0.94).

Specific Heat Capacity Analysis

The specific heat capacity of the samples was determined by applying a differential scanning calorimeter *Netzsch DSC214 Polyma* in a working range of 25–170 °C at a constant heating rate of 10°C/min by using aluminum crucibles; the flow rate of dynamic dry nitrogen gas was 20 ml min^{-1}, and the weights of the tested samples were equal to ~4 mg. Individual C_p values at different temperatures were determined according to the following equation:

$$C_p = \frac{m_{standard}}{m_{sample}} \cdot \frac{DSC_{sample} - DSC_{bas}}{DSC_{standard} - DSC_{bas}} \cdot C_{p,standard} \quad (2.7)$$

where: $C_{pstandard}$ is the table values of the specific heat of the standard, J/g·K; $m_{standard}$ is the mass of the standard, mg; m_{sample} is the mass of the sample, mg; DSC_{sample} is the value of the DSC signal at temperature *T* obtained from the sample curve, μV; $DSC_{standard}$ is the value of the DSC signal at temperature *T* obtained from the standard curve, μV; DSC_{sbas} is the value of the DSC signal at temperature *T* obtained from the baseline, μV.

Fourier Transform Infrared Spectroscopy (FT-IR)

The FT-IR spectra of the samples were recorded with the help of a spectrometer *PerkinElmer FT–IR system Spectrum X*. The specimens were prepared by mixing 1 mg of the sample in 200 mg of KBr. The spectral analysis was performed in the range of 400–4000 cm^{-1} with the spectral resolution of 1 cm^{-1}.

Simultaneous Thermal Analysis (STA)

STA (differential scanning calorimetry – DSC and thermogravimetry – TG) was employed for measuring the thermal stability and the phase transformation of the samples. The tests were carried out by using two different apparatuses:

1) *Netzsch instrument STA 409 PC Luxx*. Parameters in use: the heating rate of 15°C/min and the temperature range from 30 °C up to 1000 °C under air atmosphere. Ceramic sample handlers and crucibles of Pt-Rh were also used.

2) *Linseis PT10 instrument. Parameters*: a heating rate of 15°C/min and the temperature range from 30 °C up to 1000 °C under air atmosphere. Ceramic sample handlers and Al crucibles were also used.

Scanning Electron Microscopy (SEM)

The SEM of the samples was performed with a *JEOL JSM-7600F* while using the accelerating voltage of 10 kV with the working distance of 8.6 and 8.7 mm.

Preparation of Thin Mixed Mg-Al or Ca-Si Oxide Films

The synthesized samples were pressed into cylinder-shaped pellets (10x20 mm) by using a *MP15 Desktop Pellet* press (12.56 kg·m/s) and additionally calcined in a high-temperature furnace *SNOL 8.2/1100* (temperature up to 1,100 °C) at

temperatures up to 200, 575 and 1000 °C for 1 h with the objective to obtain nano-sized compounds.

RCA cleaning (146) for 60 min was used for the preparation of different substrates: Si wafer, silicon oxide (SiO_2) with thickness of 1 μm on Si wafer and aluminum oxide (Al_2O_3). RCA cleaning was followed by ion-plasma processing, when the substrates were exposed to O_2 RF plasma in the camera of a *JSC Kvartz Plasma-600-T* device at a pressure of 133 Pa (*RF*=13.56 MHz, *P*=0.3 W/cm^2, *t*=5 min) (146).

The electron beam evaporation technique (147) was applied for the formation of thin films. As targets for e-beam evaporation, pre-prepared precursor pellets were used. The evaporation of the thin films was operated at a pressure of $7 \cdot 10^{-1}$ Pa, and the e-gun power was set at 10 kW. During the evaporation process, the temperature of the substrate was kept constant at around 180 °C, and the thickness of the thin film was controlled by a quartz microbalance sensor. The evaporation rate of thin films was equal to ~0.6 nm/s (147).

The surface morphology of thin films was carried out in air at room temperature by using a *Microtestmachines NT-206* atomic force microscope and SPM-data processing software *SurfaceXplorer*. A V-shaped silicon cantilever (with its spring constant equaling 3 N/m, and the tip curvature radius being at 10.0 nm, and the cone angle of 20°) operating in the contact image mode with a 3 μm x 3 μm field of view was used. The surface of thin films was characterized by the roughness parameters (the root mean square roughness (R_q), skewness (R_{sk}), kurtosis (R_{ku}) and the mean height (Z_{mean}) (148).

The microhardness of thin films with the most different surface roughness and growth mechanism levels was measured by a micro-indenter *Fischerscope HM2000* (149). A Vickers-type diamond indenter was used. In all the cases, a 4 mN load was applied. Five repeat indentations were made for each sample, and the measured values are given as an average of all the measurements (149).

The microstructure of Mg-Al mixed oxide thin films was examined by scanning electron microscopy (SEM) on a *Raith e_LiNE plus* ultra high resolution scanning electron microscope equipped with an in-lens detector and a conventional secondary electron detector as well as an energy dispersive X-ray spectrometer *Bruker QUANTAX 200* equipped with a 5th generation *Si-Drift Detector* with <129eV energy resolution.

3. Results and Discussions

3.1 Synthesis of Compounds Featuring Specific Properties in $MgCO_3$-Al_2O_3-H_2O Stirred Suspensions

To date, most of the researches still focus on the multistep synthesis of hydrotalcite-type compounds by combining the most common methods, such as co-precipitation, sol-gel, ion exchange or other methods involving hydrothermal or microwave treatment. However, all of the options are denoted by a number of drawbacks: it is a multistep process, it is difficult to obtain high crystallinity compounds, strong agglomeration of primary particles often takes place, the products with poor morphology and particle size distribution are obtained, and, also, this route produces large amounts of waste (150, 151). Thus the search for a simpler synthesis method is still a highly relevant topic.

Recently, Bankauskaite (140) successfully synthesized hydrotalcite-type compounds by applying direct hydrothermal treatment. The above listed compounds were obtained in pure state and with alkali (corresponding to 5%, 15% and 25% of Na_2O or K_2O from the mass of dry materials) additive mixtures under saturated steam pressure (130–200 ºC) when the duration of isothermal curing was equal to 1, 4, 8, 24, 48, 72 and 168 hours whereas the molar ratios of the primary mixtures (Mg/Al) varied from 2 to 3. Bankauskaite established that the optimal conditions of hydrotalcite synthesis in $Mg_5(CO_3)_4(OH)_2{\cdot}4H_2O$ and γ-Al_2O_3 mixtures are as follows: the temperature of isothermal curing is 200 °C, the duration is 1 h, and the primary mixture Mg/Al molar ratio is 2. Moreover, the addition of NaOH and KOH into the mixtures induces not only the interaction between the raw materials but also changes the sequence of the obtained intermediate compounds by reducing the hydrotalcite formation temperature and/or duration (140). For this reason, the application of direct microwave or hydrothermal stirred synthesis with the objective of obtaining hydrotalcite from solid initial materials was carried out so that we could fully understand the effect of these types of materials treatment.

It was determined that, in non-stoichiometric mixtures (Mg/Al=1), after 1 hour of microwave synthesis at a temperature of 200 °C, alongside the main product hydrotalcite (ICDD File No. 70-2151; with *d*-spacing equaling 0.751, 0.379, 0.256 nm), boehmite (ICDD File No. 05-0190; with *d*-spacing equaling 0.610, 0.317, 0.185 nm), magnesite (ICDD File No. 78-2442; with *d*-spacing equaling 0.276, 0.251, 0.210 nm) and gibbsite (ICDD File No. 07-0324; with *d*-spacing equaling 0.484, 0.436 nm) were formed (Fig. 3.1, a, curve *MW*). It should be noted that the same compounds were also obtained during hydrothermal treatment (Fig. 3.1, a, curve *HS*). However, in this case, highly active γ-Al_2O_3 intensively participated in the formation of gibbsite because the intensity of the main diffraction maximum typical of the mentioned compound was higher than the intensity of the hydrotalcite main peak (Fig. 3.1, a, curve *HS*).

The materials of this chapter have previously been published as: Zadavičiūtė Skirmantė; Baltakys Kęstutis; Bankauskaitė Agnė. The Effect of Microwave and Hydrothermal Treatments on the Properties of Hydrotalcite: a Comparative Study. In: *Journal of Thermal Analysis and Calorimetry*. 2017 (127), 189–196, ISSN 1388-6150.

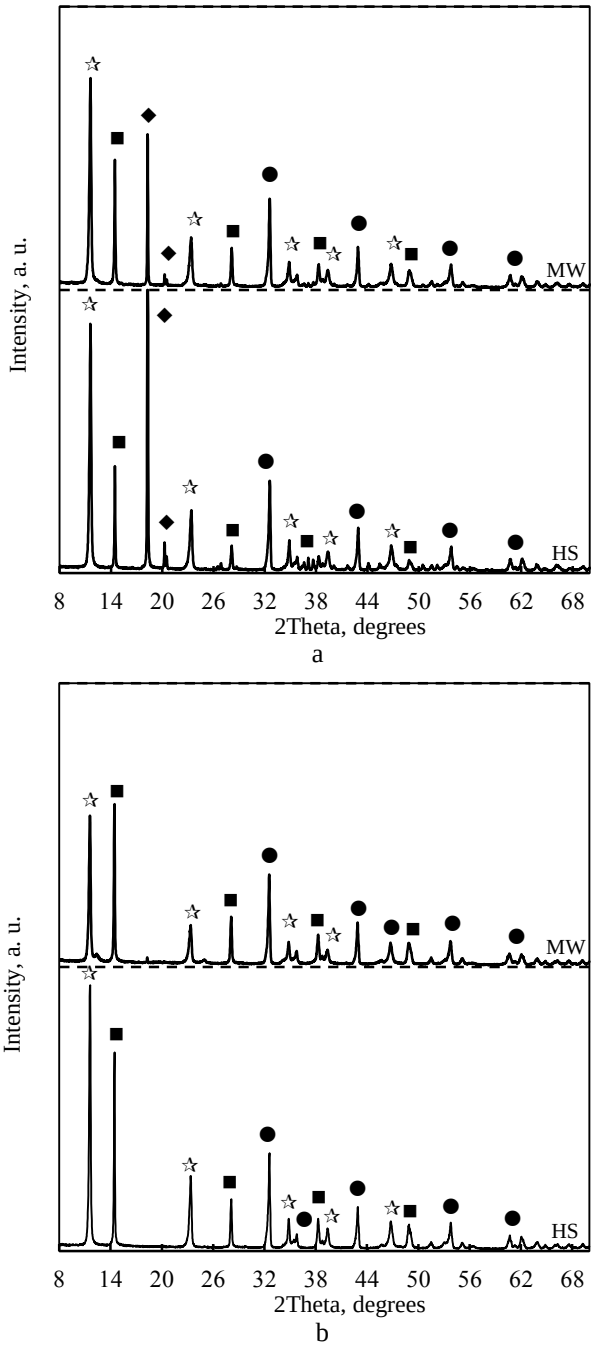

Fig. 3.1 X-ray diffraction patterns of products synthesized for 1 h (a) and 3 h (b) by using hydrothermal (HS) and microwave (MW) treatment when the molar ratio of the primary mixtures (Mg/Al) was equal to 1. Indices: ☆ – hydrotalcite, ● – magnesite, ■ – boehmite, ♦ – gibbsite

It was determined that the results of STA analysis of the synthesis products were in good agreement with the previous data: the heat values of gibbsite dehydration (252–292 °C) increased from 51.74 J/g to 164.58 J/g while the mass loss went up from 1.95% to 4.85% in comparison with microwave treatment (Table 3.1; Fig. 3.2). Moreover, double thermal conversion (which can be assigned to the decarbonization of hydrotalcite and the decomposition of magnesite) was observed within the 478–618 °C temperature range denoted by a mass loss of 20.24% for MW and 19.36% for HS (Fig. 3.2, a). Meanwhile, the other endothermic effects can be related to (Fig. 3.2, a):

- within the 184–252 °C temperature interval – to the loss of crystallization water in hydrotalcite;
- within the 294–365 °C temperature interval – to the loss of OH^- groups which are bonded with Al^{3+}.
- within the 373–471 °C temperature interval – to the decarbonization of hydrotalcite. However, the latter processes overlapped with boehmite dehydration taking place at 300–480 °C (152).

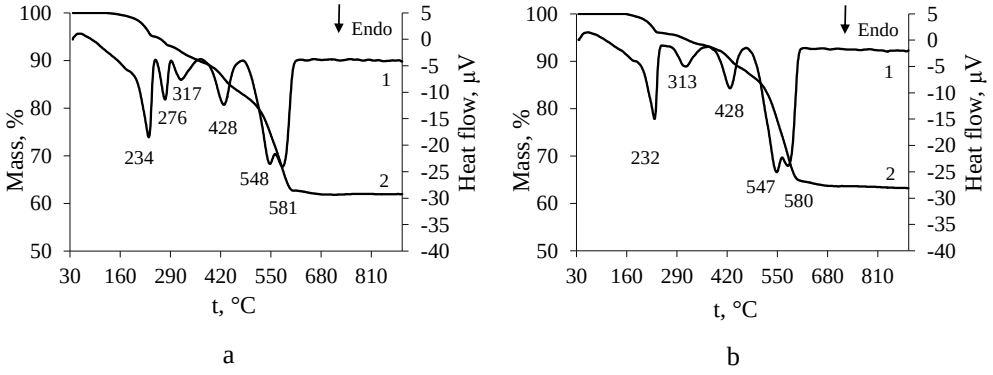

Fig. 3.2 STA curves (1 representing *DSC*, and 2 showing *TG*) of the products synthesized for 1 h (a) and 3 h (b) by using microwave treatment when the molar ratio of the primary mixtures (Mg/Al) was equal to 1

Moreover, when the duration of synthesis was extended to 3 h, the interaction between the initial materials was mostly accelerated by the hydrothermal treatment because a higher crystallinity hydrotalcite was obtained (Fig. 3.1, b; curve *HS*). These results were confirmed by STA analysis: the heat values of the removal of crystallization water were within 184–252 °C as determined by its structure; the mass loss increased from 117.10 J/g (for *MW*) to 157.63 J/g (for *HS*) and from 3.49% (for *MW*) to 4.58% (for *HS*), respectively (Fig. 3.2, b; Table 3.1). Moreover, it was observed that, during hydrothermal and microwave synthesis, gibbsite recrystallized to boehmite because the peaks characteristic of the first compound disappeared in XRD patterns as well as in DSC curves (252–292 °C) (Fig. 3.1, Fig. 3.2). Furthermore, the intensity typical of boehmite diffraction maximums was higher than that of 1 h for both types of synthesis (Fig. 3.1, b). However, the endothermic effects of hydrotalcite dehydroxylation and decarbonization as well as the dehydration of boehmite within

the 268–471 °C temperature interval overlap and cannot be distinguished (Fig. 3.2, b).

Table 3.1 The thermal characteristics of synthesis products at different durations of hydrothermal and microwave treatment in the mixtures with the molar ratio of Mg/Al=1

Preparation method	The duration of synthesis, h	Temperature range, °C	Heat of thermal effect, J/g	Mass loss, %
Hydrothermal synthesis	1	184–252	133.74	4.50
		252–302	164.58	4.85
		302–365	36.47	2.94
		373–471	109.32	6.03
		478–618	492.34	19.36
	3	184–252	157.63	4.58
		268–365	77.12	3.23
		373–471	129.43	6.42
		478–618	574.35	21.60
Microwave synthesis	1	184–252	129.75	4.17
		252–292	51.74	1.95
		294–365	45.60	3.01
		373–471	114.59	6.39
		478–618	526.97	20.24
	3	184–252	117.10	3.49
		268–365	56.32	2.45
		373–471	100.59	5.26
		478–618	608.71	22.71

In order to induce the interaction between raw materials, the molar ratio of the primary mixtures (Mg/Al) was increased to 2. It was determined that the formation of hydrotalcite under hydrothermal and microwave conditions was significantly affected by the molar ratio of the primary mixtures and the duration of synthesis. In comparison to the mixtures with a lower molar ratio (Mg/Al=1), after 1 h of hydrothermal and microwave treatment, the intensity of the hydrotalcite main peak only slightly decreased from 296 cps to 250 cps and from 258 cps to 238 cps, respectively (Fig. 3.1, a; Fig. 3.3, a).

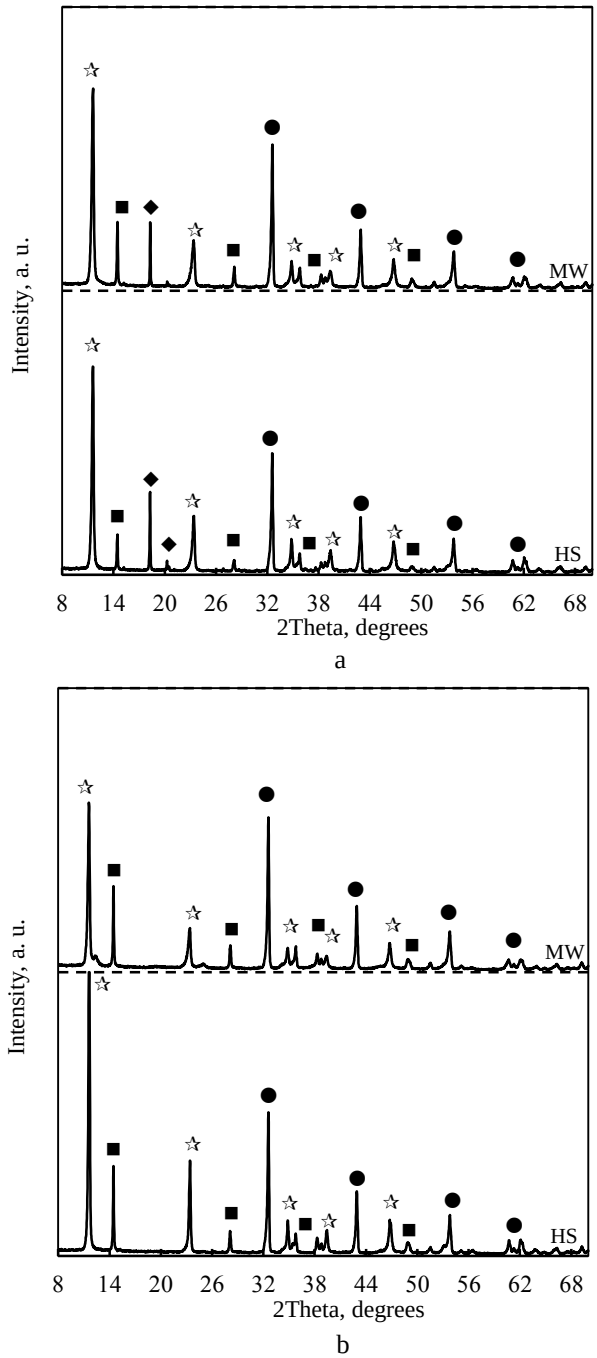

Fig. 3.3 X-ray diffraction patterns of products synthesized for 1 h (a) and 3 h (b) by using hydrothermal (*HS*) and microwave (*MW*) treatment when the molar ratio of primary mixtures (Mg/Al) was equal to 2. Indices: ☆ – hydrotalcite, ● – magnesite, ■ – boehmite, ♦ – gibbsite

Meanwhile, according to the data of STA analysis, the heat values of the loss of crystallization water from its structure and the mass loss in both cases remained almost the same, i.e., it varied from 129.75 J/g (4.17%) to 132.18 J/g (4.29%) for microwave synthesis and from 133.74 J/g (4.50%) to 144.89 J/g (4.69%) for hydrothermal synthesis (Table 3.1; Table 3.2). Also, in the mixtures with a higher Mg/Al ratio, a significant decrement in the amount of gibbsite was observed (Fig. 3.1; a; Fig. 3.3, a). In this case, the heat values of gibbsite dehydration (252–292 °C) as well as the mass loss decreased by ~3–3.5 times and ~2–2.5 times, respectively (Table 3.1; Table 3.2).

Table 3.2 The thermal characteristics of synthesis products at different durations of hydrothermal and microwave treatment in the mixtures with the molar ratio of Mg/Al=2

Preparation method	The duration of synthesis, h	Temperature range, °C	Heat of thermal effect, J/g	Mass loss, %
Hydrothermal synthesis	1	184–252	144.89	4.69
		256–292	47.21	1.90
		294–365	59.57	3.24
		373–471	140.12	6.68
		478–618	585.08	23.79
	3	184–252	153.40	4.98
		268–365	80.95	3.01
		373–471	150	6.35
		478–618	649.92	25.49
Microwave synthesis	1	184–252	132.18	4.29
		252–285	17.78	1.02
		292–365	48.80	2.88
		373–471	131.32	6.51
		478–618	636.19	25.52
	3	184–252	108.15	3.24
		268–365	58.88	2.47
		373–471	110.19	4.96
		478–618	707.45	27.27

It should be noted that due to an excess of magnesium in the system, the intensity of diffraction maximums typical of magnesite significantly increased from 98 to 176 cps for *MW* and from 107 to 140 cps for *HS* (Fig. 3.1, a; Fig. 3.3, a). These results were confirmed by STA analysis. The increment in the heat values of decarbonization of hydrotalcite and the decomposition of magnesite (478–618 °C) as well as in the mass loss were also observed: from 526.97 J/g to 636.19 J/g and from 20.24% to 25.52% for *MW* and from 492.34 J/g to 585.08 J/g and from 19.36% to 23.79% for *HS* (Table 3.1; Table 3.2). Meanwhile, the remaining thermal conversions only changed slightly.

It was observed that by prolonging the duration of the synthesis to 3 h (in the case of microwave treatment) the intensity of the main diffraction peak of hydrotalcite decreased from 238 cps to 209 cps (Fig. 3.3, curve *MW*). It is clearly visible from the

data of STA analysis: the heat values of the removal of crystallization water from its structure and the mass loss also decreased from 132.18 J/g (4.29%) to 108.15 J/g (3.24%) (Table 3.2). Meanwhile, under hydrothermal conditions, the highest crystallinity of hydrotalcite was obtained, i.e., the intensity of the main diffraction maximum typical of this compound increased from 250 cps to 471 cps (Fig. 3.3, curve *HS*). The same trend was observed when evaluating the results of STA analysis (Table 3.2). Also, as well as in the mixtures with a lower molar ratio (Mg/Al=1), after 3 h of both syntheses, gibbsite recrystallized to boehmite (Fig. 3.1, b; Fig. 3.3, b).

The previously obtained results were in good agreement with the data of SEM analysis (Fig. 3.4). It was observed that the products showed three different types of crystal morphology: thin hexagonal hydrotalcite plates and plate-like pentagonal crystals typical of boehmite as well as rhombohedral $MgCO_3$ crystals. Also, the method used for the preparation of hydrotalcite significantly affected the crystal shape of the latter compound. It was determined that, after 3 h of microwave synthesis, smaller crystals of hydrotalcite with indefinite structure were formed, whereas, under hydrothermal conditions, larger hydrotalcite crystals with a clear hexagonal shape were obtained (Fig. 3.4).

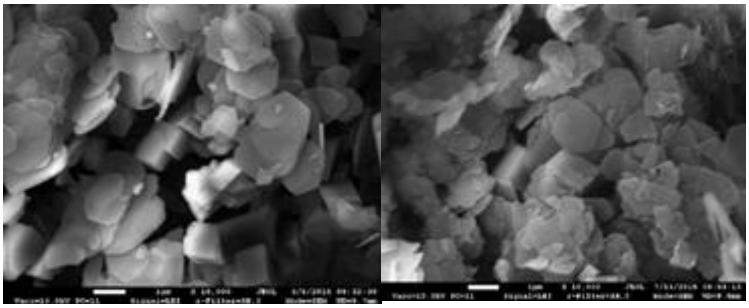

a b

Fig. 3.4 SEM images of products synthesized for 3 h (a – *MW*, b – *HS*) when the molar ratio of primary mixtures (Mg/Al) was equal to 2. Magnification: 10000 times

Moreover, it was established that the crystallite size of hydrotalcite depends on the duration of synthesis and on the molar ratio of Mg/Al only when hydrothermal treatment is applied (Fig. 3.5). It was determined that, in the mixtures with a lower molar ratio (Mg/Al=1), by prolonging the duration of isothermal curing to 3 h, the researched parameter increased from 40.06 nm to 44.70 nm. Meanwhile, in the samples with a molar ratio (Mg/Al) of 2, the crystallite size of hydrotalcite significantly increased from 37.85 nm to 52.45 nm. On the contrary, in the case of microwave treatment, when the molar ratio of primary mixtures (Mg/Al) was equal to 1 and the duration of synthesis was extended to 3 h, the crystallite size of the latter compound remained almost the same (~38.50 nm). Meanwhile, in the samples with a higher molar ratio (Mg/Al=2), it varied within the 33.89–36.25 nm range (Fig. 3.5).

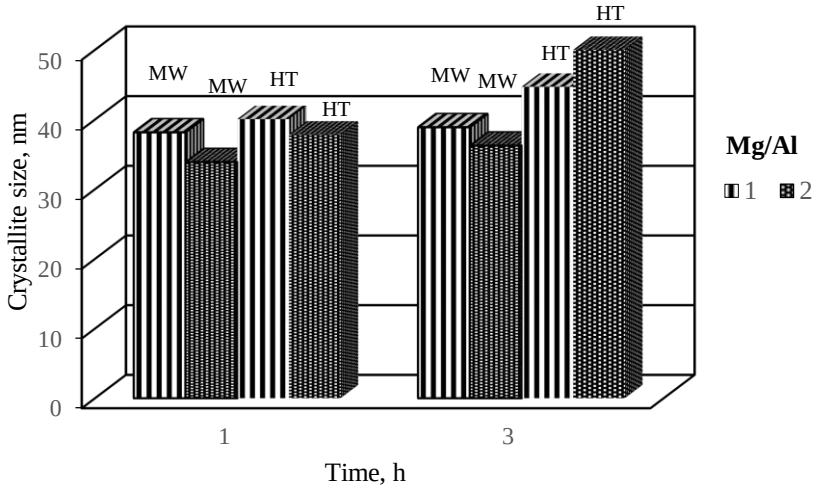

Fig. 3.5 The dependence of the hydrotalcite crystallite size on the duration of microwave and hydrothermal treatment when the molar ratio of primary mixtures (Mg/Al) was equal to 1 and 2

To sum up, it was determined that the formation of hydrotalcite under hydrothermal and microwave conditions is significantly affected by the molar ratio of the primary mixtures and on the duration of the synthesis. It should be underlined that under all the experimental conditions, the lower crystallinity hydrotalcite was obtained whenever microwave treatment was applied. The decrease in the intensity of the main diffraction peak characteristic of the above mentioned compound was observed even by prolonging the synthesis duration to 3 h (Mg/Al=1 and 2). Moreover, the crystallite size of hydrotalcite varied within the 33.89–38.50 nm range. The opposite effect was observed during hydrothermal treatment: the intensity of the main diffraction maximum typical of hydrotalcite increased with the increasing duration and the molar ratio of the primary mixtures (Mg/Al=2). Moreover, in both cases, the interaction of the initial materials proceeded faster when the Mg/Al molar ratio was equal to 2 because a smaller amount of intermediate compounds, such as magnesite and boehmite, was formed. It should also be noted that the highest hydrotalcite crystallinity and crystallite size (40.06–52.45 nm) were obtained when the hydrothermal synthesis duration was equal to 3 h and the molar ratio of primary mixtures (Mg/Al) was equal to 2.

3.2 The Effect of Post-Synthesis Methods on the Properties of Hydrotalcite-Type Compounds

A number of researchers focused on tailoring the final properties of the materials mainly by changing the synthesis process/conditions or by applying post-synthesis treatment because such parameters as crystallinity, particle size, thermal stability and other parameters typical of LDHs play an important role in their application (32).

Despite the significant progress achieved in the preparation of LDHs, LDHs particles obtained via such common methods as co-precipitation, reconstruction, ion-exchange and calcination-rehydration are usually loose powders of irregular aggregates.

Therefore, thermal or mechanochemical activation of synthesized precursors as post-synthesis treatment are often employed with the objective to modify the structural and surface properties of LDHs.

In the following part of this thesis, the effect of solid-state sintering conditions (575 °C, 1000 °C; 1 h) on the thermal stability of the samples which were synthesized by different techniques (MW at 1 h; HS at 3 h) was evaluated in order to form a mixed Mg-Al oxide which can be obtained within the 500–1000 ºC temperature range (49, 153, 154).

It was established that the method used for the synthesis of hydrotalcite did not affect the formation sequence of compounds during solid-sintering (Fig. 3.6). After 1 h of calcination at a temperature of 575 °C, only magnesium oxide (ICDD File No. 77-2179; *d*-spacing equaling 0.244, 0.211, 0.149 nm), aluminum oxide (ICDD File No. 29-0063; *d*-spacing equaling 0.199, 0.139 nm) were detected in the calcination products. However, alongside the above mentioned oxides, the diffraction maximums characteristic of an unidentified compound (*d*-spacing equaling 0.304 nm) were also observed in the XRD curves of *HS* and *MW* samples (Fig. 3.6, a). Moreover, when the calcination temperature was increased to 1000 °C, mixed magnesium aluminum oxide compounds (ICDD File No. 21-1152; *d*-spacing equaling 0.470, 0.284, 0.244, 0.203, 0.155, 0.143 nm) were formed (Fig. 3.6, b). It is important to note that the intensity of the diffraction maximums typical of magnesium oxide increased from 55 cps to 150 cps (HS-3h) and from 54 cps to 123 cps (MW-1h), whereas the diffraction peaks characteristic of aluminum oxide remained virtually the same (Fig. 3.6).

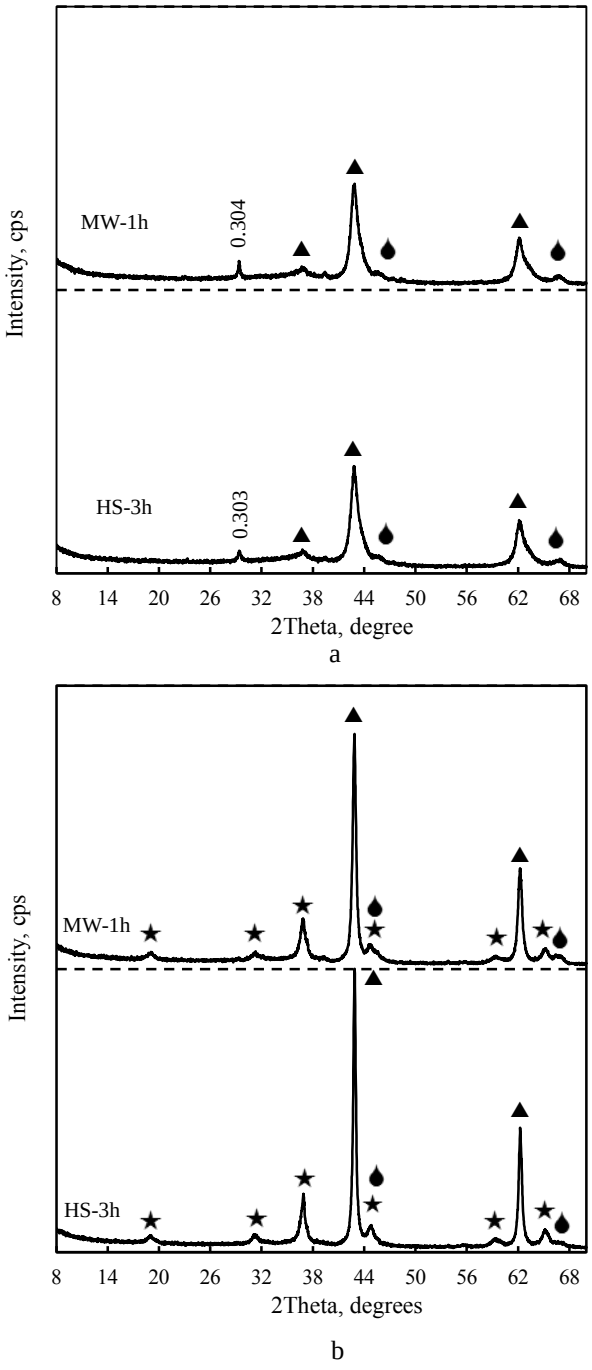

Fig. 3.6 X-ray diffraction patterns of samples calcined at 575 °C (a) and 1000 °C (b) for 1 h. Indices: ▲ – magnesium oxide, ♦ – aluminum oxide, ★ – mixed Mg-Al oxide

Thus the obtained results showed that the applied microwave or hydrothermal synthesis of hydrotalcite did not influence its thermal stability because, in both cases, after 1 h of calcination at a temperature of 575 °C, only magnesium oxide and aluminum oxide were obtained in the calcination products, whereas at a temperature of 1000 °C, alongside the above listed compounds, mixed magnesium aluminum oxide was formed.

For this reason, due to the formed higher crystallinity main synthesis product, the effect of the mechanochemical treatment conditions only on the properties of hydrothermally treated hydrotalcite was investigated.

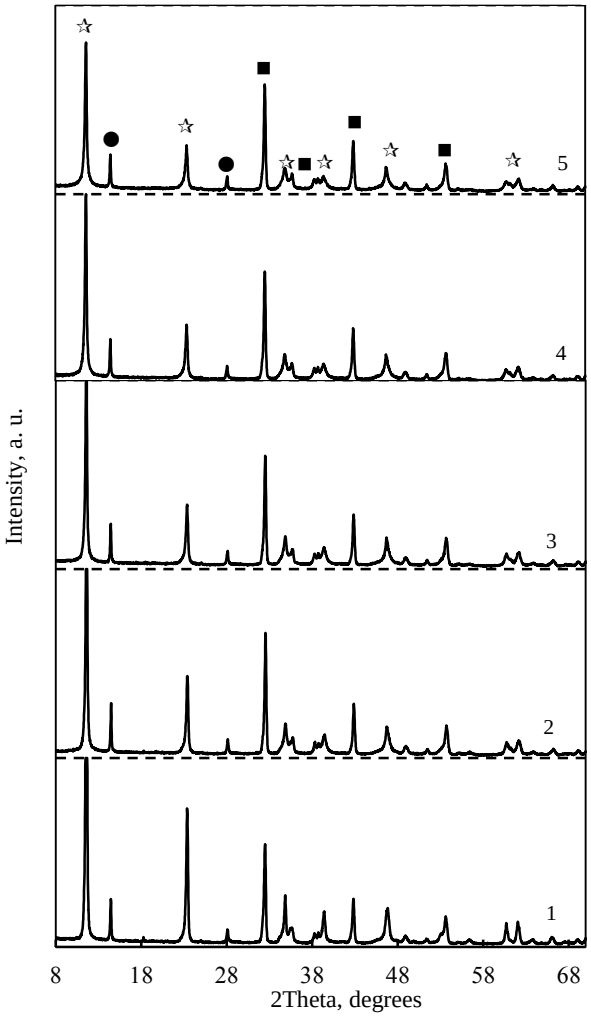

Fig. 3.7 X-ray diffraction patterns of the synthesis products before and after 5 min of mechanochemical treatment at different vibrating frequencies: 1 denotes 0 rpm; 2 stands for 650 rpm, 3 represents 750 rpm, 4 shows the values for 850 rpm; 5 depicts 950 rpm. Indices: ☆ – hydrotalcite, ● – boehmite ■ – magnesite

As expected, the mechanochemical treatment conditions played an important role with regard to the order of the crystal structure of hydrotalcite: the intensity of all the hydrotalcite peaks gradually decreased by prolonging the duration of the above outlined treatment up to 5 min. It should be noted that the intensity of the main diffraction peak of hydrotalcite decreased by ~31% at 650 rpm, while at 950 rpm it decreased approximatelly by 55% (Fig. 3.7, curves 2 and 5). However, the crystalline structure of the synthesis products was retained.

The same tendency was observed by evaluating the calculated data of the areas of the basic reflection (with *d*-spacing equaling 0.751 nm), which is typical of hydrotalcite: the decrement in this parameter with the increasing vibrating frequencies and/or the duration of the treatment was observed (Fig. 3.8). At the beginning of mechanochemical processing (0.5 min), the basic diffraction peak areas of hydrotalcite were slightly reduced from 3% (at 650 rpm) to 14% (at 950 rpm). Meanwhile, the further treatment (up to 3 min) resulted in a significant decrement of the areas by ~46% when 850 and 950 rpm vibrating frequencies were applied – this clearly indicates the weakening of the main hydrotalcite reflection.

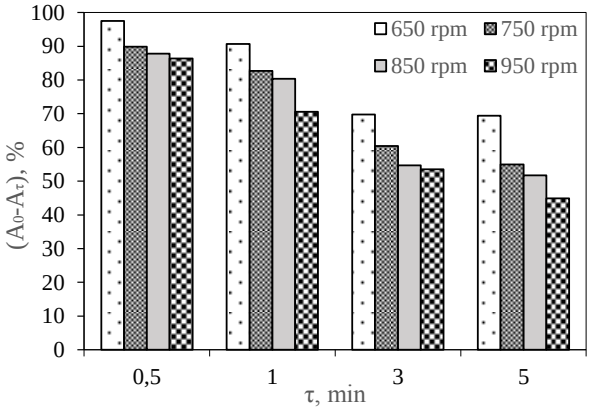

Fig. 3.8 The dependence of the main diffraction peak area of hydrotalcite on the duration of mechanochemical treatment at different vibrating frequencies. Indices: A_0 – the main diffraction peak area of hydrotalcite; A_τ – the main diffraction peak area of hydrotalcite at a different duration of mechanochemical treatment

The broadening and weakening of the diffraction maximums can be explained by the combined effect of the particle size reduction or by the formation of amorphous phases. This claim was also confirmed by the results of the calculated crystallite size of hydrotalcite. It was determined that within the first minutes (0.5 min and 1 min) of mechanochemical treatment, the conditions of the latter process did not affect the values of this specific parameter, i.e., the average crystallite size was equal to ~47.36 nm because not only the weakening but also the broadening of the diffraction peaks was observed (Fig. 3.7; Fig. 3.9). Moreover, when the duration of the treatment was extended and the vibration frequencies varied within the 650–950 rpm range, the values of the hydrotalcite crystallite size were reduced from 47.28 nm to 38.77 nm.

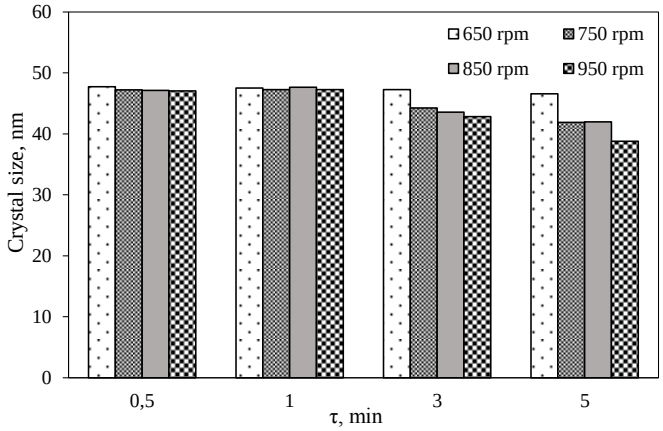

Fig. 3.9 The dependence of the hydrotalcite crystallite size on the duration of mechanochemical treatment at different vibrating frequencies

Secondly, the results of the particle size and the distribution of products were in good agreement with the previously obtained data (Fig. 3.10). It was determined that the particles with a diameter larger than 63 μm (19%), 80 μm (22%) and 425 μm (19%) were dominating in the samples after synthesis. Also, as expected, after 1 min of mechanochemical treatment at 950 rpm, a larger amount of smaller particles (~63 μm) was obtained in the products (19–22%) whereas other fractions were reduced: particles with a diameter of 425 μm by 10%, and particles with a diameter of 80 μm by 20% (Fig. 3.10, b). Moreover, in terms of the intermediate particle size distribution (106 μm and 212 μm), the same phenomenon was observed. However, when the duration of mechanochemical treatment was extended to 5 min, the amount of larger particles significantly decreased by 4% (>425 μm) and by 8% (>212 μm), and, in this case, even 34% of the smaller particles (<63 μm) achieved domination in the obtained products (Fig. 3.10, c).

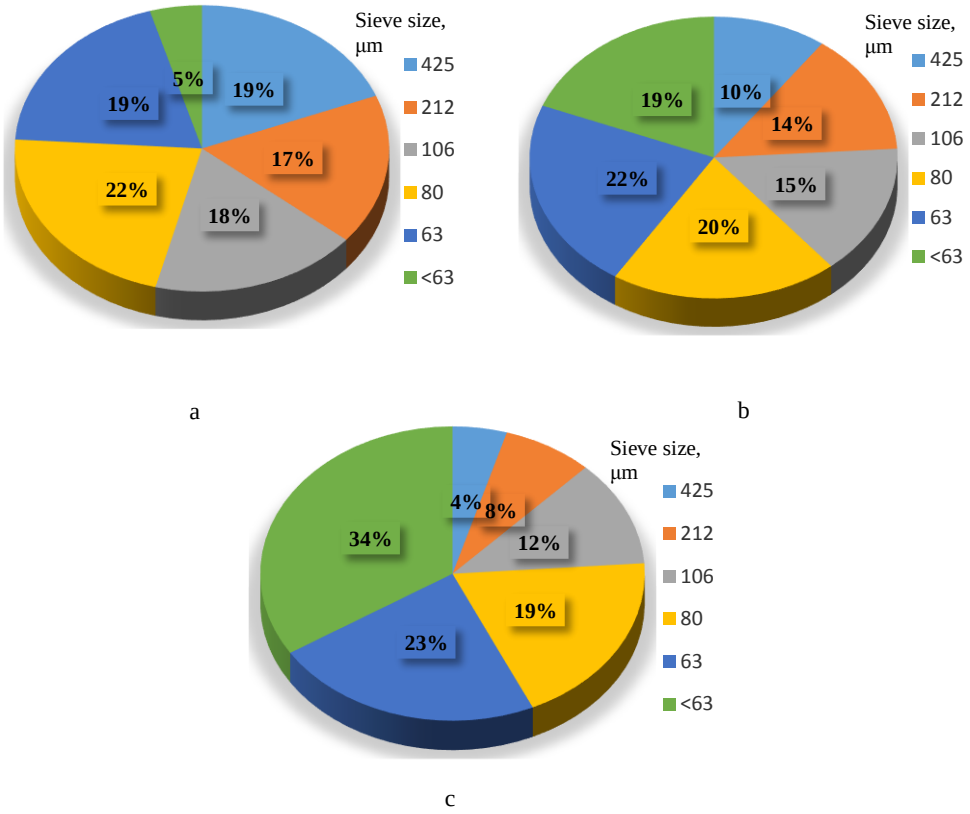

Fig 3.10 Distribution of the particle sizes in the synthesis products prior to mechanochemical treatment (a) and: b – after 1 min, c – after 5 min of mechanochemical treatment at a vibration frequency of 950 rpm

The data of STA analysis showed that the changes in both the intensity and the temperature of the endothermic effects in DSC curves indicated structural alterations of the compounds during mechanochemical treatment. Due to the latter process (5 min; 950 rpm), the crystallization water and CO_3^- groups were removed from the hydrotalcite crystal structure (Fig. 3.11). This is clearly demonstrated in the DSC curves (Fig. 3.11, b): not only the temperatures of typical thermal conversions were shifted but also the values of the absorbed heat of the endothermic effects significantly decreased from 272.83 J/g to 93 J/g (Fig. 3.11, b; 226 °C), from 112.54 J/g to 22.76 J/g (Fig. 3.11, b, 321 °C), from 143.97 J/g to 46.29 J/g (Fig. 3.11, b; 417 °C) and also from 499.82 J/g to 168.97 J/g (Fig. 3.11, b; 576 °C).

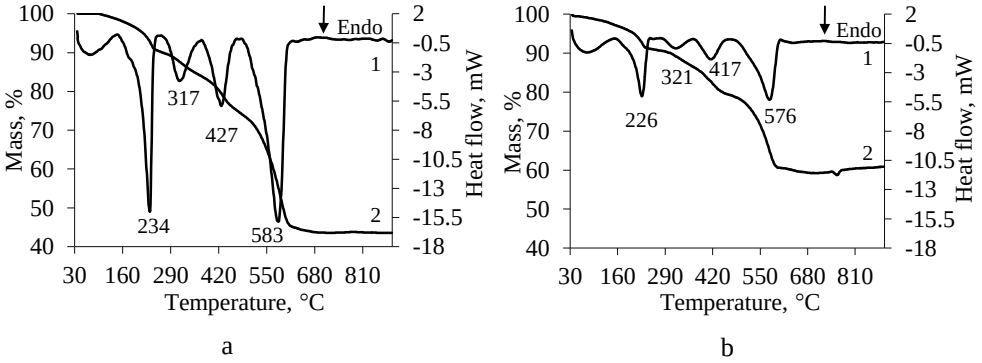

Fig. 3.11 STA curves (1 for *DSC*, 2 for *TG*) of the products synthesized without mechanochemical treatment (a) and after 5 min (b) of mechanochemical treatment at 950 rpm vibration frequency

It was determined that the results of SEM analysis confirmed the previously obtained data (Fig. 3.12). As shown above in this thesis, thin hexagonal hydrotalcite and pentagonal boehmite plates as well as rhombohedral $MgCO_3$ crystals formed in the synthesis products (Fig. 3.4, b). It should be underlined that mechanochemical treatment significantly altered the morphological properties of the obtained products. After 5 min at 950 rpm, flake-like crystals of an irregular size and shape denoted by a rougher surface were observed (Fig. 3.12).

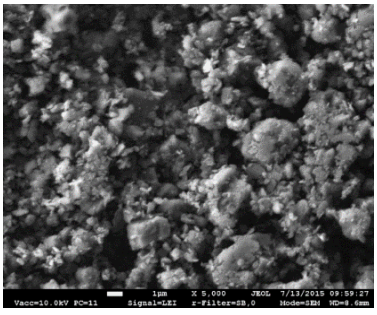

Fig. 3.12 SEM images of products synthesized after 5 min of mechanochemical treatment at 950 rpm vibration frequency. Magnification: 5000 times

In order to examine the capacity of the ground samples to reconstruct their structure, the products obtained after mechanochemical treatment were rehydrated for 1 h in distilled water (Fig. 3.13). The reconstruction of the synthesis product was calculated from the intensity change of the basic reflection (0.751 nm) when the intensity (I_{max}) of the main hydrotalcite diffraction peak after the synthesis was equal to 100% and I was measured at the intensity of the main hydrotalcite diffraction peak after a different duration of mechanochemical treatment. It was determined that the latter processing conditions exert significant influence on the reconstruction properties of the treated samples. However, it should be underlined that, in the case of products ground for 0.5 min, the layered structure was fully reconstructed (100%), and the latter process did not depend on the selected vibrating frequency. Meanwhile,

the ability of hydrotalcite to reconstruct its structure decreased with the increasing duration of mechanochemical treatment and vibrating frequency (Fig. 3.13).

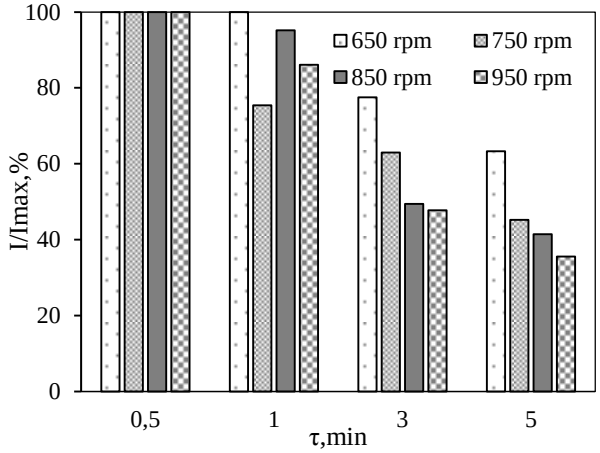

Fig. 3.13 The dependence of the intensity of the main hydrotalcite diffraction peak (with *d*-spacing being at 0.751 nm) on the duration of mechanochemical treatment at different vibrating frequencies

To sum up, the presented results show that mechanochemical post-synthesis treatment altered the properties of the synthesized hydrotalcite. It was determined that the crystallite size gradually decreased with the increasing duration of grinding. Moreover, after 5 min of mechanochemical treatment (950 rpm), the particles with a diameter smaller than 63 μm were the most common in the products (35%). Meanwhile, flake-like crystals of irregular sizes and shapes denoted by a rougher surface were observed in the ground samples. Besides, the capacity of hydrotalcite to reconstruct its structure decreased with the increasing duration and vibrating frequency of mechanochemical treatment.

3.3 Adsorption Capacity of Layered Inorganic Adsorbents for the Transition Metal Ions

With the rapid development of industries, wastewater with toxic substances is still being directly or indirectly discharged into the environment (155, 156). Due to the stringent regulations for contamination with transition metals, their removal has become a serious environmental problem (157). Currently, the main researches are focucing on the search for low-cost and easily available adsorbents capable of removing transition metal ions from wastewater. Inorganic materials, such as zirconium phosphates, aluminosilicates, clay minerals, hydroxyapatite and others, are often used as adsorbents for the treatment of water contaminated with transition metal ions (157–159).

However, to date, two other groups of compounds – calcium silicate hydrates and layered double hydroxides – have been receiving significant attention in attempts to resolve environmental remediation issues (95). They are usually used as excellent adsorbents serving for the removal of pollutants from aqueous solutions due to their

low cost, easy preparation, a large surface area, good chemical stability and, importantly, high ion exchangeability (134, 160, 161). For this reason, the adsorption capacity of transition metal ions into the structure of layered inorganic adsorbents was determined in the present research.

Single metal ion adsorption by layered inorganic adsorbents

The obtained results showed that the adsorption of Co^{2+} ions proceeded slower at the beginning of the process: after 30 s, the amount of the ions adsorbed by gyrolite was equal to 3 mg Co^{2+}/g when the initial concentration was 0.25 g/dm^3 (Fig. 3.14, curve 1). It was determined that the adsorption rate slightly increased by prolonging the experiment duration to 15 min due to the change in the quantity of the incorporated Co^{2+} ions (14.66 mg Co^{2+}/g). After 15 min, equilibrium was attained, and the removal of the investigated ions by gyrolite was complete (Fig. 3.14, curve 2).

Meanwhile, the uptake of Co^{2+} ions proceeded differently when using calcined hydrotalcite (575 °C, 1 h). In this case, a higher amount of the researched ions was intercalated into its crystal structure under all the experimental conditions: the amount of the adsorbed Co^{2+} ions reached 10.47 mg Co^{2+}/g after 30 s and 20.09 mg Co^{2+}/g after 60 min of reaction.

The materials of this chapter have been published as: Bankauskaitė Agnė; Eisinas Anatolijus; Baltakys Kęstutis; Zadavičiūtė Skirmantė. A Study on the Intercalation of Heavy Metal Ions in a Wastewater by Synthetic Layered Inorganic Adsorbents. In: *Desalination and Water Treatment*. Philadelphia, PA: Taylor & Francis. 2015 (56), 1576–1586, ISSN 1944-3994.

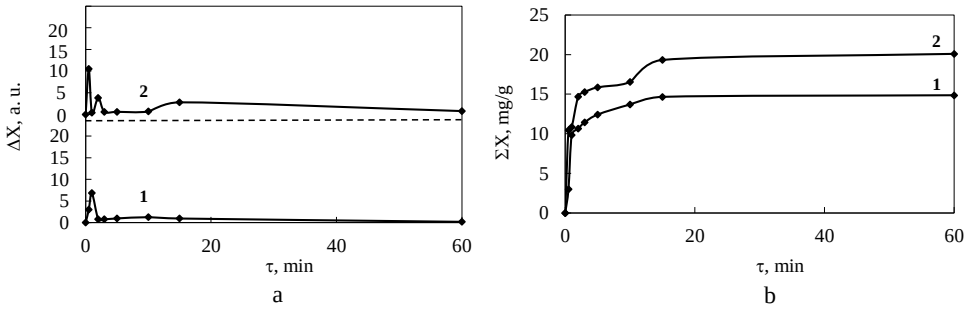

Fig. 3.14 Co^{2+} adsorption from $Co(NO_3)_2 \cdot 6H_2O$ solution differential (a) and integral (b) kinetic curve; adsorbents: 1 denotes gyrolite; 2 represents calcined hydrotalcite

Moreover, it was determined that within 30 s of the course of the adsorption experiment, the removal efficiency of Zn^{2+} ions for both adsorbents was equal to 50%, i.e., approximately from 12 to 13 mg Zn^{2+}/g (Fig. 3.15, curve 1). Besides, the reaction equilibrium was achieved at a different period of time: after five minutes when gyrolite was being used, and after 2–3 min when calcined hydrotalcite was being used (Fig. 3.15, curve 2). However, at the end of the process, a considerable amount of Zn^{2+}

ions (21.75 mg Zn^{2+}/g) was incorporated into the structure of gyrolite, while calcined hydrotalcite only adsorbed a smaller quantity (16.63 mg Zn^{2+}/g).

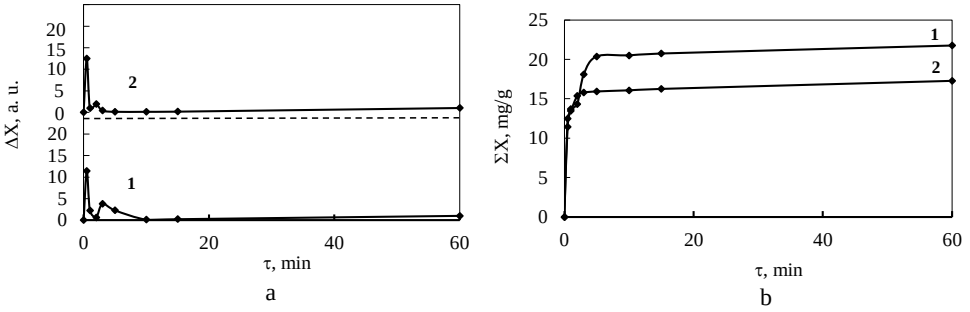

Fig. 3.15 Zn^{2+} adsorption from $Zn(NO_3)_2 \cdot 6H_2O$ solution differential (a) and integral (b) kinetic curves; adsorbents: 1 denotes gyrolite; 2 represents calcined hydrotalcite

It was observed that the uptake of Mn^{2+} ions was more rapid than the uptake of zinc ions. In this case, after 30 s of reaction, the removal efficiency of both adsorbents reached 70%, i.e., approximately from 17 to 18 mg Mn^{2+}/g (Fig. 3.16, curve 1). Furthermore, the elimination of ions from a manganese nitrate solution by gyrolite (20.73 mg Mn^{2+}/g) was completed after 5 min because the equilibrium was attained, whereas calcined hydrotalcite showed a slightly higher adsorption rate. However, the maximum amount of intercalated manganese ions (23.66 mg Mn^{2+}/g) was obtained only after 15 minutes (Fig. 3.16, curve 2).

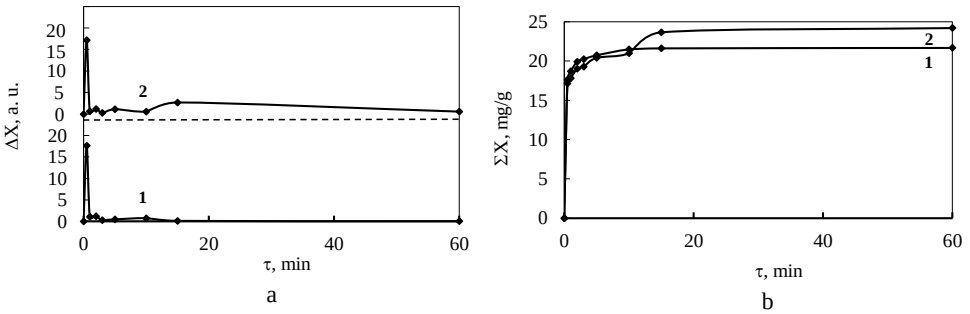

Fig. 3.16 Mn^{2+} adsorption from $Mn(NO_3)_2 \cdot 4H_2O$ solution differential (a) and integral (b) kinetic curves; adsorbents: 1 represents gyrolite; 2 denotes calcined hydrotalcite

The adsorption dependency on the chemical nature of the adsorbents and the transition metal solutions was confirmed by the experimental data of Ni^{2+} removal from an aqueous solution (Fig. 3.17). As shown in curve 1, during the first minute of the test, the uptake of the presently discussed ions is very slow due to the small quantity of adsorbed ions, i.e., only ~10 mg Ni^{2+}/g is taken by both synthetic layered inorganic adsorbents. Interestingly, when using calcined hydrotalcite, the process

equilibrium is attained only after 15 min, whereas it is reached two times faster in the case of gyrolite (Fig. 3.17, curve 2 after 5 min). However, calcined hydrotalcite adsorbed a larger amount of Ni^{2+} ions (24.39 mg Ni^{2+}/g) in comparison with the researched compound (18.96 mg Ni^{2+}/g).

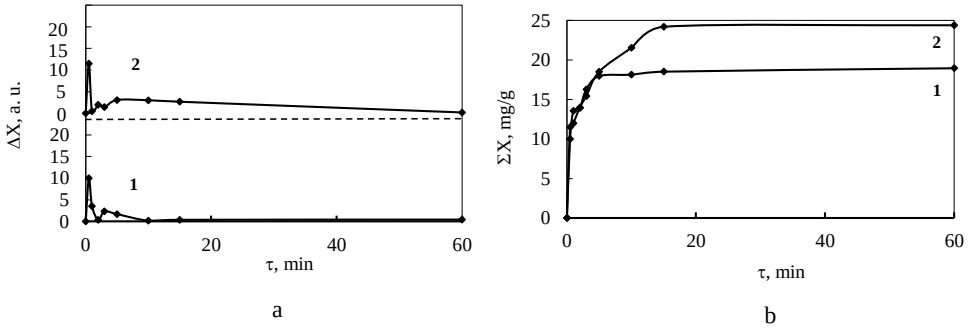

Fig. 3.17 Ni^{2+} adsorption from $Ni(NO_3)_2 \cdot 6H_2O$ solution differential (a) and integral (b) kinetic curves; adsorbents: 1 represents gyrolite; 2 denotes calcined hydrotalcite

It should be noted that the intrusion of metal ions into the adsorbent structures also depends on the pH of the solution due to the extremely high and selective uptake of Fe^{3+} ions. It was determined that the elimination of the researched ions was completed within 30 s because all the iron ions (~98–99%) were adsorbed (Fig. 3.18).

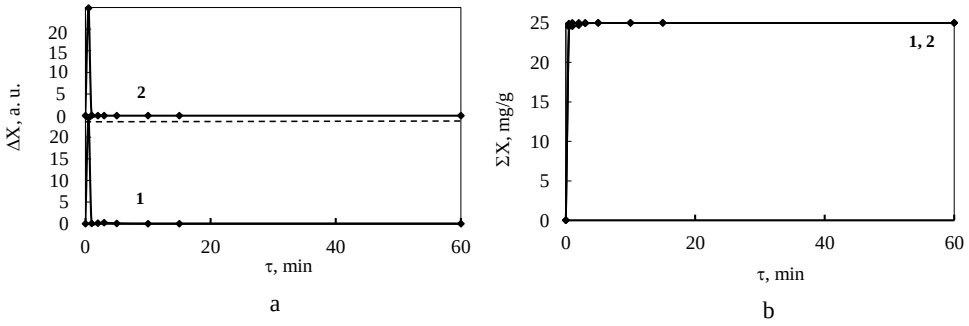

Fig. 3.18 Fe^{3+} adsorption from $Fe(NO_3)_3 \cdot 6H_2O$ solution differential (a) and integral (b) kinetic curves; adsorbents: 1 represents gyrolite; 2 denotes calcined hydrotalcite

It is clearly seen that the adsorption of Co^{2+}, Ni^{2+}, Zn^{2+}, Mn^{2+}, Fe^{3+} from aqueous solutions by synthetic layered inorganic adsorbents is a complex process. It was determined that, during the ion exchange process, $Ca^{2+} \leftrightarrow Me^{x+}$ and $Mg^{2+} \leftrightarrow Me^{x+}$ reactions typical of gyrolite and calcined hydrotalcite were found to be non-stoichiometric (Table 3.3). The uptake of Me^{x+} ions by the solids was lower than Ca^{2+} or Mg^{2+} ions leached. In the case of Fe^{3+} ions, after 60 min, the amount of the adsorbed Fe^{3+} was equal to 0.45 mmol/g, whereas the quantity of the leached Ca^{2+} ions equaled 0.68 mmol/g. The non-stoichiometry arised due to the leaching of Ca^{2+} ions from the

interlayers of the gyrolite crystal lattice. The same tendency was observed with calcined hydrotalcite. The main reason of the three times higher quantity of the leached Mg^{2+} ions (e.g., with iron nitrate; $\sum X=0.45$ mmol Fe^{3+}/g $\sum X=1.4$ mmol Mg^{2+}/g) can be explained by this compound's capacity to reconstruct its structure. During this process, due to the initial pH value of the transition metal ion solutions, the crystallinity of hydrotalcite is changed: in the acidic and neutral media, the intensity of the main diffraction maximum varies from 1130 a. u. to 1734 a. u., respectively. Meanwhile, the intensity of the diffraction peaks typical of as-synthesized HT was equal to 9590 a. u. For this reason, an extra amount of Mg^{2+} ions is leached to the reaction medium, which suggests that not all of the ions are participating in the reconstruction process.

Table 3.3 The amount of the adsorbed and leached metal ions

Me^{x+} ions	Layered inorganic adsorbents			
	Calcined hydrotalcite		Gyrolite	
	The amount of adsorbed Me^{x+}, mmol/g	The amount of leached Mg^{2+}, mmol/g	The amount of adsorbed Me^{x+}, mmol/g	The amount of leached Ca^{2+}, mmol/g
Fe^{3+}	0.45	1.4	0.45	0.68
Co^{2+}	0.34	0.9	0.31	0.51
Ni^{2+}	0.41	1.2	0.35	0.44
Zn^{2+}	0.26	0.5	0.33	0.55
Mn^{2+}	0.44	1.0	0.39	0.55

Thus the selectivity sequence of adsorption (according to the duration of the explored process from the slower to faster intercalation of the investigated ions into the adsorbent structure) can be represented as:

$$Co^{2+}<Zn^{2+}<Mn^{2+}<Ni^{2+}<Fe^{3+}$$

whereas in the case of calcined hydrotalcite the sequence is:

$$Co^{2+}<Ni^{2+}<Mn^{2+}<Zn^{2+}<Fe^{3+}$$

Since industrial effluents contain several pollutant substances, it is necessary to study the simultaneous adsorption of the multi-component system (162, 163). This type of adsorption depends not only on the adsorbent dosage and the particle size but also on the competition of transition metal ions (i.e., their valence, concentration, atomic radius), the solution's pH, the contact time and the temperature (164, 165).

Simultaneous adsorption by synthetic gyrolite

In order to evaluate multiple adsorbates which usually dominate in wastewater, experiments of simultaneous adsorption were performed in a mixture of Co^{2+}, Ni^{2+}, Cu^{2+}, Zn^{2+}, Mn^{2+}, Fe^{3+} ion solutions (0.25 g Me^{x+}/dm^3) at a temperature of 25 °C by the above mentioned layered inorganic adsorbents.

It is worth noting that the latter research with calcined hydrotalcite was performed by Bankauskaite (140). The scholar showed that this compound adsorbed almost all the Co^{2+}, Ni^{2+}, Cu^{2+}, Zn^{2+}, Mn^{2+}, Fe^{3+} ions (~99.8%). For this reason, the experiments were only carried out with synthetic gyrolite.

It was determined that simultaneous adsorption proceeded intensively at the beginning of the process because, after 30 s, the amount of the ions adsorbed by gyrolite reached 93%, i.e., it measured approximately 139 mg Me^{x+}/g. After the first minutes, equilibrium was attained, and the adsorption of the above outlined ions was complete – gyrolite adsorbed 24.73 mg Zn^{2+}/g, 24.51 mg Co^{2+}/g, 23.71 mg Ni^{2+}/g, 24.95 mg Mn^{2+}/g, 23.00 mg Cu^{2+}/g and 23.54 mg Fe^{3+}/g (Table 3.4). It is evidently seen that these values differ from the data obtained while performing single metal ion adsorption (Figs. 3.14-3.17).

This chapter has been published as: Zadavičiūtė Skirmantė; Baltakys Kęstutis; Eisinas Anatolijus; Bankauskaitė Agnė. Simultaneous adsorption at 25 °C and the eculiarities of Gyrolite Substituted with Heavy Metals. In: *Journal of Thermal Analysis and Calorimetry*. Dordrecht: Springer. 2017 (127), pp. 335–343, ISSN 1388-6150.
Zadavičiūtė Skirmantė; Baltakys Kęstutis; Eisinas Anatolijus. Adsorption Kinetic Parameters of Fe^{3+} and Ni^{2+} Ions by Gyrolite. In: *Materials Science=Medžiagotyra*. 2015 (21), pp. 117–122, ISSN 1392-1320.

Table 3.4 The amount of metal ions adsorbed by gyrolite after 60 min of experiment at 25 ºC

Time, Min	The amount of adsorbed of Me^{x+} ions, mg/g					
	ΣX (Zn^{2+})	ΣX (Co^{2+})	ΣX (Ni^{2+})	ΣX (Mn^{2+})	ΣX (Cu^{2+})	ΣX (Fe^{3+})
0.5	24.08	22.72	23.00	24.11	22.01	23.08
1	24.21	23.04	23.22	24.22	22.21	23.13
2	24.27	23.25	23.29	24.32	22.29	23.22
3	24.39	23.49	23.40	24.49	22.40	23.25
5	24.43	23.70	23.51	24.81	22.60	23.32
10	24.62	24.05	23.58	24.91	22.82	23.39
15	24.67	24.34	23.68	24.92	22.93	23.50
60	24.73	24.51	23.71	24.95	23.00	23.54

Moreover, the presented results showed that, during the intrusion of transition metal ions into the gyrolite structure, calcium ions were released from their crystal

lattices into the solution. It was established that most Ca^{2+} ions were released within the first minutes of the reaction because, after 30 s, their concentration was equal to 34.16 mg Ca^{2+}/g (Table 3.5). By prolonging the experiment duration, the concentration of calcium ions increased with the increasing duration of adsorption, and, after 60 min, the amount of ions was equal to 48.03 mg Ca^{2+}/g (Table 3.5).

Table 3.5 The amount of calcium ions leached from the gyrolite structure

The amount of leached Ca^{2+} ions									
Time, min	0	0.5	1	2	3	5	10	15	60
ΣX, mg/g	0	34.16	44.55	45.08	46.08	47.04	47.50	47.93	48.03
pH value	2.28	3.42	3.53	4.01	4.23	4.67	5.12	5.12	5.12

Besides, the pH value increased from 2.28 to 5.12 at the beginning of adsorption when the adsorbent was mixed with a transition metal ion solution (Table 3.5). Presumably, this change could be attributed to the degree of release of Ca^{2+} ions from the structure of gyrolite into the solution.

Furthermore, the examination revealed that the intrusion of transition metal ions into the gyrolite structure proceeded via two types of chemical reaction: *substitution* and *exchange*. The ion exchange occured between divalent or trivalent ions because 36.8% of Ca^{2+} ions were replaced by transition metal ions, whereas the remaining part ($Ca^{2+}\leftrightarrow Me^{x+}$) of these ions was combined by gyrolite as the addition reaction took place: gyrolite-Ca^{0}+$Me^{x+}\leftrightarrow$gyrolite-Me^{0}+Ca^{2+}.

In order to confirm that the adsorption reactions are not reversible processes, after the adsorption process, gyrolite substituted with Me^{x+} ions was dried and immersed in distilled water. It was proved that Me^{x+} ions did not appear in the solution after 60 minutes at a temperature of 25 °C. Thus our results show that gyrolite acts as a chemisorbent – but not like the usual adsorbent.

In this case, the selectivity sequence of gyrolite according to the duration of adsorption can be proposed as follows:

$$Fe^{3+}>Ni^{2+}>Zn^{2+}>Mn^{2+}>Cu^{2+}>Co^{2+}$$

Also, in order to determine the kinetic parameters of simultaneous adsorption, the researched reactions were described by a pseudo-first order equation and a pseudo-second order equation.

The calculated linear dependence suggested that pseudo-first order equation (2.3) did not fit well with the description of the simultaneous adsorption mechanism of transition metal ions, because the values of the obtained correlation coefficients (R^2) were quite low (R^2=0.48–0.69), and the calculated $q_{e(cal.)}$ values disagreed with the experimental $q_{e(exp.)}$ values (Table 3.6).

Table 3.6 Kinetic parameters of pseudo-first order kinetic models

Me^{x+}	R^2	$q_{e(exp.)}$, mg/g	$q_{e(cal.)}$, mg/g
Zn^{2+}	0.54	24.73	1.47
Ni^{2+}	0.62	23.71	1.50
Mn^{2+}	0.69	24.95	1.87
Co^{2+}	0.62	24.51	3.23
Cu^{2+}	0.62	23.00	2.09
Fe^{3+}	0.48	23.54	1.16

Meanwhile, by using the pseudo-second order kinetics equation (2.5), the equilibrium adsorption capacity ($q_{e(exp.)}$) and second order constants k_2 (g/mg·min) were determined experimentally from linear equations as outlined below:

adsorption of Zn^{2+} ions by gyrolite (Fig. 3.19, a):

$$y=0.0405x+0.0013^1 \quad (3.1)$$

adsorption of Mn^{2+} ions by gyrolite (Fig. 3.19, b):

$$y=0.04x+0.0016^1 \quad (3.2)$$

adsorption of Ni^{2+} ions by gyrolite (Fig. 3.19, a):

$$y=0.0422x+0.0013^1 \quad (3.3)$$

adsorption of Co^{2+} ions by gyrolite (Fig. 3.19, c):

$$y=0.041x+0.0037^1 \quad (3.4)$$

adsorption of Cu^{2+} ions by gyrolite (Fig. 3.19, c):

$$y=0.0435x+0.0024^1 \quad (3.5)$$

adsorption of Fe^{3+} ions by gyrolite (Fig. 3.19, b):

$$y=0.0426x+0.0011^1 \quad (3.6)$$

[1] where: $y = \frac{\tau}{q_\tau}$ and $x = \tau$, when $x = 0$, $y = \frac{1}{k_2 q_e^2}$

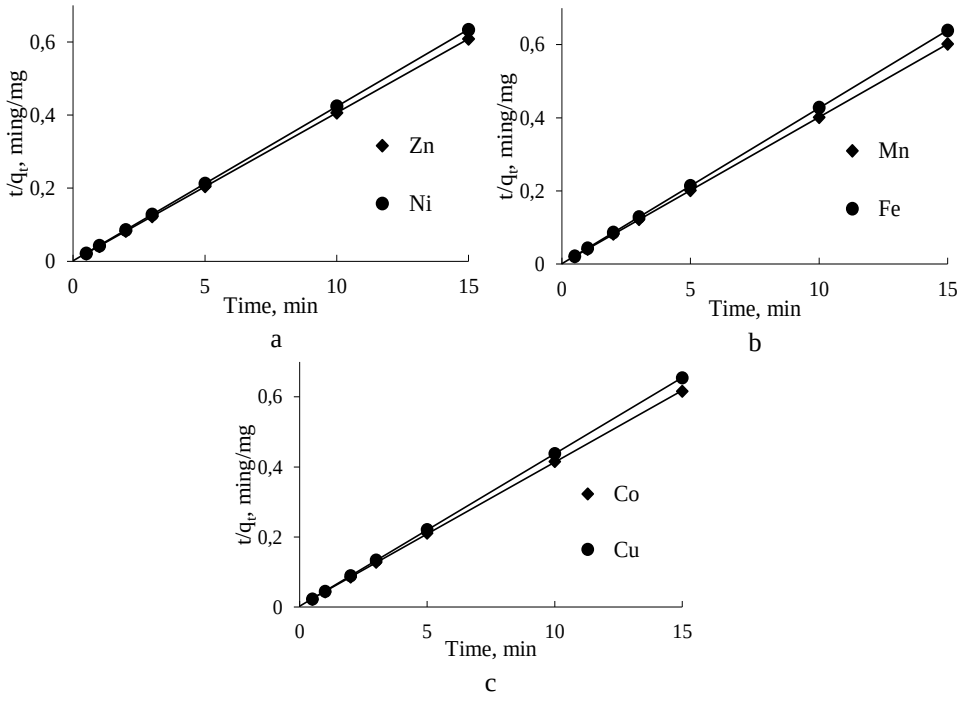

Fig. 3.19 Pseudo-second order kinetic plots in solutions

The obtained results showed that Ho equation can be used to describe the mechanism of the simultaneous adsorption of Me^{x+} ions by gyrolite because the values of the correlation coefficient (R^2) were almost equal to 1, which indicates that the pseudo-second order equation adequately describes the experimental data (Table 3.7). It was determined that the largest adsorption rate constant (k_2) was observed for iron ions (k_2=1.65 g/min·mg), whereas the minimum k_2 value was obtained for cobalt ions (k_2=0.45 g/min·mg). Besides, an agreement between $q_{e(exp.)}$ experimental and $q_{e(cal.)}$ calculated values of the pseudo-second order model was observed (Table 3.7). This data agreed with the experimental results and confirmed that transition metal ions were chemisorbed by gyrolite.

Table 3.7 The kinetic parameters of the pseudo-second order kinetic model

Me^{x+}	R^2	$q_{e(exp.)}$, mg/g	$q_{e(cal.)}$, mg/g	k_2, g/min·mg
Zn^{2+}	1	24.73	24.69	1.26
Ni^{2+}	1	23.71	23.70	1.37
Mn^{2+}	1	24.95	25	1.00
Co^{2+}	0.99	24.51	24.39	0.45
Cu^{2+}	1	23.00	22.99	0.79
Fe^{3+}	1	23.54	23.47	1.65

In order to evaluate gyrolite stability after adsorption, the investigated compound was characterized by numerous methods of instrumental analysis.

X-ray diffraction data analysis showed that, after the reaction with transition metal ions, the structure of gyrolite remained stable in the solution although the intensity of typical diffraction peaks slightly decreased due to the desorption of calcium ions into the reaction medium (Fig. 3.20, a; Fig. 3.21, a). It is worth mentioning that only gyrolite (ICDD File No. 42-1452; *d*-spacing equaling 2.2371, 1.1262, 0.8371, 0.4197 nm) was observed after adsorption in the XRD pattern, and its structure remained stable when the values of the solution pH varied within the 5.86–10.61 range. The presented results were in good agreement with the data obtained by Baltakys *et al*. (138).

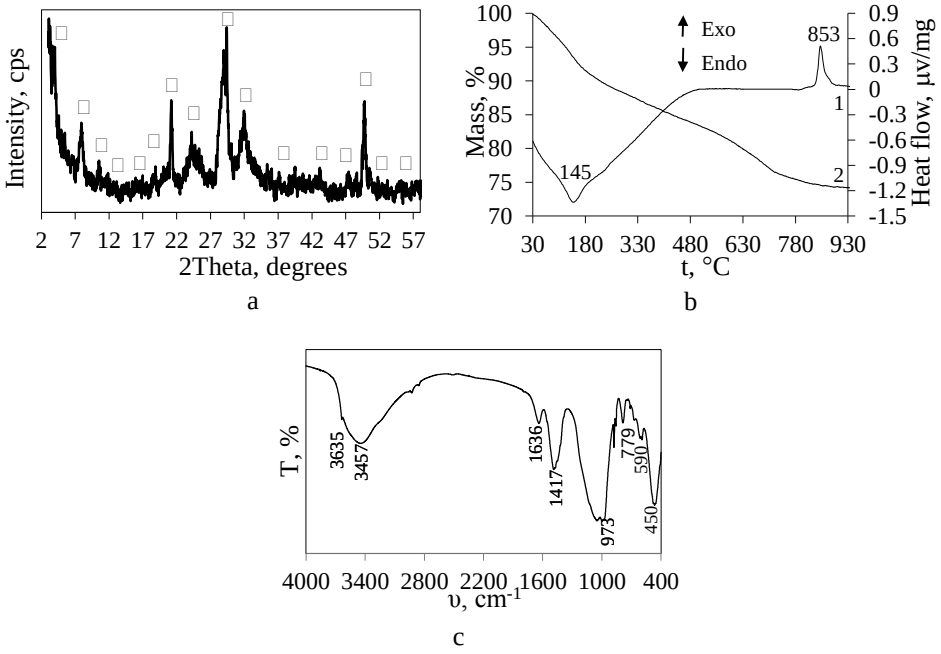

Fig. 3.20 X-ray diffraction pattern (a), STA curves (b) (1 for *DSC*, 2 for *TG*) and FT-IR spectrum (c) of gyrolite. The duration of hydrothermal synthesis at 200 °C is 48 h. Indexes: □ denotes gyrolite

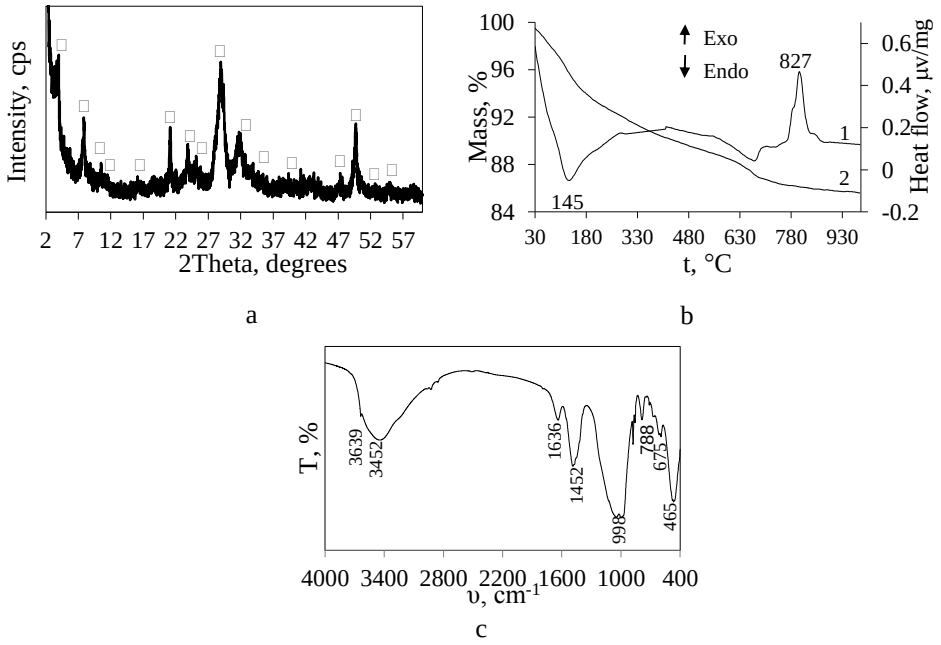

Fig. 3.21 X-ray diffraction pattern (a), STA curves (b) (1 denotes *DSC*, 2 represents *TG*) and FT-IR spectrum (c) of gyrolite substituted with transition metal ions. Indexes: □ stands for gyrolite

The obtained XRD results were also confirmed by STA and FT-IR analysis. In the DSC curve, the same thermal effects in both samples (before and after the adsorption process) were identified: the endothermic effect at 145 °C typical of water dehydration and the exothermic effect at 853 °C; 827 °C is characteristic of the formation of wollastonite (Fig. 3.20, b; Fig. 3.21, b).

The FT-IR spectrum showed a sharp peak near 3639 cm^{-1} which is visible only in the gyrolite spectrum and proves that clearly distinguished OH^- positions exist in the structure of this compound which are connected only with Ca atoms and are not influenced by hydrogen bridge links. A wide absorption band near 3457 cm^{-1} means the opposite – that molecular water forms hydrogen bridge links in the interlayers. The bands in the range of 1636 cm^{-1} frequency are assigned to $\delta(H_2O)$ vibrations and confirm this presumption. Also, a doublet near ~590 and ~612 cm^{-1} was identified and assigned to Si-O-Si bending vibrations, whereas the band at ~973 cm^{-1} relates to the Si-O stretching mode of non-binding oxygens, while the band at ~645 cm^{-1} refers to Si-O-Si bonds (Fig. 3.20, c; Fig. 3.21, c).

Thus the experimentally obtained data showed that the intercalation of Co^{2+}, Ni^{2+}, Cu^{2+}, Zn^{2+}, Mn^{2+}, Fe^{3+} ions into the structure of gyrolite proceeds via two types of chemical reaction: substitution ($Ca^{2+} \leftrightarrow Me^{x+}$) and addition (gyrolite-$Ca^0+Me^{x+} \leftrightarrow$gyrolite-$Me^0+Ca^{2+}$). Besides, the adsorption reactions are irreversible: all the explored ions were adsorbed by chemical interaction, which was proved by the pseudo-second kinetic model.

Simultaneous adsorption by synthetic hydrotalcite

It is worth mentioning that many studies (41, 125, 126) have been conducted on the uptake of transition metal ions by calcined hydrotalcite; however, the scholarly literature data concerning the adsorption of these ions by synthetic hydrotalcite is limited. It is well-known that Co^{2+}, Cu^{2+} and Cr^{3+} ions play an important role as active components in LDHs-derived catalysts (166–168). To date, intercalated with the above mentioned ions Mg/Al based LDHs are very promising precursors of the catalysts for various heterogeneous reactions: $DeNO_x$ (169), DeN_2O (170), VOCs incineration (171), SCO of ammonia (172) and others (173, 174). For this reason, in the next part of this work, simultaneous adsoption of Co^{2+}, Cu^{2+} and Cr^{3+} ions (0.25 g Me^{x+}/dm^3) by hydrothermally treated hydrotalcite (Mg/Al=2, 200 °C, 3 h) at various (25–45 ºC) temperatures was performed.

The materials presented in this chapter have been published as: Zadavičiūtė Skirmantė; Bankauskaitė Agnė; Baltakys Kęstutis; Eisinas Anatolijus. The Study of Cp Determination of Hydrotalcite Intercalated with Heavy Metal Ions. In: *Journal of Thermal Analysis and Calorimetry*. Dordrecht: Springer. 2018 (131), pp. 521–527, ISSN 1388-6150.

Table 3.8 The total amount of adsorbed metal ions after 30 min of simultaneous adsorption within the 25–45 °C temperature range

The amount of adsorbed Me^{x+} ions at different temperatures	Time, min		0.5	1	3	5	10	15	30
	25 °C	ΣX(Co^{2+}), mg/g	3.07	4.49	6.71	8.64	9.74	11.15	12.16
		ΣX(Cu^{2+}), mg/g	9.16	16.57	17.13	17.56	19.06	20.14	19.48
		ΣX(Cr^{3+}), mg/g	9.32	9.70	9.98	10.54	11.32	22.52	24.36
	35 °C	ΣX(Co^{2+}), mg/g	1.78	4.97	16.28	16.47	16.68	16.89	16.97
		ΣX(Cu^{2+}), mg/g	8.00	8.32	12.99	15.93	17.20	17.61	17.96
		ΣX(Cr^{3+}), mg/g	9.32	10.68	18.82	20.09	20.87	21.20	21.42
	45 °C	ΣX(Co^{2+}), mg/g	6.91	8.28	9.31	10.41	10.44	11.12	12.69
		ΣX(Cu^{2+}), mg/g	9.79	10.94	13.18	13.41	13.64	14.12	14.63
		ΣX(Cr^{3+}), mg/g	7.89	11.81	12.49	12.95	16.53	17.85	18.54

It was determined that, after 30 min of simultaneous adsorption, the total amount of adsorbed Cu^{2+} and Cr^{3+} ions decreased by increasing the reaction temperature up to 45 °C: from 19.48 mg to 14.63 mg Cu^{2+}/g and from 24.36 mg to 18.54 mg Cr^{3+}/g,

respectively. Meanwhile, in the case of Co^{2+} ions, the discussed process was more complex: the increment at 35 °C as well as the decrement at 45 °C in the adsorption capacity of hydrotalcite for the above mentioned ions was observed. Due to a higher reaction rate, equilibrium was attained within the first minutes of the process (Table 3.8).

Thus it should be indicated that the amounts of adsorbed transition metal ions by hydrotalcite reached 75% at 25 °C and 35 °C temperatures and 61% at a temperature of 45 °C (Table 3.8). Besides, under all the experimental conditions, the selectivity sequence of hydrotalcite according to the amount of transition metal ions can be proposed as follows:

$$Co^{2+}<Cu^{2+}<Cr^{3+}$$

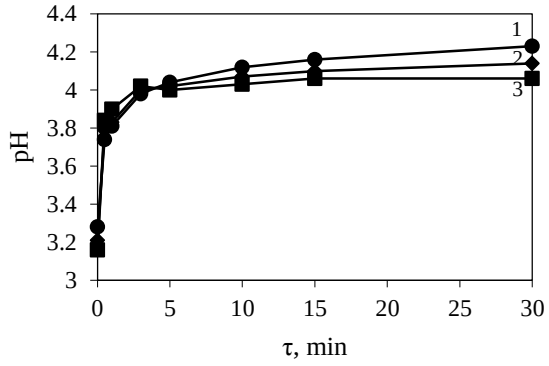

Fig. 3.22 pH values during adsorption at various temperatures: 1 at 25 °C; 2 at 35 °C; 3 at 45 °C

Meanwhile, the investigation of hydrotalcite stability after completing the process revealed that, at a temperature of 25 °C, its structure remained stable, and no other compounds were identified in the XRD pattern (Fig. 3.23, a). However, when the temperature was increased to 35 °C, the partial destruction of the latter compound proceeded because the intensity of the main diffraction peak (with *d*-spacing measuring 0.751 nm) decreased from 454 cps to 317 cps (Fig. 3.23, b). These results were in good agreement with the pH of the reaction media. Due to the release of CO_3^{2-} anions from the adsorbent interlayer into the solution, the reaction media became more acidic, i.e., the decrement in the values of pH from 4.23 to 4.14 was observed (Fig. 3.22). Moreover, no admixtures were identified in the XRD pattern (Fig. 3.23, b). It should be underlined that at a higher reaction temperature (45 °C), not only the cation but also the anion adsorption took place: alongside hydrotalcite, other LDHs with intercalated NO_3^- anions were formed. This can be explained by the accelerated mobility of ions, which resulted in the reduced adsorption capacity of transition metals (Fig. 3.23, c).

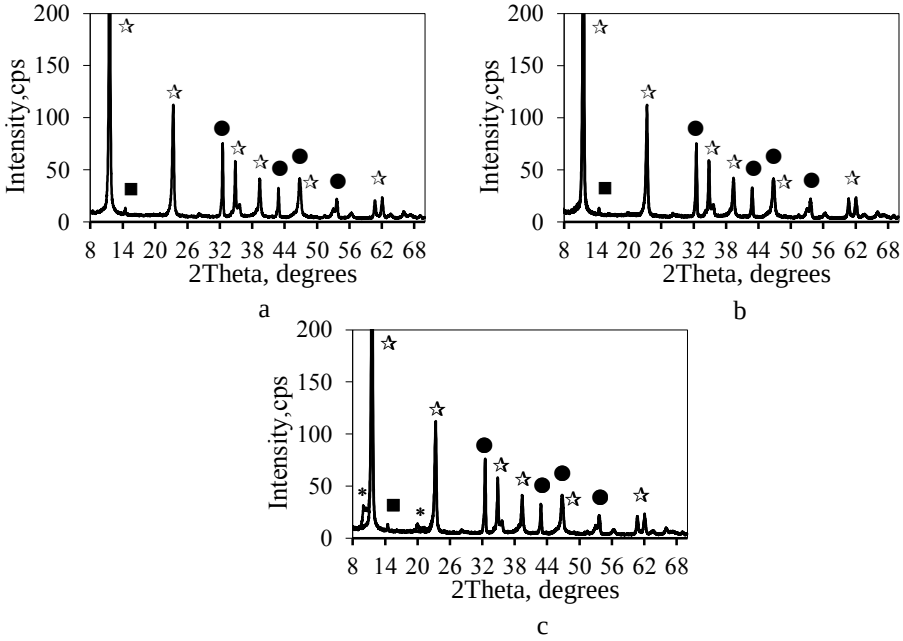

Fig. 3.23 X-ray diffraction patterns after adsorption at temperatures of 25 °C (a), 35 °C (b) and 45 °C (c). Indices: ☆ – hydrotalcite, ● – magnesite, ■ – boehmite, ∗ – magnesium aluminum nitrate hydroxide hydrate

Moreover, the evaluation of the kinetic parameters of simultaneous adsorption by hydrotalcite showed that the pseudo-first kinetic model could not be used for the description of Co^{2+}, Cu^{2+} and Cr^{3+} ions (Table 3.9). The agreement between $q_{e(exp.)}$ experimental and $q_{e(cal.)}$ calculated values was observed only for the pseudo-second order model. It should be indicated that the largest rate constant (k_2) at a temperature of 25 °C was typical of chrome ions (k_2=0.33 g/min·mg), whereas the minimum k_2 value at a temperature of 35 °C was obtained for cobalt ions (k_2=0.02 g/min·mg). It was established that the rate constants of Cr^{3+} ions depended on the temperature: k_2 decreased (k_2=0.33–0.05 g/min·mg) when the temperature of adsorption increased from 25 °C to 45 °C. This data confirmed the presupposition that transition metal ions are chemisorbed by hydrotalcite (Table 3.9).

Table 3.9 Kinetic parameters of pseudo-first and pseudo-second order kinetic models

Metal ions	Adsorption temperature, °C	$q_{e(exp.)}$, mg/g	Pseudo-first order			Pseudo-second order		
			R^2	$q_{e(cal.)}$, mg/g	k_1, min^{-1}	R^2	$q_{e(cal.)}$, mg/g	k_2, g/min·mg
Cu^{2+}	25	19.48	0.83	7.68	0.24	0.99	19.72	0.16
	35	17.96	0.96	11.68	0.25	0.99	18.86	0.05
	45	14.63	0.73	5.11	0.17	0.99	14.29	0.24
Co^{2+}	25	12.16	0.97	9.55	0.15	0.99	12.22	0.04
	35	16.98	0.81	8.83	0.34	0.92	21.27	0.02
	45	12.69	0.69	6.10	0.10	0.99	11.29	0.19
Cr^{3+}	25	24.36	0.73	21.35	0.12	0.99	11.48	0.33
	35	21.42	0.91	11.56	0.29	0.99	22.37	0.06
	45	18.54	0.94	12.26	0.19	0.99	18.69	0.05

Thus it was determined that the adsorption temperature as well as the nature of Cu^{2+}, Co^{2+} and Cr^{3+} ions had a significant influence on the uptake of the above listed ions by hydrotalcite samples. When this specific parameter was increased from 25 °C to 35 °C, the structure of hydrotalcite became unstable and, at a higher reaction temperature (45 °C), not only cation but also anion adsorption took place.

To sum up, it can be stated that the adsorption capacities of both layered compounds strongly depended on the chemical nature of the involved transition metal ion solutions. Besides, it was determined that the above mentioned reactions are irreversible, and that both compounds act as chemisorbents. The latter statement was also proved by the calculation of the pseudo-second order model.

3.4 Study of C_p Determination for Hydrotalcite Samples Intercalated with Transition Metal Ions

The application of LDHs is mainly affected by their physical and chemical properties (175). The specific heat basically represents the thermal storage capacity of a system, but it is also useful to calculate other related quantities, such as dynamic thermal conductivity and diffusivity (176). However, information scarcity in the scholarly literature concerning the measurements of specific heat capacity of pure and intercalated with transition metals hydrotalcite is evident. This is why the following experiment was devised to examine their effect on hydrotalcite-specific heat capacity.

The materials presented in this chapter have been published as: Zadavičiūtė Skirmantė; Bankauskaitė Agnė; Baltakys Kęstutis; Eisinas Anatolijus. The Study of C_p Determination of Hydrotalcite Intercalated with Heavy Metal Ions. In: *Journal of Thermal Analysis and Calorimetry*. Dordrecht: Springer. 2018 (131), pp. 521–527, ISSN 1388-6150.

It was determined that with the increasing adsorption temperature from 25 °C to 45 °C, the amount of intercalated transition metal ions into the adsorbent was 75%, 74% and 61%, respectively. It should be noted that chromium ions intercalated mostly into the adsorbent structure (~ 40% of the amount of adsorbed transition metal ions) independently from the adsorption conditions (Fig. 3.24).

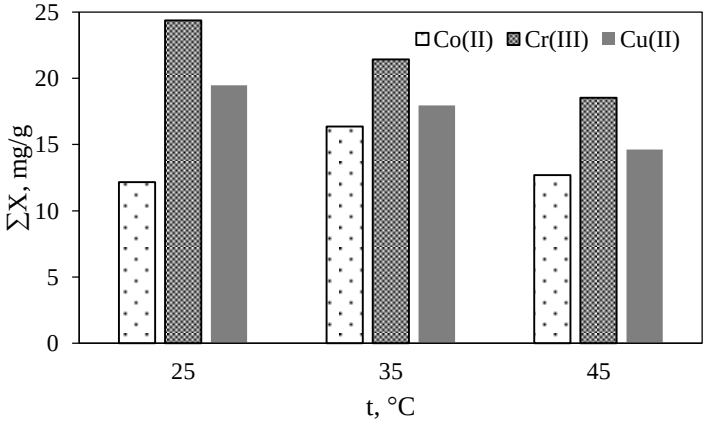

Fig. 3.24 The total amount of adsorbed metal ions after 30 min of simultaneous adsorption within the 25–45 °C temperature range

It was determined that, during the dehydroxilation of brucite-like layers (276–311 °C) as well as during the destruction of the interlayer (439–465 °C), the absorbed heat values were changed: from 971.9 μVs mg^{-1} to 867.3 μVs mg^{-1} within the 276–311 °C temperature range and from 454 μVs mg^{-1} to 633.1 μVs mg^{-1} within the 439–465 °C temperature interval, which clearly indicates the intercalation of NO_3^- anions (177) (Fig. 3.25).

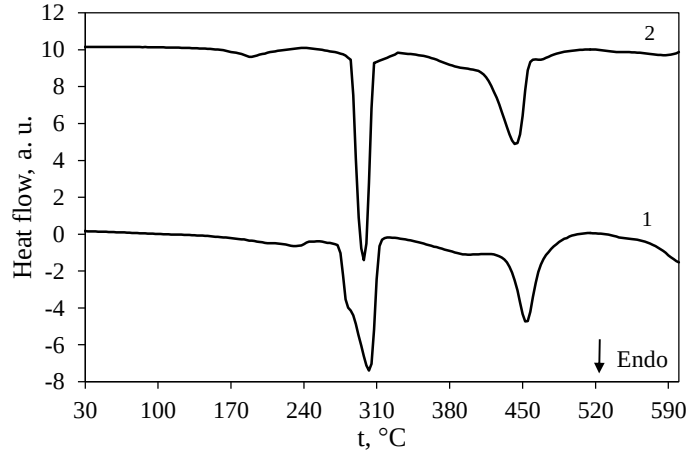

Fig. 3.25 The DSC curves of the samples after synthesis (1) and adsorption at a temperature of 45 °C (2)

It should be underlined that the C_p values can only be accurately determined if no thermal conversion takes place in the investigated materials. For this reason, according to the results of DSC analysis, the 25–170 °C temperature range was selected for the calculation of C_p values of pure and intercalated with transition metal hydrotalcite samples.

It was determined that the presence of Cu^{2+}, Co^{2+} and Cr^{3+} ions in the structure of the latter compound coupled with the appropriate adsorption temperature showed important impact on the specific heat capacity of hydrotalcite (Fig. 3.26). Due to the intercalation of the researched ions, in comparison with the as-synthesized hydrotalcite (C_p=2.47 J/g·K) sample, the lower values of C_p were obtained at 25 °C (C_p=2.39 J/g·K) and 35 °C (C_p=2.44 J/g·K) temperatures. Meanwhile, after 30 min of adsorption at 45 °C, the value of specific heat was higher and equal to 2.60 J/g·K due to the formation of new LDHs.

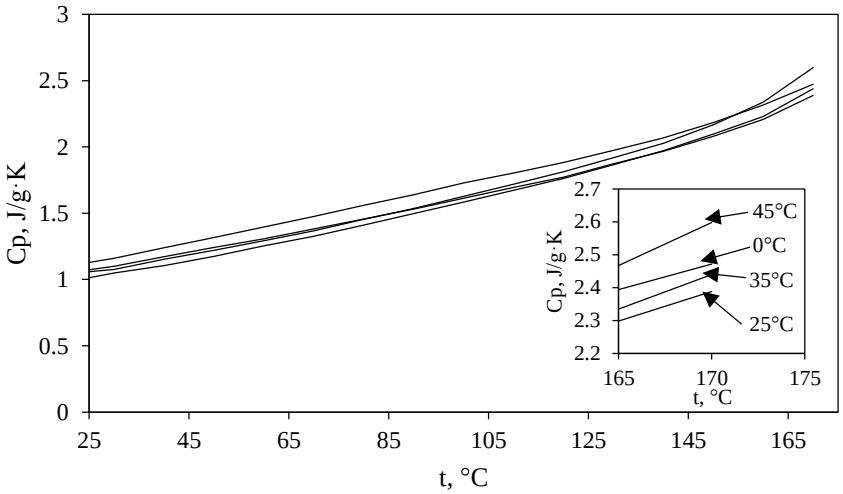

Fig. 3.26 Adsorption temperature dependence on the specific heat capacities of pure and intercalated with transition metal hydrotalcite samples

It was determined that the heat capacity of hydrotalcite samples was mainly affected by the adsorption temperature. At 25 °C and 35 °C, due to the intercalation of the investigated ions into the structure of the latter compound, lower values of C_p were obtained: 2.39 J/g·K and 2.44 J/g·K, respectively. Meanwhile, when the operating temperature was increased to 45 °C, the highest specific heat capacity was reached (C_p=2.60 J/g·K).

3.5 Formation of Thin Mixed Metal Oxide Films from the Targets Possessing Specific Properties of Electron Beam Evaporation

Diverse techniques have been used to prepare LDHs or their mixed oxide films on inorganic substrates. Usually, two methods are applied: physical deposition (e.g.,

pulsed laser deposition, spin coating) and *in situ* growth or substrate-induced growth (178–181). Recently, a new area of application of gyrolite and hydrotalcite was suggested: these compounds can be used as a precursor for the fabrication of thin films (182). It is known that one of the existing methods of preparation of such materials is electron beam (e-beam) evaporation, which results in dense, high quality thin films featuring the required properties (183). It should be noted that, during the evaporation process, thin film growth on different substrates may affect the inferior adhesion between the film and the substrate, poor wear resistance and mechanochemical stability of the evaporated thin films (184). Also, many important physical and chemical properties of thin films depend on their microstructure and texture. However, scholarly literature discussing the mechanical properties of thin films prepared from different gyrolite or hydrotalcite targets is fairly limited. For this reason, the final part of this thesis undertakes to investigate the roughness parameters of thin films prepared from different targets based on gyrolite or hydrotalcite by applying e-beam evaporation.

The formation of thin mixed Mg-Al oxide films based on hydrotalcite

It was determined that after 1 h of calcination at a temperature of 200 °C, the intensity of the main diffraction peaks characteristic of hydrotalcite slightly decreased due to the release of crystallization water (Fig. 3.27, curve 1). In this case, partial dehydration of gibbsite took place because significant decrease in the intensity of the diffraction peaks typical of the latter compound from 115 cps to 47 cps was observed (Fig. 3.3, a; Fig. 3.27, curve 1).

Moreover, when the calcination temperature was increased to 575 °C, magnesium (ICDD File No. 77-2179; *d*-spacing equaling 0.244, 0.211 and 0.149 nm) and aluminum (ICDD File No. 29-0063; *d*-spacing equaling 0.199 and 0.139 nm) oxides were obtained in the system. However, an unidentified small intensity diffraction peak (its *d*-spacing equaled 0.303 nm) was also observed in the XRD pattern (Fig. 3.27, curve 2). As expected, at the calcination temperature of 1000 °C, mixed Mg-Al oxide (ICDD File No. 21-1152; *d*-spacing equaling 0.303 nm) was obtained (Fig. 3.27, curve 3). However, alongside the above mentioned compound, magnesium oxide and traces of aluminum oxide were also formed.

Therefore, calcined precursors featuring various mineralogical compositions were used as targets for thin film deposition in order to evaluate their effect on the structural and textural properties of thin mixed Mg-Al oxide films. It should be noted that the above mentioned films were labeled as MMO-200, MMO-575 and MMO-1000 according to the calcination temperatures of the targets.

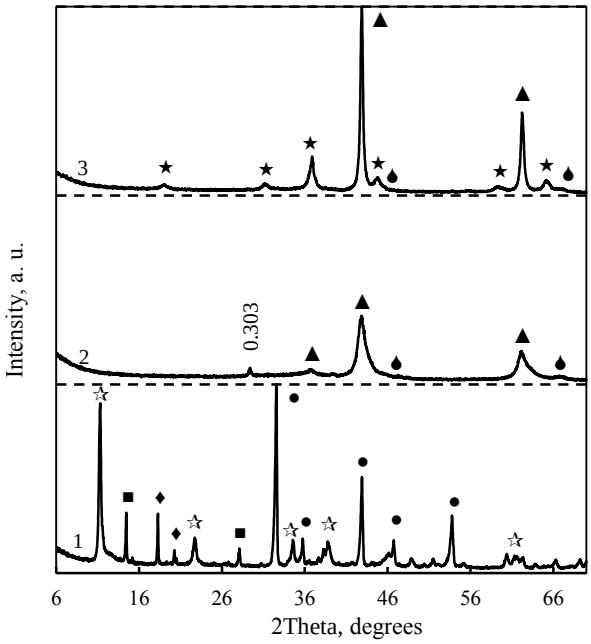

Fig. 3.27 X-ray diffraction patterns of precursors calcined at 200 °C (curve 1), 575 °C (curve 2) and 1000 °C (curve 3) temperatures. Indices: ☆ – hydrotalcite, ● – magnesite, ■ – boehmite, ♦ – gibbsite

It was determined that mixed Mg-Al oxide (ICDD File No. 21-1152; *d*-spacing equaling 0.242 and 0.140 nm) was observed in all the formed thin films by using different targets or substrates (Fig. 3.28). Besides, alongside the explored compounds, magnesium (ICDD File No. 45-0946; *d*-spacing equaling 0.211 and 0.148 nm) and aluminum (ICDD File No. 45-0946; *d*-spacing equaling 0.211 and 0.148 nm) oxides were identified in the XRD patterns.

It is clearly visible that the calcination temperature of the targets should not exceed 1000 °C because the crystallization of thin mixed Mg-Al oxide films took place slower, i.e., the lowest intensity diffraction peaks of these compounds were observed in comparison with MMO-200 or MMO-575 samples (Fig. 3.28, curves 3). Moreover, the obtained results were in good agreement with the data provided in scholarly literature because LDHs calcinated within the temperature range of 550–600 °C show better texture and morphological parameters (185, 186). In this case, 5–7 times higher intensity of the diffraction maximums typical of mixed Mg-Al oxide were observed in the formed thin films (Fig. 3.28, curves 2). Also, it was determined that due to reflections of the substrate components which were identified in all the formed thin film samples, the intensities of mixed Mg-Al oxide decreased and broadened.

Moreover, it was determined that the high amount of crystallization water in the target structure exerted negative influence on the e-beam evaporation process (Fig.

3.28, curves 1). For this reason, the calcination temperatures of the target preparation should be higher than 500 °C.

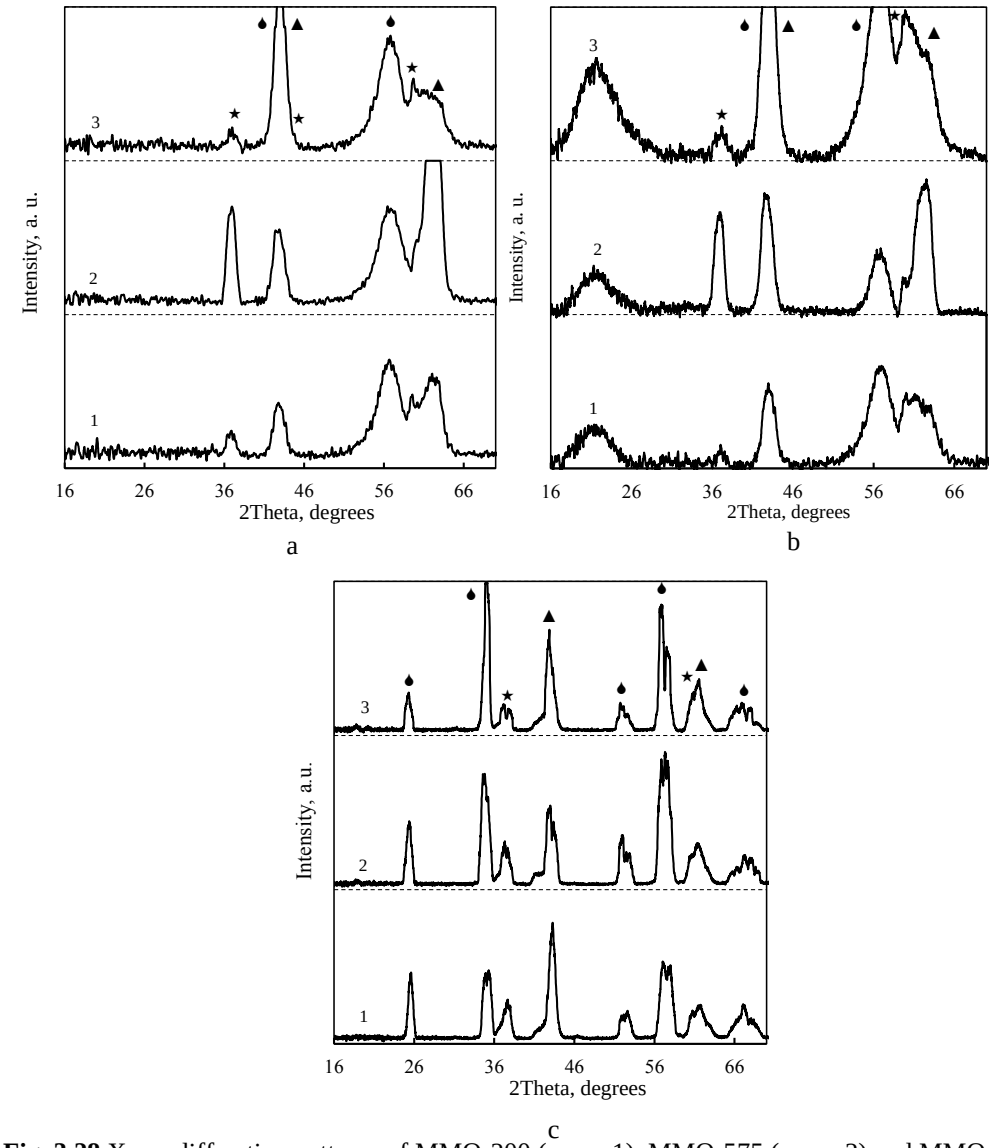

Fig. 3.28 X-ray diffraction patterns of MMO-200 (curve 1), MMO-575 (curve 2) and MMO-1000 (curve 3) thin films on different substrates: a – Si, b – Si/SiO_2, c – Al_2O_3. Indices: ▲ – magnesium oxide, ♦ – aluminum oxide, ★ – mixed Mg-Al oxide

AFM investigations revealed the formation of thin mixed Mg-Al oxide films with different topographies (Fig. 3.29). It was determined that mostly the calcination conditions influenced the growth mechanism of thin films deposited on different substrates. During evaporation, MMO-575 and MMO-1000 samples corresponded to a very smooth and dense surface without dramatic changes in the microstructure,

whereas MMO-200 thin films grew in the localized areas – hillocks. Besides, all the obtained thin films were well adhered to the substrate.

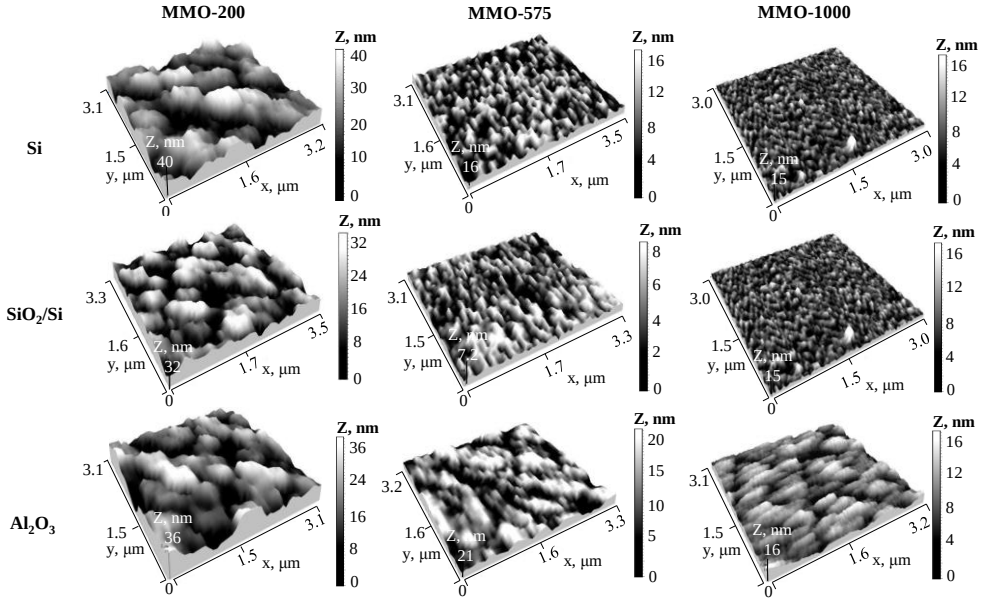

Fig. 3.29 AFM surface topography images of MMO thin films deposited on different substrates (Si, SiO_2/Si, Al_2O_3)

It is known that the mechanical stability of the deposited films strongly depends on their surface morphology. As previously obtained results show, MMO-575 and MMO-1000 thin films feature a similar mechanism of film growth; meanwhile, MMO-200 films only grew in the localized areas. For this reason, in order to evaluate the microhardness, the samples with the most different surface roughness and growth mechanism were chosen, i.e., MMO-200 and MMO-1000 thin films deposited on Si substrate.

It was determined that the values of Vickers hardness are equal to 540 HV and 560 HV, while Young's modulus remains relatively constant at 104 GPa and 108 GPa, respectively. It should be noted that the values of the latter parameter were shown to be 25% lower compared to the values provided by other authors (187) whereas Vickers hardness was practically in the same range. This inadequacy could be explained by the amount of magnesium and aluminum in the material because the change in the values of the discussed parameters in one or the other direction represents saturation of magnesium or aluminum (or other elements) (188).

It is known that if the surface is excessively rough, heavy abrasive wear will appear, which can ultimately lead to adhesion or scuffing (177). However, for very smooth surfaces, strong adhesive force and adhesive wear can already be detected under very small loads (189). For this reason, the mechanical properties of thin films were also characterized by evaluating the roughness parameters (Table 3.10, Fig. 3.30, Fig. 3.31).

It was determined that the lowest kurtosis value (R_{ku}=2.59), which shows that a bumpy surface is getting formed, was characteristic of the MMO-200 film deposited on Si substrate. Meanwhile, the highest R_{ku} value (R_{ku}=8.24), which was typical of the MMO-1000 film deposited on Si substrate, indicates the predominance of a spiky surface. It should be emphasized that the perfectly random surface was characteristic of the MMO-575 thin film deposited on Si substrate because its R_{ku} value was close to 3 (Table 3.10).

Table 3.10 The values of roughness parameters of MMO thin films according to AFM analysis

	MMO-200		MMO-575		MMO-1000	
Substrates	R_{ku}	Z_{mean}, nm	R_{ku}	Z_{mean}, nm	R_{ku}	Z_{mean}, nm
Si	2.59	19.81	3.02	8.39	8.24	4.07
SiO_2/Si	2.94	18.23	3.06	3.71	6.13	4.15
Al_2O_3	3.55	22.57	3.33	12.07	2.83	9.61

It was determined that the mechanical properties of thin films strongly depend on the chemical composition of both targets and substrates. The lowest root mean square roughness (R_q) of 1.13 nm was observed for MMO-575 and MMO-1000 thin films deposited on SiO_2/Si substrate with the surface elements featuring a mean height of 3.71 and 4.15 nm, respectively; meanwhile, the highest R_q value (7.14 nm) was detected for the MMO-200 sample deposited on Si substrate with a mean height of 19.81 nm (Fig. 3.30; Table 3.10).

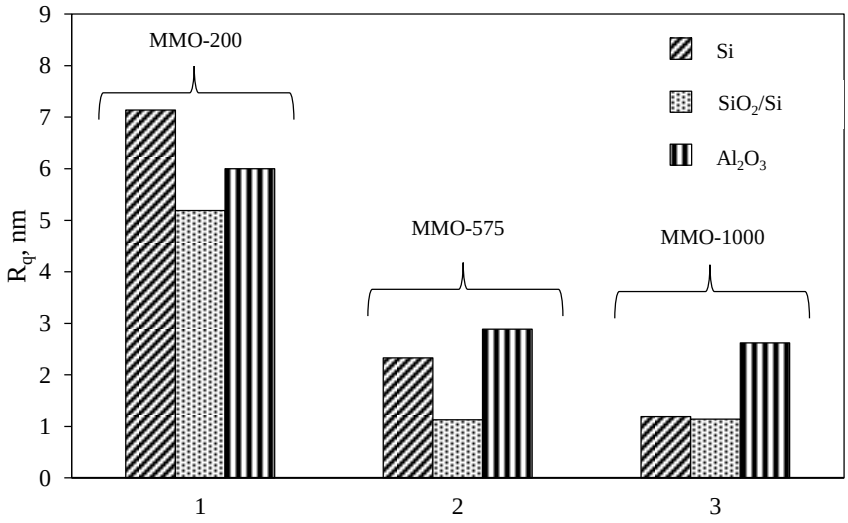

Fig. 3.30 Root mean square roughness (R_q) dependence of MMO-200, MMO-575 and MMO-1000 thin films

Moreover, the most prominent asymmetry of surface elements was characteristic of the MMO-200 film deposited on Al_2O_3 substrate as well as of the MMO-1000 film deposited on Si substrate because, in the case of the MMO-200 sample, the lowest negative skewness parameter was obtained (R_{sk}=-0.40) thus showing the predominance of valleys, i.e., a profile with its peaks removed, or a profile with deep scratches (Fig. 3.31). Meanwhile, in the case of the MMO-1000 film, the highest positive R_{sk} value (R_{sk}=0.89) was observed, which indicates a peaked surface, i.e., a profile with valleys filled in or a profile with high peaks. It should be noted that the homogeneous and symmetrical growth of thin films was only obtained by using the target calcined at a temperature of 575 °C because R_{sk} values were close to point zero (Fig. 3.31).

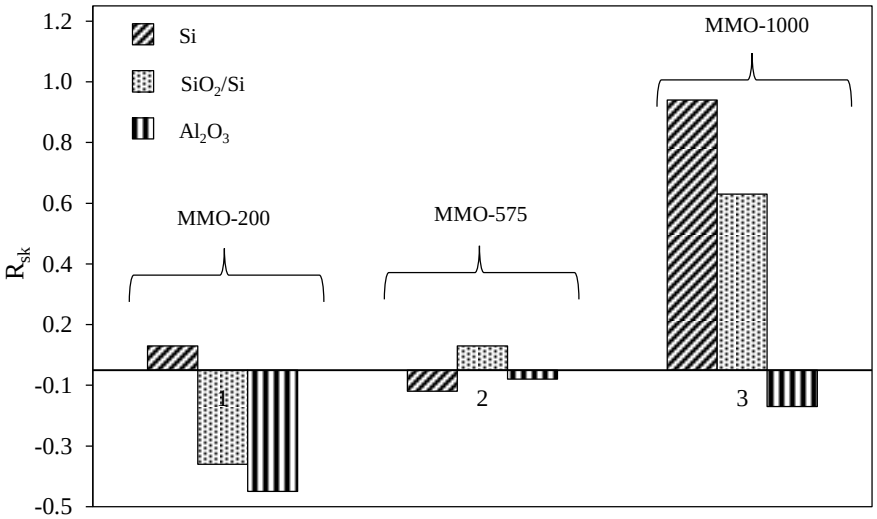

Fig. 3.31 Distribution of the skewness parameter of CHT-200, CHT-575 and CHT-1000 thin films evaporated on different substrates

The SEM view of the cross-section of MMO-575 thin film deposited on the Si substrate is presented in Fig. 3.32. The image reveals a strong aligned microstructure characterized by closed packed nanocolumns, which clearly shows that a dense thin film was formed.

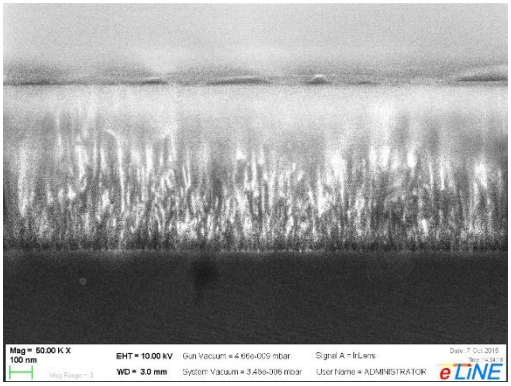

Fig. 3.32 SEM image of the cross-section of MMO-575 thin film deposited on Si substrate

The formation of thin Ca-Si oxide films based on gyrolite

Two different targets were used for the formation of thin films based on gyrolite. The mineralogical composition and the structure stability of both targets are presented in Fig. 3.33. The X-ray diffraction data showed that after 1 h of calcination at a temperature of 200 °C, the intensity of the main diffraction peaks characteristic of gyrolite decreased due to the release of crystallization water (Fig. 3.33, a). Moreover, when the calcination temperature was increased to 1000 °C, wollastonite (ICDD File No. 73-1110; *d*-spacing equaling to 0.384, 0.351, 0.331 and 0.299 nm) was obtained in the XRD pattern (Fig. 3.33, b).

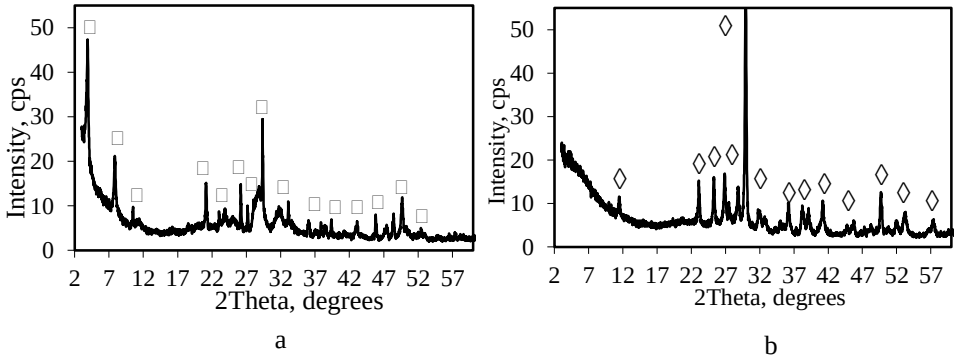

Fig. 3.33 X-ray diffraction patterns of precursors calcined at 200 °C (a) and 1000 °C (b) temperatures. Indices: □ denotes gyrolite, ◊ represents wollastonite

Therefore, as in the case of hydrotalcite, thin films based on gyrolite were formed on Si, SiO_2/Si and Al_2O_3 substrates, and the roughness parameters were evaluated. These films were labeled as Gyr-200 and Gyr-1000 according to the calcination temperatures of the targets.

The results of AFM topographies showed that the mineralogical composition of both targets and substrates influenced the growth mechanism of thin films. It was discovered that Gyr-200 and Gyr-1000 samples deposited on Si and SiO_2/Si substrates corresponded to a smooth and dense surface without dramatic changes in microstructure. Meanwhile, the thin film on the Al_2O_3 substrate grew in localized areas (hillocks). It should be noted that thin Gyr-1000 films developed a more similar mechanism of film growth than Gyr-200 films. This data was confirmed by the calculation of the roughness parameters (Table 3.11).

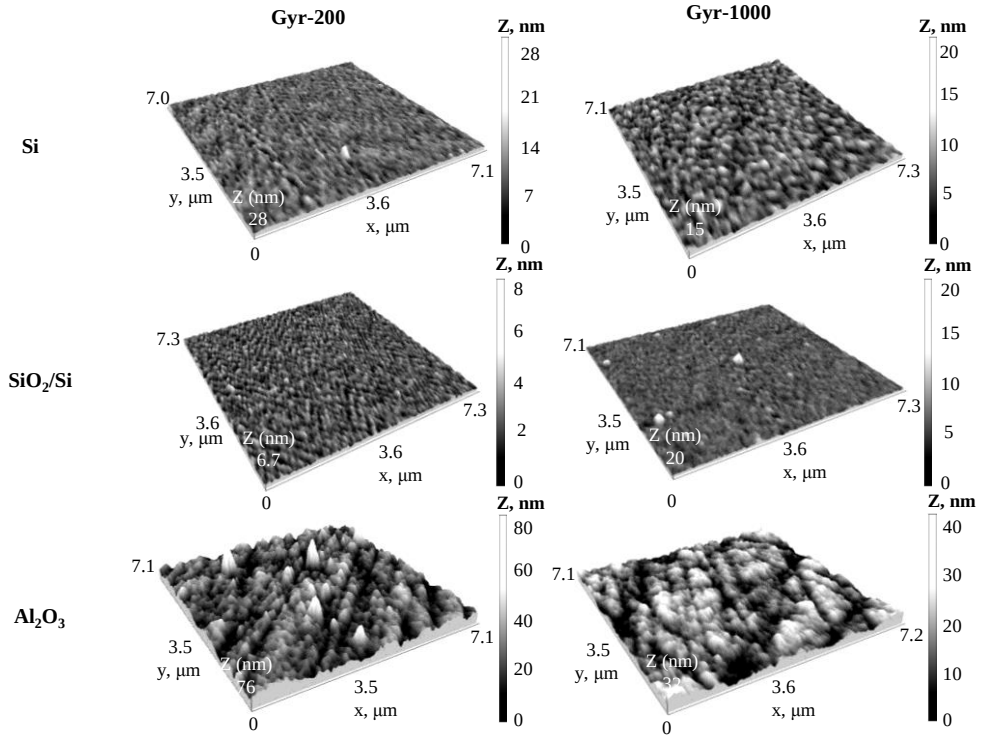

Fig. 3.34 AFM surface topography images of gyrolite thin films deposited on different substrates (Si, SiO_2/Si, Al_2O_3)

It was determined that the highest root mean square roughness of 6.48 nm was observed for the Gyr-200 film deposited on Al_2O_3 substrate with a mean height of 22.83 nm. Meanwhile, thin Gyr-1000 film deposited on SiO_2/Si substrate with the surface elements featuring a mean height of 3.94 nm showed the lowest *Rq* value of 1.01 nm. It is worth noting that under all experimental conditions, Gyr-200 films possessed surfaces of higher roughness than Gyr-1000 films, except for those deposited on Si substrate (Table 3.11).

Moreover, the highest positive skewness parameter was characteristic of the Gyr-1000 film deposited on SiO_2/Si substrate (R_{sk}=2.53), which indicates that a peaked surface is formed, i.e., a profile with valleys filled in or a profile with high peaks are present. It should be noted that, close to the zero points, R_{sk} values were obtained by using SiO_2/Si substrate with a target calcined at a temperature of 200 °C and also with

a target calcined at a temperature of 1000 °C which was deposited on Si and Al_2O_3 substrates. It clearly showed that homogeneous and symmetrical growth was characteristic of the researched thin films (Table 3.11).

The other roughness parameter, kurtosis (R_{ku}), which shows the predominance of high peaks, was characteristic of almost all the investigated films because the values of the researched parameter were higher than 3. However, only the thin Gyr-1000 film deposited on Si and Al_2O_3 substrates had a perfectly random surface because its R_{ku} value was close to 3 (Table 3.11).

Table 3.11 Values of roughness parameters of thin films according to AFM analysis

Substrates	Parameters	Gyr-200	Gyr-1000
Si	R_q, nm	1.33	1.80
	R_{sk}	1.23	0.14
	R_{ku}	18.50	3.14
	Z_{mean}, nm	8.42	7.69
SiO_2/Si	R_q, nm	1.38	1.01
	R_{sk}	0.07	2.53
	R_{ku}	3.45	8.10
	Z_{mean}, nm	6.47	3.94
Al_2O_3	R_q, nm	6.48	4.50
	R_{sk}	0.86	-0.03
	R_{ku}	8.01	2.95
	Z_{mean}, nm	22.83	16.18

Thus, according to the obtained results, it can be stated that the electron beam evaporation technique is suitable for the formation of thin films. Technologically, it is more convenient to evaporate thin films by using MMO-575, MMO-1000 or Gyr-1000 samples as targets because, in the case of MMO-200 or Gyr-200 pallets, due to the presence of crystallization water in the structure of the synthesis products, discharge was observed in the vacuum chamber during the evaporation process.

The analysis of the microstructure of both thin films revealed that the surface topography mainly depends on the nature of the selected precursors and substrates. The dense and smooth surface of thin films was obtained by using MMO-575 and MMO-1000 targets, whereas hillocks were formed on the surface of MMO-200 thin films deposited on all the substrates. Irrespectively of the choice of the substrate, homogeneous and symmetrical growth of thin films was obtained by using the MMO-575 target (R_{sk} values were close to 0). Meanwhile, in the case of thin gyrolite films, the substrate played a significant role on the values of R_{sk}. Homogeneous and symmetrical growth was observed for the Gyr-200 target deposited on SiO_2/Si substrate and for the Gyr-1000 target deposited on Si and Al_2O_3.

3.6 Technological Recommendations for the Synthesis of Compounds Featuring Specific Properties under Periodic Operation in Production

On the grounds of the data obtained in this research, a principal technological scheme for the synthesis of compounds with specific properties under periodic

operation in production was proposed (Fig. 3.35). The optimal parameters of Mg-Al synthesis were determined on the grounds of the results obtained in this work, i.e., by using magnesium carbonate and γ-Al_2O_3 mixture, when the molar ratio (Mg/Al) is equal to 2. Hydrothermal or microwave synthesis is carried out in stirred suspensions when the water-to-solid ratio (W/S) is equal to 10, saturated water vapor temperature is set at 200 °C, and the duration of synthesis varies from 1 to 3 h. Per one operating/work cycle, 100 kg of solid raw materials (23.29 kg Al_2O_3 and 76.71 kg $MaCO_3$) and 1000 kg of water was used during the research.

On the grounds of the research, the main production stages can be described as follows: the required amounts of $MgCO_3$ and γ-Al_2O_3 compounds are weighed by the weight dispensers (3) and supplied to the mixer/adsorber (5), in which, the required amount of water is added from the reservoir (2) by using a volumetric dispenser (4). The obtained suspension is supplied by a pump to an autoclave (6) or to microwave reactors (7). If the synthesis of compounds is performed by selecting the first method, the initial products are treated in the autoclave (6) at a temperature of 200 °C for 3 h. If the second method is applied, the synthesis of compounds is carried out in the microwave reactor (7) at a temperature of 200 ° C for 1 h. After hydrothermal/microwave treatment, the product is supplied to a reservoir of suspension (9), in which, after sedimentation, the excess water is removed with a pump (8), and then the product is placed into a filtration unit and into a pulverous dryer (10). During this process, pellets of a diameter of 0.75–1.00 mm with a moisture content of 1.5–2% are produced. Finally, the product can be used for adsorption, or it can be transported to a chamber furnace which works under periodic operation (12), and then calcined at a higher temperature (>500 ºC) for 1 h. The calcined product (mixed metal oxides) can also be used for the adsorption, thin film formation, or it can be delivered to the product packaging warehouse.

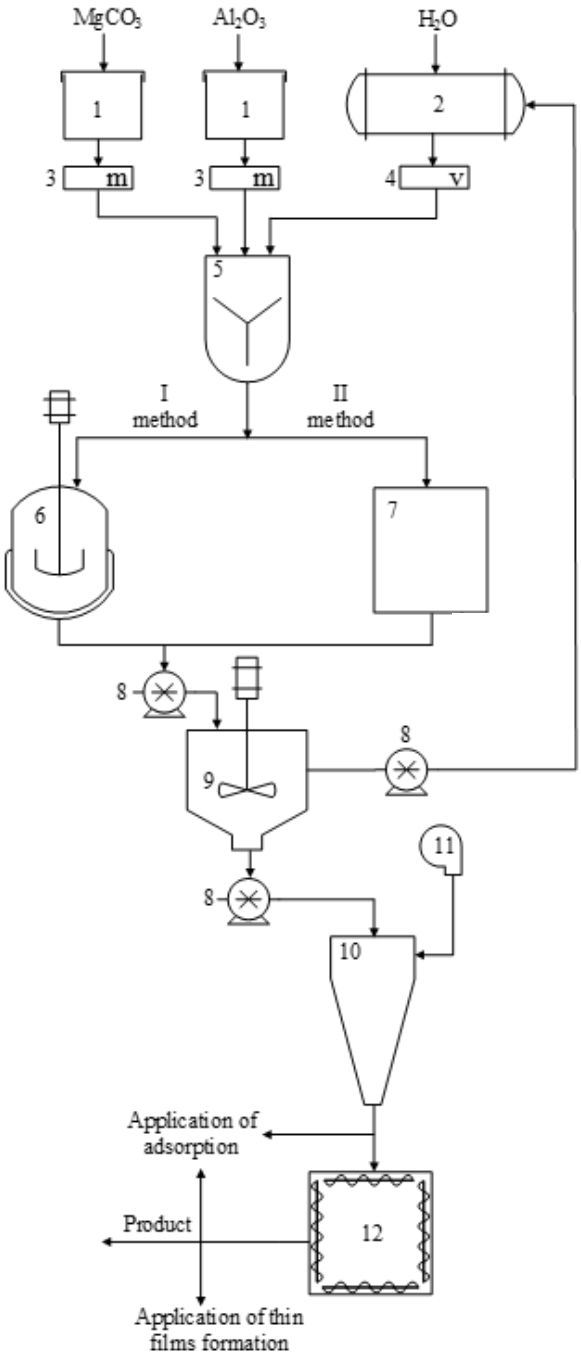

Fig. 3.35 Principal technological scheme of the synthesis of compounds with specific properties under periodic operation in production: 1 – a batcher of raw materials; 2 – a reservoir of water; 3 – weight dispensers; 4 – a volume dispenser; 5 – a mixer/adsorber; 6 – an autoclave; 7 – a microwave reactor; 8 – a pump; 9 – a reservoir of suspension; 10 – a pulverous dryer; 11 – a heater; 12 – a chamber furnace

Conclusions

1. The formation of compounds denoted by specific properties in the $MgCO_3$-Al_2O_3-H_2O stirred suspension is induced by hydrothermal treatment. During the hydrothermal treatment, it was observed that the intensity of the main diffraction maximum typical of hydrotalcite increased from 296 cps to 471 cps, and the crystallite sizes increased from 40.06 nm to 52.45 nm with the increasing duration and the molar ratio of the primary mixtures (Mg/Al=1 or 2). Meanwhile, the lower crystallinity in the compound was obtained when microwave synthesis was applied, i.e., the intensity of the main diffraction maximum decreased from 258 cps to 209 cps, and the crystallite sizes were reduced from 38.50 nm to 36.25 nm. By changing the conditions of the activation methods (i.e., mechanochemical and thermal ones), the mineralogical composition and the morphological properties of the researched compounds can be controlled.
2. It was determined that synthetic oxides and silicate compounds simultaneously adsorbed almost all the cations (Zn^{2+}, Cu^{2+}, Co^{2+}, Ni^{2+}, Mn^{2+}, Fe^{3+} and Cr^{3+}) in the liquid medium. The chemical and mineralogical composition of the researched compounds and the adsorption temperature significantly influenced the adsorption capacity of the transition metal ions and the duration at which the equilibrium was attained (3–10 min).
3. It was examined that, regardless of the pH value of the initial solution, the adsorption reactions characteristic of synthetic gyrolite and hydrotalcite are irreversible because the major part of the investigated ions was intercalated in the crystal structure of the adsorbents according to the chemical interaction which was confirmed by the pseudo-second kinetic model.
4. It was determined that thin films with various thickness (from 4 nm to 23 nm) which were obtained from calcined precursors can be formed on various substrates (Si, SiO_2/Si and Al_2O_3) by using the electron beam evaporation method. It was also established that, in order to receive the appropriate roughness parameters (R_q, R_{sk}, R_{ku} and Z_{mean}) of the researched films, the synthesized oxides and silicate compounds should be activated at temperatures higher than 500 ºC because the presence of crystallization water in the structure of the target leads to the discharge in the vacuum chamber.
5. The principal scheme of the synthesis of compounds with specific properties under periodic operation in production including hydrothermal/microwave synthesis and activation methods was offered.

References

1. BANERJEE, S. and GAUTAM, P.K. (2016). Layered Double Hydroxides Nanomaterials for Water Remediation. In: *Nanomaterials for Wastewater Remediation*. 2016, pp. 161–188. ISBN 9780128046098.
2. QU, J., QIWU, Z., XUEWEI, L., XIAOMAN, H. and SHAOXIAN, S. (2016). Mechanochemical Approaches to Synthesize Layered Double Hydroxides: a Review. In: *Applied Clay Science*. 2016, vol. 119, No. 2, pp. 185–192. doi: 10.1016/j.clay.
3. COSTA, F.R., ABDEL-GOAD, M., WAGENKNECHT, U. and HEINRICH, G. (2005). Nanocomposites Based on Polyethylene and Mg-Al Layered Double Hydroxide. I. Synthesis and Characterization. In: *Polymer*. 2005, vol. 46, No. 12, pp. 4447–4453. doi: 10.1016/j.polymer.2005.02.027.
4. WEN, T., WU, X., TAN, X., WANG, X. and XU, A. (2013). One-Pot Synthesis of Water-Swellable Mg-Al Layered Double Hydroxides and Graphene Oxide Nanocomposites for Efficient Removal of As(V) from Aqueous Solutions. In: *ACS Applied Materials and Interfaces*. 2013, vol. 5, No. 8, pp. 3304–3311. doi: 10.1021/am4003556.
5. COSTA, F.R. (2007). Mg-Al Layered Double Hydroxide: A Potential Nanofiller and Flame-Retardant for Polyethylene: PhD Dissertation. Dresden University of Technology.
6. MILLS, S.J., CHRISTY, A.G., GÉNIN, J.-M. R., KAMEDA, T. and COLOMBO, F. (2012). Nomenclature of the Hydrotalcite Supergroup: Natural Layered Double Hydroxides. In: *Mineralogical Magazine*. 2012, vol. 76, No. 5, pp. 1289–1336. doi: 10.1180/minmag.2012.076.5.10.
7. BENÍCIO, L.P.F., SILVA, R.A., LOPES, J.A., EULÁLIO, D., DOS SANTOS, R.M.M., DE AQUINO, L.A., VERGÜTZ, L., NOVAIS, R.F., DA COSTA, L.M., PINTO, F.G. and TRONTO, J. (2015). Hidróxidos duplos lamelares: Nanomateriais para aplicações na agricultura. In: *Revista Brasileira de Ciencia do Solo*. 2015, vol. 39, No. 1, pp. 1–13. doi: 10.1590/01000683rbcs20150817.
8. ZHAO, Y., LI, F., ZHANG, R., EVANS, D.G. and DUAN, X. (2002). Preparation of Layered Double-Hydroxide Nanomaterials with a Uniform Crystallite Size Using a New Method Involving Separate Nucleation and Aging Steps. In: *Chemistry of Materials*. 2002, vol. 14, No. 10, pp. 4286–4291. doi: 10.1021/cm020370h.
9. GU, Z., ATHERTON, J.J. and XU, Z.P. (2015). Hierarchical Layered Double Hydroxide Nanocomposites: Structure, Synthesis and Applications. In: *Chem. Commun.* 2015, vol. 51, No. 15, pp. 3024–3036. doi: 10.1039/C4CC07715F.
10. CHANG, Z., EVANS, D.G., DUAN, X., VIAL, C., GHANBAJA, J., PRÉVOT, V., DE ROY, M. and FORANO, C. (2005). Synthesis of [Zn-Al-CO_3] Layered Double Hydroxides by a Coprecipitation Method under Steady-State Conditions. In: *Journal of Solid State Chemistry*. 2005, vol. 178, No. 9, pp. 2766–2777. doi: 10.1016/j.jssc.2005.06.024.
11. ALAM, M.N. and POTIYARAJ, P. (2017). Synthesis of Nano Zinc Hydroxide via Sol-Gel Method on Silica Surface and Its Potential Application in the

Reduction of Cure Activator Level in the Vulcanization of Natural Rubber. In: *Journal of Sol-Gel Science and Technology*. 2017, vol. 81, No. 3, pp. 903–911. doi: 10.1007/s10971-016-4248-0.
12. TYAGI, S.B., KHARKWAL, A., KHARKWAL, M. and SHARMA, R. (2017). Synthesis and Characterization of Layered Double Hydroxides Containing Optically Active Transition Metal Ion. In: *Solid State Sciences*. 2017, vol. 63, pp. 93–102. doi: 10.1016/j.solidstatesciences.
13. ROSA, R., LEONELLI, C., VILLA, C. and PRIARONE, G. (2013). Microwave-Assisted Melt Reaction Method for the Intercalation of Carboxylic Acid Anions into Layered Double Hydroxides. In: *Journal of Microwave Power and Electromagnetic Energy*. 2013, vol. 47, No. 1, pp. 12–23. doi: 10.1080/08327823.2013.11689843.
14. PAREDES, S.P., VALENZUELA, M.A., FETTER, G. and FLORES, S.O. (2011). TiO_2/ MgAl Layered Double Hydroxides Mechanical Mixtures as Efficient Photocatalysts in Phenol Degradation. In: *Journal of Physics and Chemistry of Solids*. 2011, vol. 72, No. 8, pp. 914–919. doi: 10.1016/j.jpcs.
15. MASCOLO, G. and MASCOLO, M.C. (2015). On the Synthesis of Layered Double Hydroxides (LDHs) by Reconstruction Method Based on the 'Memory Effect'. In: *Microporous and Mesoporous Materials*. 2015, vol. 214, pp. 246–248. doi: 10.1016/j.micromeso.
16. LU, X., MENG, L., LI, H., DU, N., ZHANG, R. and HOU, W. (2013). Facile Fabrication of Ibuprofen-LDH Nanohybrids via a Delamination/ Reassembling Process. In: *Materials Research Bulletin*. 2013, vol. 48, pp. 1512–1517. doi: 10.1016/j.materresbull.2012.12.057.
17. ZENG, H., DENG, X., WANG, Y. and LIAO, K. (2009). Preparation of Mg-Al Hydrotalcite by Urea Method and Its Catalytic Activity for Transesterification. In: *AIChE Journal*. 2009, vol. 55, No. 5, pp. 1229–1235. doi: 10.1002/aic.
18. SHARMA, S.K., KUSHWAHA, P.K., SRIVASTAVA, V.K., BHATT, S.D. and JASRA, R.V. (2007). Effect of Hydrothermal Conditions on Structural and Textural Properties of Synthetic Hydrotalcites of Varying Mg/Al Ratio. In: *Industrial and Engineering Chemistry Research*. 2007, vol. 3, pp. 4856–4865. doi: 10.1021/ie061438w.
19. SALOMAO, R., MILENA, L.M., WAKAMATSU, M.H. and PANDOLFELLI, V.C. (2011). Hydrotalcite Synthesis via Co-Precipitation Reactions Using MgO and $Al(OH)_3$ Precursors. In: *Ceramics International*. 2011, vol. 37, pp. 3063–3070. doi: 10.1016/j.ceramint.2011.05.034.
20. CHUBAR, N., GILMOUR, R., GERDA, V., MIČUŠÍK, M., OMASTOVÁ, M., HEISTER, K., MAN, P., FRAISSARD, J. and ZAITSEV, V. (2017). Layered Double Hydroxides as the Next Generation Inorganic Anion Exchangers: Synthetic Methods Versus Applicability. In: *Advances in Colloid and Interface Science*. 2017, vol. 245, No. April, pp. 62–80. doi: 10.1016/j.cis.
21. PANDA, H.S., SRIVASTAVA, R. and BAHADUR, D. (2008). Stacking of Lamellae in Mg/Al Hydrotalcites: Effect of Metal Ion Concentrations on Morphology. In: *Materials Research Bulletin*. 2008, vol. 43, pp. 1448–1455. doi: 10.1016/j.materresbull.

22. SMALENSKAITE, A., VIEIRA, D.E.L., SALAK, A.N., FERREIRA, M.G.S., KATELNIKOVAS, A. and KAREIVA, A. (2017). A Comparative Study of Co-Precipitation and Sol-Gel Synthetic Approaches to Fabricate Cerium-Substituted Mg/Al Layered Double Hydroxides with Luminescence Properties. In: *Applied Clay Science*. 2017, vol. 143, pp. 175–183. doi: 10.1016/j.clay.
23. BUDHYSUTANTO, W.N., KRAMER, H.J.M., VAN AGTERVELD, D., TALMA, A.G. and JANSENS, P.J. (2010). Pre-Treatment of Raw Materials for the Hydrothermal Synthesis of Hydrotalcite-like Compounds. In: *Chemical Engineering Research and Design*. 2010, vol. 88, No. 11, pp. 1445–1449. doi: 10.1016/J.CHERD.2009.10.010.
24. LIAO, L., ZHAO, N. and XIA, Z. (2012). Hydrothermal Synthesis of Mg-Al Layered Double Hydroxides (LDHs) from Natural Brucite and $Al(OH)_3$. In: *Materials Research Bulletin*. 2012, vol. 47, No. 11, pp. 3897–3901. doi: 10.1016/j.materresbull.
25. WANG, Y., LUO, S., WANG, Z. and FU, Y. (2013). Structural and Textural Evolution of Nanocrystalline Mg-Al Layered Double Hydroxides during Mechanical Treatment. In: *Applied Clay Science*. 2013, vol. 80–81, pp. 334–339. doi: 10.1016/j.clay.
26. BANKAUSKAITE, A. and BALTAKYS, K. (2011). The Hydrothermal Synthesis of Hydrotalcite by Using Different Partially Soluble and Insoluble in Water Magnesium and Aluminium Components. In: *Science of Sintering*. 2011, vol. 43, No. 3, pp. 261–275. doi: 10.2298/SOS1103261B.
27. XU, Z. P., QING, G. and LU, M. (2005). Hydrothermal Synthesis of Layered Double Hydroxides (LDHs) from Mixed MgO and Al_2O_3: LDH Formation Mechanism. In: *Chemistry of Materials*. 2005, No. 2, pp. 1055–1062. doi: 10.1021/cm048085g.
28. FAHAMI, A. and BEALL, G.W. (2016). Mechanosynthesis and Characterization of Hydrotalcite like Mg-Al-SO_4-LDH. In: *Materials Letters*. 2016, vol. 165, pp. 192–195. doi: 10.1016/j.matlet.
29. FAHAMI, A., AL-HAZMI, F.S., AL-GHAMDI, A.A., MAHMOUD, W.E. and BEALL, G.W. Structural Characterization of Chlorine Intercalated Mg-Al Layered Double Hydroxides: A Comparative Study between Mechanochemistry and Hydrothermal Methods. In: *Journal of Alloys and Compounds*. 2016, vol. 683, pp. 100–107. doi: 10.1016/j.jallcom.
30. ZHANG, F., DU, N., SONG, S., LIU, J. and HOU, W. (2013). Mechano-Hydrothermal Synthesis of Mg_2Al–NO_3 Layered Double Hydroxides. In: *Journal of Solid State Chemistry*. 2013, vol. 206, No. 3, pp. 45–50. doi: 10.1016/j.jssc.
31. ZHANG, F., DU, N., LI, H., LIU, J. and HOU, W. (2014). Synthesis of Mg–Al–Fe–NO_3 Layered Double Hydroxides via a Mechano-Hydrothermal Route. In: *Solid State Sciences*. 2014, vol. 32, No. 3, pp. 41–47. doi: 10.1016/j.solidstatesciences.
32. BENITO, P., HERRERO, M., LABAJOS, F.M. and RIVES, V. (2010). Effect of Post-Synthesis Microwave-Hydrothermal Treatment on the Properties of Layered Double Hydroxides and Related Materials. In: *Applied Clay Science*. 2010, vol. 48, No. 1–2, pp. 218–227. doi: 10.1016/j.clay.

33. TAO, Y., ZHU, H., LI, R., LI, Z., LIU, J., WANG, G. and GU, Z. (2013). Microwave Synthesis of Nickel/Cobalt Double Hydroxide Ultrathin Flowerclusters with Three-Dimensional Structures for High-Performance Supercapacitors. In: *Electrochimica Acta*. 2013, vol. 111, pp. 71–79. doi: 10.1016/j.electacta.
34. PRAKRUTHI, H.R., JAI PRAKASH, B.S. and BHAT, Y.S. (2015). Microwave Assisted Synthesis of Glycerol Carbonate over LDH Catalyst: Activity Restoration through Rehydration and Reconstruction. In: *Journal of Molecular Catalysis A: Chemical*. 2015, vol. 408, pp. 214–220. doi: 10.1016/j.molcata.
35. KULYUKHIN, S.A. and KRASAVINA, E.P. (2016). Sorption of U(VI) onto Layered Double Hydroxides and Oxides of Mg and Al, Prepared Using Microwave Radiation. In: *Radiochemistry*. 2016, vol. 58, No. 4, pp. 405–408. doi: 10.1134/S1066362216040093.
36. HE, J., WEI, M., LI, B., KANG, Y., EVANS, D.G. and DUAN, X. (2006). Preparation of Layered Double Hydroxides. In: *Layered Double Hydroxides*. 2006, vol. 119, pp. 89–119. doi: 10.1007/430_006.
37. MENG, Z., ZHANG, Y., ZHANG, Q., CHEN, X., LIU, L., KOMARNENI, S. and LV, F. (2017). Novel Synthesis of Layered Double Hydroxides (LDHs) from Zinc Hydroxide. In: *Applied Surface Science*. 2017, vol. 396, pp. 799–803. doi: 10.1016/j.apsusc.
38. THOMAS, G.S., RADHA, A.V., KAMATH, P.V. and KANNAN, S. (2006). Thermally Induced Polytype Transformations among the Layered Double Hydrodides (LDHs) of MgZn with Al. In: *Journal of Physical Chemistry B*. 2006, vol. 110, No. 25, pp. 12365–12371. doi: 10.1021/jp061377f.
39. FORANOA, C., HIBINO, T., LEROUX, F. and TAVIOT-GUÉHO, C. (2006). Chapter 13.1 Layered Double Hydroxides. In: *Developments in Clay Science*. 2006, vol. 1, pp. 1021–1095. doi: 10.1016/S1572-4352(05)01039-1.
40. WANG, D., ZHANG, X., LIU, CH., CHENG, T.T., WEI, W. and SUN, Y. (2015). Transition Metal-Modified Mesoporous Mg-Al Mixed Oxides: Stable Base Catalysts for the Synthesis of Diethyl Carbonate from Ethyl Carbamate and Ethanol. In: *Applied Catalysis A: General*. 2015, vol. 505, pp. 478–486. doi: 10.1016/j.apcata.
41. ZHANG, Z., LIAO, M., ZENG, H.Y., XU, S., LIU, X., DU, J., ZHU, P. and HUANG, Q. (2014). Temperature Effect on Chromium(VI) Removal by Mg/Al Mixed Metal Oxides as Adsorbents. In: *Applied Clay Science*. 2014, vol. 102, pp. 246–253. doi: 10.1016/j.clay.
42. COSANO, D., ESQUINAS, C., JIMÉNEZ-SANCHIDRIÁN, C. and RUIZ, J.R. (2016). Use of Raman Spectroscopy to Assess the Efficiency of MgAl Mixed Oxides in Removing Cyanide from Aqueous Solutions. In: *Applied Surface Science*. 2016, vol. 364, pp. 428–433. doi: 10.1016/j.apsusc.
43. KOVANDA, F., ROJKA, T., BEZDIČKA, P., JIRÁTOVÁ, K., OBALOVÁ, L., PACULTOVÁ, K., BASTL, Z. and GRYGAR, T. (2009). Effect of Hydrothermal Treatment on Properties of Ni-Al Layered Double Hydroxides and Related Mixed Oxides. In: *Journal of Solid State Chemistry*. 2009, vol. 182, No. 1, pp. 27–36. doi: 10.1016/j.jssc.

44. ZHANG, Z., LIAO, M., ZENG, H.Y., XU, S., LIU, X., DU, J., ZHU, P. and HUANG, Q. (2014). Temperature Effect on Chromium (VI) Removal by Mg/Al Mixed Metal Oxides as Adsorbents. In: *Applied Clay Science*. 2014, vol. 102, pp. 246–253. doi: 10.1016/j.clay.
45. COSANO, D., ESQUINAS, C., JIMÉNEZ-SANCHIDRIÁN, C. and RUIZ, J.R. (2016). Use of Raman Spectroscopy to Assess the Efficiency of MgAl Mixed Oxides in Removing Cyanide from Aqueous Solutions. In: *Applied Surface Science*. 2016, vol. 364, pp. 428–433. doi: 10.1016/j.apsusc.
46. WANG, D., ZHANG, X., LIU, CH., CHENG, T.T., WEI, W. and SUN, Y. (2015). Transition Metal-Modified Mesoporous Mg-Al Mixed Oxides: Stable Base Catalysts for the Synthesis of Diethyl Carbonate from Ethyl Carbamate and Ethanol. In: *Applied Catalysis A: General*. 2015, vol. 505, pp. 478–486. doi: 10.1016/j.apcata.
47. KOWALIK, P., KONKOL, M., KONDRACKA, M., PRÓCHNIAK, W., BICKI, R. and WIERCIOCH, P. (2013). Memory Effect of the CuZnAl-LDH Derived Catalyst Precursor – *In Situ* XRD Studies. In: *Applied Catalysis A: General*. 2013, vol. 464–465, pp. 339–347. doi: 10.1016/j.apcata.
48. BASTIANI, R., ZONNO, I.V., SANTOS, I.A.V., HENRIQUES, C.A. and MONTEIRO, J.L.F. (2004). Influence of Thermal Treatments on the Basic and Catalytic Properties of Mg,Al-Mixed Oxides Derived from Hydrotalcites. In: *Brazilian Journal of Chemical Engineering*. 2004, vol. 21, No. 2, pp. 193–202. ISSN 0104-6632.
49. BANKAUSKAITE, A., BALTAKYS, K. and MEZINSKIS, G. (2014). Modified Hydrotalcites Application as Precursors for (Na, K)Mg/Al Spinel-Type Compounds Formation. In: *Journal of Thermal Analysis and Calorimetry*. 2014, vol. 118, No. 2, pp. 711–718. doi: 10.1007/s10973-014-3737-z.
50. BASĄG, S., KOVANDA, F., PIWOWARSKA, Z., KOWALCZYK, A., PAMIN, K. and CHMIELARZ, L. (2017). Hydrotalcite-Derived Co-Containing Mixed Metal Oxide Catalysts for Methanol Incineration : Role of Cobalt Content, Mg/Al Ratio and Calcination Temperature. In: *Journal of Thermal Analysis and Calorimetry*. 2017, vol. 129, No. 3, pp. 1301–1311. doi: 10.1007/s10973-017-6348-7.
51. KOMARNENI, S. and STOUT, S. (2002). A Microwave-Assisted Method for the Rapid Removal of Potassium from Phlogopite. In: *Clays Clay Miner*. 2002, vol. 50, pp. 248–253. doi: 10.1346/000986002760832847.
52. RIVERA, J.A., FETTER, G. and BOSCH, P. (2006). Microwave Power Effect on Hydrotalcite Synthesis. In: *Microporous and Mesoporous Materials*. 2006, vol. 89, No. 1–3, pp. 306–314. doi: 10.1016/j.micromeso.
53. BENITO, P., LABAJOS, F.M., ROCHA, J. and RIVES, V. (2006). Influence of Microwave Radiation on the Textural Properties of Layered Double Hydroxides. In: *Microporous and Mesoporous Materials*. 2006, vol. 94, No. 1–3, pp. 148–158. doi: 10.1016/j.micromeso.
54. HERRERO, M., BENITO, P., LABAJOS, F.M. and RIVES, V. (2007). Nanosize Cobalt Oxide-Containing Catalysts Obtained through Microwave-Assisted

Methods. In: *Catalysis Today*. 2007, vol. 128, No. 3–4, pp. 129–137. doi: 10.1016/j.cattod.
55. BENITO, P., LABAJOS, F.M. and RIVES, V. (2006). Microwave-Treated Layered Double Hydroxides Containing Ni^{2+} and Al^{3+}: The Effect of Added Zn^{2+}. In: *Journal of Solid State Chemistry*. 2006, vol. 179, No. 12, pp. 3784–3797. doi: 10.1016/j.jssc.
56. CROSS, H.E., PARKES, G. and BROWN, D.R. (2012). Microwave Calcination of Cu/Mg/Al Hydrotalcite Catalyst Precursor. In: *Applied Catalysis A: General*. 2012, vol. 429–430, pp. 24–30. doi: 10.1016/j.apcata.2012.03.046.
57. TAKEHIRA, K. (2017). Recent Development of Layered Double Hydroxide-Derived Catalysts − Rehydration, Reconstitution, and Supporting, Aiming at Commercial Application. In: *Applied Clay Science*. 2017, vol. 136, pp. 112–141. doi: 10.1016/j.clay.
58. PEROTTI, G.F., BARUD, H.S., RIBEIRO, S.J.L. and CONSTANTINO, V.R.L. (2014). Bacterial Cellulose as a Template for Preparation of Hydrotalcite-like Compounds. *Journal of the Brazilian Chemical Society*. 2014, vol. 25, No. 9, pp. 1647–1655. doi: 10.5935/0103-5053.20140153.
59. BASAHEL, S.N., AL-THABAITI, S., NARASIMHARAO, K., AHMED, N.S. and MOKHTAR, M. (2014). Nanostructured Mg–Al Hydrotalcite as Catalyst for Fine Chemical Synthesis. In: *Journal of Nanoscience and Nanotechnology*. 2014, vol. 14, No. 2, pp. 1931–1946. doi: 10.1166/jnn.
60. SAJID, M. and BASHEER, CH. (2016). Layered Double Hydroxides: Emerging Sorbent Materials for Analytical Extractions. In: *TrAC Trends in Analytical Chemistry*. 2016, vol. 75, pp. 174–182. doi: 10.1016/J.TRAC.
61. ASHEKUZZAMAN, S.M. and JIANG, J.Q. (2014). Study on the Sorption-Desorption-Regeneration Performance of Ca-, Mg- and CaMg-Based Layered Double Hydroxides for Removing Phosphate from Water. In: *Chemical Engineering Journal*. 2014, vol. 246, pp. 97–105. doi: 10.1016/j.cej.
62. EZEH, C.I., HUANG, X., YANG, X., SUN, CH. and WANG, J. (2017). Sonochemical Surface Functionalization of Exfoliated LDH: Effect on Textural Properties, CO_2 Adsorption, Cyclic Regeneration Capacities and Subsequent Gas Uptake for Simultaneous Methanol Synthesis. In: *Ultrasonics Sonochemistry*. 2017, vol. 39, pp. 330–343. doi: 10.1016/j.ultsonch.
63. WANG, Y., LI, Q., BO, L., WANG, X., ZHANG, T., LI, S., REN, P. and WEI, G. (2016). Synthesis and Oil Absorption of Biomorphic MgAl Layered Double Oxide/Acrylic Ester Resin by Suspension Polymerization. In: *Chemical Engineering Journal*. 2016, vol. 284, pp. 989–994. doi: 10.1016/j.cej.
64. BANKAUSKAITE, A. and BALTAKYS, K. (2015). Thermal, Texture and Reconstruction Properties of Hydrotalcites Substituted with Na^+ or K^+ Ions. In: *Journal of Thermal Analysis and Calorimetry*. 2015, vol. 121, No. 1, pp. 227–233. doi: 10.1007/s10973-015-4499-y.
65. LV, L., HE, J., WEI, M., EVANS, D.G., DUAN, X. (2006). Factors Influencing the Removal of Fluoride from Aqueous Solution by Calcined Mg–Al–CO_3 Layered Double Hydroxides. In: *Journal of Hazardous Materials*. 2006, vol. 133, No. 1–3, pp. 119–128. doi: 10.1016/j.jhazmat.

66. STANIMIROVA, T.S., KIROV, G. and DINOLOVA, E. (2001). Mechanism of Hydrotalcite Regeneration. In: *Journal of Materials Science Letters*. 2001, vol. 20, No. 5, pp. 453–455. doi: 10.1023/A: 1010914900966.
67. ANGELESCU, E., PAVEL, O. D., BÎRJEGA, R., FLOREA, M. and ZĂVOIANU, R. (2008). The Impact of the 'Memory Effect' on the Catalytic Activity of Mg/Al; Mg,Zn/Al; Mg/Al,Ga Hydrotalcite-like Compounds Used as Catalysts for Cycloxene Epoxidation. In: *Applied Catalysis A: General*. 2008, vol. 341, No. 1–2, pp. 50–57. doi: 10.1016/j.apcata.
68. PAVEL, O.D., BÎRJEGA, R., CHE, M., COSTENTIN, G., ANGELESCU, E. and ŞERBAN, S. (2008). The Activity of Mg/Al Reconstructed Hydrotalcites by 'Memory Effect' in the Cyanoethylation Reaction. In: *Catalysis Communications*. 2008, vol. 9, No. 10, pp. 1974–1978. doi: 10.1016/j.catcom.
69. LIN, Y., FANG, Q. and CHEN, B. (2014). Metal Composition of Layered Double Hydroxides (LDHs) Regulating ClO^-_4 Adsorption to Calcined LDHs via the Memory Effect and Hydrogen Bonding. In: *Journal of Environmental Sciences (China)*. 2014, vol. 26, No. 3, pp. 493–501. doi: 10.1016/S1001-0742(13)60462-3.
70. RIVES, V., CARRIAZO, D. and MARTIN, C. (2010). Heterogeneous Catalysis by Polyoxometalate-Intercalated Layered Double Hydroxides. In: *Pillared Clays and Related Catalysts*. 2010, pp. 319–397. ISBN: 978-1-4419-6669-8
71. ZHAO, Q., TIAN, S., YAN, L., ZHANG, Q. and NING, P. (2015). Novel HCN Sorbents Based on Layered Double Hydroxides: Sorption Mechanism and Performance. In: *Journal of Hazardous Materials*. 2015, vol. 285, pp. 250–258. doi: 10.1016/j.jhazmat.
72. OKADA, K., YOSHIZAKI, H., KAMESHIMA, Y. and NAKAJIMA, A. (2008). Effect of the Crystallinity of Kaolinite Precursors on the Properties of Mesoporous Silicas. In: *Applied Clay Science*. 2008, vol. 41, No. 1–2, pp. 10–16. doi: 10.1016/j.clay.
73. LADEWIG, K., NIEBERT, M., XU, Z.P., GRAY, P.P. and LU, G.Q. (2010). Controlled Preparation of Layered Double Hydroxide Nanoparticles and Their Application as Gene Delivery Vehicles. In: *Applied Clay Science*. 2010, vol. 48, No. 1–2, pp. 280–289. doi: 10.1016/j.clay.
74. CHEN, J.J., THOMAS, J.J., TAYLOR, H.F.W. and JENNINGS, H.M. (2002). Solubility and Structure of Calcium Silicate Hydrate. In: *Cement and Concrete Research*. 2002, vol. 34, No. 9, pp. 1499–1519.
75. JEFFREY, J.CH., JEFFREY, J., THOMAS, H.F.W., TAYLOR, J. and HAMLIN, M. (2004). Solubility and Structure of Calcium Silicate Hydrate. In: *Cement and Concrete Research.* 2004, vol. 34, No. 9, pp. 1499–1519. doi: 10.1016/j.cemconres.2004.04.034
76. NONAT, A. (2004). The Structure and Stoichiometry of C-S-H. In: *Cement and Concrete Research.* 2004, vol. 34, No. 9, pp. 1521–1528. doi: 10.1016/j.cemconres.2004.04.035.
77. GARD, J.A., TAYLOR, H.F.W. (1976). Calcium Silicate Hydrate (H). In: *Cement and Concrete Research*. 1976, vol. 6, No. 5, p. 667–677. doi: 10.1016/0008-8846(76)90031-4.

78. RICHARDSON, I.G. (2008). The Calcium Silicate Hydrates. In: *Cement and Concrete Research*. 2008, vol. 38, No. 2, pp. 137–158. doi: 10.1016/j.cemconres.2007.11.005
79. BONACCORSI, E., MERLINO, S. and TAYLOR, H.F.W. (2004). The Crystal Structure of Jennite, $Ca_9Si_6O_{18}(OH)_6 \cdot 8H_2O$. In: *Cement and Concrete Research*. 2004, vol. 34, No. 9, pp. 1481–1488. doi: 10.1016/j.cemconres.
80. TAYLOR, H.F.W. (1986). Proposed Structure for Calcium Silicate Hydrate Gel. In: *Journal of the American Ceramic Society*. 1986, vol. 96, No. 6, pp. 464–467. doi: 10.1111/j.1151-2916.1986.tb07446.x.
81. BONACCORSI, E., MERLINO, S. and TAYLOR, H.F.W. (2004). The Crystal Structure of Jennite, $Ca_9Si_6O_{18}(OH)_6 \cdot 8H_2O$. In: *Cement and Concrete Research.* 2004, vol. 34, No. 9, pp. 1481–1488. doi: 10.1016/j.cemconres.2003.12.033.
82. MITSUDA, T. and TAYLOR, H.F.W. (1975). Influence of Aluminium on the Conversion of Calcium Silicate Hydrate Gels into 11 Å Tobermorite at 90°C and 120°C. In: *Cement and Concrete Research.* 1975, vol. 5, No. 3, pp. 203–209. doi: 10.1016/0008-8846(75)90001-0.
83. KURCZYK, H.G. and SCHWIETE, H.E. (1962). Concerning the Hydration Productrs of C3S and β-C2S. In: *Proceedings of the 4th International Symposium on the Chemistry of Cement*. 1962, vol. 1, pp. 349–358.
84. STADE, H. and WIEKER, W. (1980). On the Structure of Ill-Crystallized Calcium Hydrogen Silicates. I. Formation and Properties of an Ill-Crystallized Calcium Hydrogen Disilicate Phase. In: *Zeitschrift für anorganische und allgemeine Chemie*. 1980, vol. 466, pp. 55–70. ISSN: 1521-3749.
85. RICHARDSON, I.G. (2004). Tobermorite/Jennite- and Tobermorite/Calcium Hydroxide-Based Models for the Structure of C-S-H: Applicability to Hardened Pastes of Tricalcium Silicate, β-Dicalcium Silicate, Portland Cement, and Blends of Portland Cement with Blast-Furnace Slag, Metakaol. In: *Cement and Concrete Research*. 2004, vol. 34, No. 9, pp. 1733–1777. doi: 10.1016/j.cemconres.
86. ILJINA, A., BALTAKYS, K. and EISINAS, A. (2015). The Influence of Hydrothermal Treatment Duration on Gyrolite Synthesis. In: *Romanian Journal of Materials*. 2015, vol. 45, No. 4, pp. 331–340.
87. STUMM, A., GARBEV, K., BEUCHLE, G., BLACK, L., STEMMERMANN, P. and NÜESCH, R. (2005). Incorporation of Zinc into Calcium Silicate Hydrates, Part I: Formation of C-S-H(I) with C/S=2/3 and Its Isochemical Counterpart Gyrolite. In: *Cement and Concrete Research*. 2005, vol. 35, No. 9, pp. 1665–1675. doi: 10.1016/j.cemconres.
88. FLINT, E.P., MCMURDIE, H.F. and WELLS, L.S. (1938). Formation of Hydrated Calcium Silicate at Elevated Temperatures and Pressures. In: *Journal of Research of the National Bureau of Standards*. 1938, vol. 21, pp. 617–638.
89. KALOUSEK, G.L. and NELSON, E.B. (1978). Hydrothermal Reactions of Dicalcium Silicate and Silica. In: *Cement and Concrete Research*. 1978, vol. 8, No. 3, pp. 283–289. doi: 10.1016/0008-8846(78)90097-2.
90. OKADA, Y., FANG, Y., ISHIDA, H. and NISHIDO, H. (1994). Dehydration Processes of Gyrolite. In: *Journal of the Ceramic Society of Japan*. 1994, vol. 102, pp. 449–455.

91. OKADA, Y., MASUDA, T., ISHIDA, H. (1995). Behavior of Silicate Anions on the Formation Processes of Gyrolite Followed by 29Si NMR. In: *Journal of the Ceramic Society of Japan*. 1995, vol. 103, No. 2, pp. 124–127.
92. SIAUCIUNAS, R. and BALTAKYS, K. (2004). Formation of Gyrolite during Hydrothermal Synthesis in the Mixtures of CaO and Amorphous SiO_2 or Quartz. In: *Cement and Concrete Research*. 2004, vol. 34, No. 11, pp. 2029–2036. doi: 10.1016/j.cemconres.
93. SHAW, S.S., HENDERSON, M.B. and CLARK, S.M. (2002). In-Situ Synchrotron Study of the Kinetics, Thermodynamics, and Reaction Mechanisms of the Hydrothermal Crystallization of Gyrolite, $Ca_{16}Si_{24}O_{60}(OH)_8 \cdot 14H_2O$. In: *American Mineralogist*. 2002, vol. 87, pp. 533–541. doi: 10.2138/am-2002-0416.
94. BALTAKYS, K. and SIAUCIUNAS, R. (2007). The Influence of Stirring and γ-Al_2O_3 or Na_2O Additives on the Gyrolite Formation in the CaO–Quartz–H_2O System. In: *Ceramics Silikaty*. 2007, vol. 51, No. 2, pp. 106–111.
95. BALTAKYS, K. and SIAUCIUNAS, R. (2010). Influence of Gypsum Additive on the Gyrolite Formation Process. In: *Cement and Concrete Research*. 2010, vol. 40, No. 3, pp. 376–383. doi: 10.1016/j.cemconres.
96. RÓŻYCKA, A., KOTWICA, Ł. and MAŁOLEPSZY, J. (2014). Synthesis of Single Phase Gyrolite in the CaO-Quartz-Na_2O-H_2O System. In: *Materials Letters*. 2014, vol. 120, pp. 166–169. doi: 10.1016/j.matlet.
97. EISINAS, A. (2013). Girolito sandaros ypatybės ir panaudojimas: daktaro disertacija/doctoral thesis. Kaunas University of Technology. Kaunas: Technologija.
98. ILJINA, A. (2017). Neutralization of AlF_3 Production Waste and Its Application for the Hydrothermal Synthesis of C-S-H: doctoral dissertation. Kaunas University of Technology. Kaunas: Technologija.
99. TEODOSIU, C., BARJOVEANU, G., SLUSER, B.R., POPA, S.A.E. and TROFIN, O. (2016). Environmental Assessment of Municipal Wastewater Discharges: a Comparative Study of Evaluation Methods. In: *International Journal of Life Cycle Assessment*. 2016, vol. 21, No. 3, pp. 395–411. doi: 10.1007/s11367-016-1029-5.
100. GOVIND, P. (2014). Heavy Metals Causing Toxicity in Animals and Fishes. In: *Research Journal of Animal Res. J. Animal, Veterinary and Fishery Sci. International Science Congress Association*. 2014, vol. 2, No. 2, pp. 17–23.
101. DIXIT, R, WASIULLAH, MALAVIYA, D., PANDIYAN, K., SINGH, U.B., SAHU, A., SHUKLA, R., SINGH, B.P., RAI, J.P., SHARMA, P.K., LADE, H. and PAUL, D. (2015). Bioremediation of Heavy Metals from Soil and Aquatic Environment: an Overview of Principles and Criteria of Fundamental Processes. In: *Sustainability (Switzerland)*. 2015, vol. 7, No. 2, pp. 2189–2212. doi: 10.3390/su7022189.
102. MOHALLAL, E. and FAUNA, S. (2015). Concentration of Heavy Metals in the Tissues of Spiny Mouse as Bio-Indicators of Pollution under Different Environmental Conditions in Egypt. In: *Egyptian Journal of Desert Research*. 2015, vol. 65, No. 1, pp. 63–76.

103. GUNATILAKE, S.K. (2015). Methods of Removing Heavy Metals from Industrial Wastewater. In: *Journal of Multidisciplinary Engineering Science Studies*. 2015, vol. 1, No. 1, pp. 12–18. doi: 10.13140/RG.2.1.3751.1848.
104. BARAKAT, M.A. (2011). New Trends in Removing Heavy Metals from Industrial Wastewater. In: *Arabian Journal of Chemistry*. 2011, vol. 4, No. 4, pp. 361–377. doi: 10.1016/j.arabjc.
105. BANKAUSKAITE, A., EISINAS, A. BALTAKYS, K., ZADAVICIUTE, S. (2015). A Study on the Intercalation of Heavy Metal Ions in a Wastewater by Synthetic Layered Inorganic Adsorbents. In: *Desalination and Water Treatment*. Philadelphia, PA: Taylor & Francis. 2015, vol. 56, No. 6, pp. 1576-1586. ISSN 1944-3994.
106. ZAWIERUCHA, I, KOZLOWSKI, C. and MALINA, G. (2016). Immobilized Materials for Removal of Toxic Metal Ions from Surface/Groundwaters and Aqueous Waste Streams. In: *Environ. Sci.: Processes Impacts*. 2016, vol. 18, No. 4, pp. 429–444. doi: 10.1039/C5EM00670H.
107. IGBERASE, E., OSIFO, P. and OFOMAJA, A. (2017). The Adsorption of Pb, Zn, Cu, Ni, and Cd by Modified Ligand in a Single Component Aqueous Solution: Equilibrium, Kinetic, Thermodynamic, and Desorption Studies. In: *International Journal of Analytical Chemistry*. 2017, vol. 2017. doi: 10.1155/2017/6150209.
108. ZAWIERUCHA, I., KOZLOWSKI, C. and MALINA, G. (2016). Immobilized Materials for Removal of Toxic Metal Ions from Surface/Groundwaters and Aqueous Waste Streams. In: *Environ. Sci.: Processes Impacts*. 2016, vol. 18, No. 4, pp. 429–444. doi: 10.1039/C5EM00670H.
109. BUASRI, A., CHAIYUT, N., TAPANG, K., JAROENSIN, S. and PANPHROM, S. (2012). Biosorption of Heavy Metals from Aqueous Solutions Using Water Hyacinth as a Low Cost Biosorbent. In: *Civil and Environmental Research*. 2012, vol. 2, No. 2, pp. 17–25.
110. VARMA, G.V., SINGH, R.K. and SAHU, V. (2013). A Comparative Study on the Removal of Heavy Metals by Adsorption Using Fly Ash and Sludge: a Review. In: *International Journal of Application or Innovation in Engineering & Management*. 2013, vol. 2, No. 7, pp. 45–56.
111. DE GISI, S., LOFRANO, G., GRASSI, M. and NOTARNICOLA, M. (2016). Characteristics and Adsorption Capacities of Low-Cost Sorbents for Wastewater Treatment: a Review. In: *Sustainable Materials and Technologies*. 2016, vol. 9, pp. 10–40. doi: 10.1016/j.susmat.
112. TRIPATHI, A. and RAWAT RANJAN, M. (2015). Heavy Metal Removal from Wastewater Using Low Cost Adsorbents. In: *Journal of Bioremediation & Biodegradation*. 2015, vol. 6, No. 6. doi: 10.4172/2155-6199.1000315.
113. LI, T., MIRAS, H. and SONG, Y.F. (2017). Polyoxometalate (POM)-Layered Double Hydroxides (LDH) Composite Materials: Design and Catalytic Applications. In: *Catalysts*. 2017, vol. 7, No. 9, p. 260. doi: 10.3390/catal7090260.
114. RICHETTA, M., MEDAGLIA, P.G., MATTOCCIA, A., VARONE, A. and PIZZOFERRATO, R. (2017). Layered Double Hydroxides: Tailoring

Interlamellar Nanospace for a Vast Field of Applications. In: *Journal of Material Science & Engineering*. 2017, vol. 6, No. 4. doi: 10.4172/2169-0022.1000360.
115. ZUBAIR, M., DAUD, M., MCKAY, G., SHEHZAD, F. and AL-HARTHI, M.A. (2017). Recent Progress in Layered Double Hydroxides (LDH)-Containing Hybrids as Adsorbents for Water Remediation. In: *Applied Clay Science*. 2017, vol. 143, pp. 279–292. doi: 10.1016/J.CLAY.
116. PELIGRO, F.R., PAVLOVIC, I., ROJAS, R. and BARRIGA, C. (2016). Removal of Heavy Metals from Simulated Wastewater by *In Situ* Formation of Layered Double Hydroxides. In: *Chemical Engineering Journal*. 2016, vol. 306, pp. 1035–1040. doi: 10.1016/j.cej.2016.08.054.
117. RUAN, X., CHEN, Y., CHEN, H., QIAN, G. and FROST, R.L. (2016). Sorption Behavior of Methyl Orange from Aqueous Solution on Organic Matter and Reduced Graphene Oxides Modified Ni-Cr Layered Double Hydroxides. In: *Chemical Engineering Journal*. 2016, vol. 297, pp. 295–303. doi: 10.1016/j.cej.
118. ZHANG, T., LI, Q., XIAO, H., MEI, Z., LU, H. and ZHOU, Y. (2013). Enhanced Fluoride Removal from Water by Non-Thermal Plasma Modified CeO_2/Mg-Fe Layered Double Hydroxides. In: *Applied Clay Science*. 2013, vol. 72, pp. 117–123. doi: 10.1016/j.clay.
119. ZHANG, B., DONG, Z., SUN, D., WU, T. and LI, Y. (2017). Enhanced Adsorption Capacity of Dyes by Surfactant-Modified Layered Double Hydroxides from Aqueous Solution. In: *Journal of Industrial and Engineering Chemistry*. 2017, vol. 49, pp. 208–218. doi: 10.1016/j.jiec.
120. THEISS, F.L., AYOKO, G.A. and FROST, R.L. (2016). Leaching of Iodide (I^-) and Iodate (IO_3^-) Anions from Synthetic Layered Double Hydroxide Materials. In: *Journal of Colloid and Interface Science*. 2016, vol. 478, pp. 311–315. doi: 10.1016/j.jcis.
121. RICHETTA, M., MEDAGLIA, P.G., MATTOCCIA, A., VARONE, A. and PIZZOFERRATO, R. (2017). Layered Double Hydroxides: Tailoring Interlamellar Nanospace for a Vast Field of Applications. In: *Journal of Material Science & Engineering*. 2017, vol. 6, No. 4. doi: 10.4172/2169-0022.1000360.
122. KAMEDA, T., TAKEUCHI, H. and YOSHIOKA, T. (2008). Uptake of Heavy Metal Ions from Aqueous Solution Using Mg–Al Layered Double Hydroxides Intercalated with Citrate, Malate and Tartrate. In: *Separation and Purification Technology*. 2008, vol. 62, pp. 330–336. doi: 10.1016/j.seppur.2008.02.001.
123. ZANG, Y., HOU, W. and XU, J. (2011). Removal of Cu (II) from $CuSO_4$ Aqueous Solution by Mg-Al Hydrotalcite-like Compounds. In: *Chinese Journal of Chemistry*. 2011, vol. 29, No. 4, pp. 847–852.
124. LI, Y., BI, H.Y. and ZANG, Y.B. (2013). Single and Simultaneous Sorption of Copper Ions and p-Cresol into Surfactant-Modified Hydrotalcite-like Compound with Chelating Ligand. In: *Separation and Purification Technology*. 2013, vol. 116, pp. 448–453. doi: 10.1016/j.seppur.
125. LIU, X., WU, Y., XU, Y. and GE, F. (2016). Preparation of Mg/Al Bimetallic Oxides as Sorbents: Microwave Calcination, Characterization, and Adsorption of Cr(VI). In: *Journal of Sol-Gel Science and Technology*. 2016, vol. 79, No. 1, pp. 122–132. doi: 10.1007/s10971-016-4018-z.

126. SUN, M., XIAO, Y., ZHANG, L., GAO, X., YAN, W., WANG, D. and SU, J. (2015). High Uptake of Cu^{2+}, Zn^{2+} or Ni^{2+} on Calcined MgAl Hydroxides from Aqueous Solutions: Changing Adsorbent Structures. In: *Chemical Engineering Journal*. 2015, vol. 272, pp. 17–27. doi: 10.1016/j.cej.
127. GONZÁLEZ, M.A., PAVLOVIC, I., ROJAS-DELGADO, R. and BARRIGA, C. (2014). Removal of Cu^{2+}, Pb^{2+} and Cd^{2+} by Layered Double Hydroxide-Humate Hybrid. Sorbate and Sorbent Comparative Studies. In: *Chemical Engineering Journal*. 2014, vol. 254, pp. 605–611. doi: 10.1016/j.cej.2014.05.132.
128. GONZÁLEZ, M.A., PAVLOVIC, I. and BARRIGA, C. (2015). Cu (II), Pb (II) and Cd (II) Sorption on Different Layered Double Hydroxides. A Kinetic and Thermodynamic Study and Competing Factors. In: *Chemical Engineering Journal*. 2015, vol. 269, pp. 221–228. doi: 10.1016/j.cej.2015.01.094.
129. CHEN, Y., PENG, J., XIAO, H., PENG, H., BU, L., PAN, Z., HE, Y., CHEN, F., WANG, X. and LI, S. (2017). Adsorption Behavior of Hydrotalcite-like Modified Bentonite for Pb^{2+}, Cu^{2+} and Methyl Orange Removal from Water. In: *Applied Surface Science*. 2017, vol. 420, pp. 773–781. doi: 10.1016/j.apsusc.
130. YANG, F., SUN, S., CHEN, X., CHANG, Y., ZHA, F. and LEI, Z. (2016). Mg-Al Layered Double Hydroxides Modified Clay Adsorbents for Efficient Removal of Pb^{2+}, Cu^{2+} and Ni^{2+} from Water. In: *Applied Clay Science*. 2016, vol. 123, pp. 134–140. doi: 10.1016/j.clay.
131. PELIGRO, F.R., PAVLOVIC, I., ROJAS, R. and BARRIGA, C. (2016). Removal of Heavy Metals from Simulated Wastewater by *In Situ* Formation of Layered Double Hydroxides. In: *Chemical Engineering Journal*. 2016, vol. 306, pp. 1035–1040. doi: 10.1016/j.cej.
132. ZHAO, J., ZHU, Y.J., WU, J., ZHENG, J.Q., ZHAO, X.Y., LU, B.Q. and CHEN, F. (2014). Chitosan-Coated Mesoporous Microspheres of Calcium Silicate Hydrate: Environmentally Friendly Synthesis and Application as a Highly Efficient Adsorbent for Heavy Metal Ions. In: *Journal of Colloid and Interface Science*. 2014, vol. 418, pp. 208–215. doi: 10.1016/j.jcis.
133. WU, J., ZHU, Y.J., CAO, S.W. and CHEN, F. (2010). Hierachically Nanostructured Mesoporous Spheres of Calcium Silicate Hydrate: Surfactant-Free Sonochemical Synthesis and Drug-Delivery System with Ultrahigh Drug-Loading Capacity. In: *Advanced Materials*. 2010, vol. 22, No. 6, pp. 749–753. doi: 10.1002/adma.
134. ILJINA, A., BALTAKYS, K. and EISINAS, A. (2015). Gyrolite Adsorption of Zn^{2+} Ions in Acidic and Alkaline Solutions. In: *Materials Science.* 2015, vol. 21, No. 1, pp. 123–128. doi: 10.5755/j01.ms.21.1.5703.
135. BANKAUSKAITE, A. and BALTAKYS, K. (2009). The Sorption of Copper Ions by Gyrolite in Alkaline Solution. In: *SCIENCE-POLAND, Materials.* 2009, vol. 27, No. 3, pp. 899–908.
136. KASPERAVICIUTE, V., BALTAKYS, K. and SIAUCIUNAS, R. (2008). The Sorption Properties of Gyrolite for Copper Ions. In: *Ceramics – Silikaty*. 2008, vol. 52, No. 2, pp. 95–101.

137. BALTAKYS, K., SIAUCIUNAS, R. and EISINAS, A. (2014). The Effect of Gyrolite Substituted with Cadmium Ions on the Hydration Kinetics of OPC at Early Stages. In: *Advances in Cement Research*. 2014, vol. 26, No. 1, pp. 1–10. ISSN: 0951-7197
138. BALTAKYS, K., EISINAS, A., BARAUSKAS, I., PRICHOCKIENE, E. and ZALECKAS, E. (2012). Removal of Zn(II), Cu(II) and Cd(II) from Aqueous Solution Using Gyrolite. In: *Journal of Scientific and Industrial Research*. 2012, vol. 71, pp. 566–572.
139. ILJINA, A., BALTAKYS, K. and EISINAS, A. (2016). The Effect of Gyrolite Structure Properties on Zn^{2+} Ion Adsorption. In: *Desalination and Water Treatment*. 2016, Vol. 57, No. 4, pp. 1756–1765. doi: 10.1080/19443994.
140. BANKAUSKAITE, A. (2014). Hidrotalcito hidroterminė sintezė, savybės ir panaudojimas: daktaro disertacija/ doctoral dissertation. Kaunas University of Technology. Kaunas: Technologija.
141. EUROPEAN COMMITTEE FOR STANDARDIZATION. (2010). *European Standard. Building Lime – Part 2: Test Methods*. LST EN 459-2:2010.
142. SIMONIN, J.P. (2016). On the Comparison of Pseudo-First Order and Pseudo-Second Order Rate Laws in the Modeling of Adsorption Kinetics. In: *Chemical Engineering Journal*. 2016, vol. 300, pp. 254–263. doi: 10.1016/j.cej.
143. RODRIGUES, A.E. and SILVA, C.M. (2016). What's Wrong with Lagergreen Pseudo First Order Model for Adsorption Kinetics? In: *Chemical Engineering Journal*. 2016, vol. 306, pp. 1138–1142. doi: 10.1016/j.cej.
144. HO, Y.S. (2006). Review of Second-Order Models for Adsorption Systems. In: *Journal of Hazardous Materials*. 2006, vol. 136, No. 3, pp. 681–689. doi: 10.1016/j.jhazmat.
145. SIMONIN, J.P. (2016). On the Comparison of Pseudo-First Order and Pseudo-Second Order Rate Laws in the Modeling of Adsorption Kinetics. In: *Chemical Engineering Journal*. 2016, vol. 300, pp. 254–263. doi: 10.1016/j.cej.
146. LAZAUSKAS, A. and GRIGALIŪNAS, V. (2012). Float Glass Surface Preparation Methods for Improved Chromium Film Adhesive Bonding. In: *Materials Science*. 2012, vol. 18, pp. 181–186.
147. ABAKEVIČIENĖ, B., GRIGALIŪNAS, V., ŠAKALIŪNIENĖ, J., VIRGANAVIČIUS, D., ŠLAPIKAS, K., MIKOLAJŪNAS, M. and TAMULEVIČIUS, S. (2014). Modelling and Fabrication of Micro-SOFC Membrane Structure. In: *Materials Science*. 2014, vol. 20, No. 2, pp. 223–227. doi: 10.5755/j01.ms.20.2.5585.
148. GADELMAWLA, E.S., KOURA, M.M., MAKSOUND, T.M.A., ELEWA, I.M. and SOLIMAN, H.H. (2002). Roughness Parameters. In: *Journal of Materials Processing Technology*. 2002, vol. 123, pp. 133–145. doi: 10.1016/S0924-0136(02)00060-2.
149. MESKINIS, S., VASILIAUSKAS, A., SLAPIKAS, K., GUDAITIS, R., TAMULEVICIUS, S. and NIAURA, G. (2012). Piezoresistive Properties and Structure of Hydrogen-Free DLC Films Deposited by DC and Pulsed-DC Unbalanced Magnetron Sputtering. In: *Surface and Coatings Technology*. 2012, vol. 211, pp. 172–175. doi: 10.1016/j.surfcoat.2011.10.004.

150. GAO, P., XIE, R., WANG, H., ZHONG, L., XIA, L., ZHANG, Z., WEI, W. and SUN, Y. (2015). Cu/Zn/Al/Zr Catalysts via Phase-Pure Hydrotalcite-like Compounds for Methanol Synthesis from Carbon Dioxide. In: *Journal of CO_2 Utilization*. 2015, vol. 11, pp. 41–48. doi: 10.1016/j.jcou.2014.12.008.
151. WANG, Z., WANG, E., GAO, L. and XU, L. (2005). Synthesis and Properties of Mg_2Al Layered Double Hydroxides Containing 5-fluorouracil. In: *Journal of Solid State Chemistry*. 2005, vol. 178, No. 3, pp. 736–741. doi: 10.1016/j.jssc.
152. KLOPROGGE, J.T., RUAN, H.D. and FROST, R.L. Thermal Decomposition of Bauxite Minerals: Infrared Emission Spectroscopy of Gibbsite, Boehmite and Diaspore. In: *Journal of Materials Science*. 2002, vol. 7, pp. 1–21.
153. KOCÍK, J., HÁJEK, M. and TROPPOVÁ, I. (2015). The Factors Influencing Stability of Ca-Al Mixed Oxides as a Possible Catalyst for Biodiesel Production. In: *Fuel Processing Technology*. 2015, vol. 134, pp. 297–302. doi: 10.1016/j.fuproc.
154. MELONI, D., MONACI, R., CUTRUFELLO, M.G., ROMBI, E. and FERINO, I. (2015). Adsorption Microcalorimetry Characterization of K-Doped MgAl Mixed Oxide Catalysts for Soybean Oil Transesterification Synthesized by Impregnation and Ball Milling Techniques. In: *Journal of Thermal Analysis and Calorimetry*. 2015, vol. 119, No. 2, pp. 1023–1036. doi: 10.1007/s10973-014-4283-4.
155. BAZRAFSHAN, E., MOHAMMADI, L., ANSARI-MOGHADDAM, A. and MAHVI, A.H. (2015). Heavy Metals Removal from Aqueous Environments by Electrocoagulation Process – A Systematic Review. In: *Journal of Environmental Health Science and Engineering*. 2015, vol. 13, No. 1, p. 74. doi: 10.1186/s40201-015-0233-8.
156. ATIEH, M.A., JI, Y. and KOCHKODAN, V. (2017). Metals in the Environment: Toxic Metals Removal. In: *Bioinorganic Chemistry and Applications*. 2017, vol. 2017, pp. 2–4.
157. BISHT, R., AGARWAL, M. and SINGH, K. (2017). Heavy Metal Removal from Wastewater Using Various Adsorbents: a Review. In: *Journal of Water Reuse and Desalination*. 2017, vol. 7, No. 4, pp. 387–419. doi: 10.2166/wrd.
158. ERDEM, E., KARAPINAR, N. and DONAT, R. (2004). The Removal of Heavy Metal Cations by Natural Zeolites. In: *Journal of Colloid and Interface Science*. 2004, vol. 280, No. 2, pp. 309–314. doi: 10.1016/j.jcis.
159. AKHTAR, F., ANDERSSON, L., OGUNWUMI, S., HEDIN, N. and BERGSTRÖM, L. (2014). Structuring Adsorbents and Catalysts by Processing of Porous Powders. In: *Journal of the European Ceramic Society*. 2014, vol. 34, No. 7, pp. 1643–1666. doi: 10.1016/j.jeurceramsoc.
160. JAMHOUR, R.M.A.Q., ABABNEH, T.S. and AL-RAWASHDEH, A.I. (2016). Adsorption Isotherms and Kinetics of Ni (II) and Pb (II) Ions on New Layered Double Hydroxides-Nitrilotriacetate Composite in Aqueous Media. In: *Advances in Analytical Chemistry*. 2016, vol. 6, No. 1, pp. 17–33. doi: 10.5923/j.aac.20160601.03.
161. CHEN, F., WU, X., BU, R. and YANG, F. (2017). Co–Fe Hydrotalcites for Efficient Removal of Dye Pollutants via Synergistic Adsorption and Degradation.

In: *RSC Advances*. 2017, vol. 7, No. 66, pp. 41945–41954. doi: 10.1039/C7RA07417D.
162. KUMAR, S., ZAFAR, M., PRAJAPATI, J.K., KUMAR, S. and KANNEPALLI, S. (2011). Modeling Studies on Simultaneous Adsorption of Phenol and Resorcinol onto Granular Activated Carbon from Simulated Aqueous Solution. In: *Journal of Hazardous Materials*. 2011, vol. 185, No. 1, pp. 287–294. doi: 10.1016/j.jhazmat.
163. REGTI, A., EL KASSIMI, A., LAAMARI, M.R. and EL HADDAD, M. (2016). Competitive Adsorption and Optimization of Binary Mixture of Textile Dyes: a Factorial Design Analysis. In: *Journal of the Association of Arab Universities for Basic and Applied Sciences*. 2016, vol. 24, pp. 1–9. doi: 10.1016/j.jaubas.
164. GISI, S.D., LOFRANO, G., GRASSI, M., NOTARNICOLA, M. (2016). Characteristics and Adsorption Capacities of Low-Cost Sorbents for Wastewater Treatment: a Review. In: *Sustainable Materials and Technologies*. 2016, vol. 9, pp. 10–40. doi: 10.1016/j.susmat.2016.06.002
165. KUMAR MEENA, A., RAJAGOPAL, CH. and MISHRA, G.K.M. *et al*. (2010). Removal of Heavy Metal Ions from Aqueous Solutions Using Chemically (Na_2S) Treated Granular Activated Carbon as an Adsorbent. In: *Journal of Scientific & Industrial Research*. 2010, vol. 69, No. June, pp. 449–453.
166. ZHANG, Q., LIPPMANN, S., GRASEMANN, A., ZHU, M. and RETTENMAYR, M. (2016). Determination of Temperature Dependent Thermophysical Properties Using an Inverse Method and an Infrared Line Camera. In: *International Journal of Heat and Mass Transfer*. 2016, vol. 96, pp. 242–248. doi: 10.1016/j.ijheatmasstransfer.
167. FACIO, J.I., BETANCOURTH, D., CEJAS BOLECEK, N.R., JORGE, G.A., PEDRAZZINI, P., CORREA, V.F., CORNAGLIA, P.S., VILDOSOLA, V. and GARCÍA, D.J. (2015). Lattice Specific Heat for the RMIn5(R=Gd, La, Y; M=Co, Rh) Compounds: Non-Magnetic Contribution Subtraction. In: *Journal of Magnetism and Magnetic Materials*. 2015, vol. 407, pp. 406–411. doi: 10.1016/j.jmmm.
168. BRÜTTING, M., HEMBERGER, F., VIDI, S., WACHTEL, J., MEHLING, H. and EBERT, H.P. (2016). Determination of Heat Capacity by Means of Longitudinal Guarded Comparative Calorimeter – Correction Methods. In: *International Journal of Thermal Sciences*. 2016, vol. 100, pp. 423–429. doi: 10.1007/3-540-29527-5.
169. CHMIELARZ, L., KUŚTROWSKI, P., RAFALSKA-ŁASOCHA, A., MAJDA, D. and DZIEMBAJ, R. (2002). Catalytic Activity of Co-Mg-Al, Cu-Mg-Al and Cu-Co-Mg-Al Mixed Oxides Derived from Hydrotalcites in SCR of NO with Ammonia. In: *Applied Catalysis B: Environmental*. 2002, vol. 35, No. 3, pp. 195–210. doi: 10.1016/S0926-3373(01)00254-5.
170. CHMIELARZ, L., RUTKOWSKA, M., KUŚTROWSKI, P., DROZDEK, M., PIWOWARSKA, Z., DUDEK, B., DZIEMBAJ, R. and MICHALIK, M. (2011). An Influence of Thermal Treatment Conditions of Hydrotalcite-like Materials on Their Catalytic Activity in the Process of N_2O Decomposition. In: *Journal of*

Thermal Analysis and Calorimetry. 2011, vol. 105, No. 1, pp. 161–170. doi: 10.1007/s10973-011-1284-4.
171. CHMIELARZ, L., PIWOWARSKA, Z., RUTKOWSKA, M., WOJCIECHOWSKA, M., DUDEK, B., WITKOWSKI, S. and MICHALIK, M. (2012). Total Oxidation of Selected Mono-Carbon VOCs over Hydrotalcite Originated Metal Oxide Catalysts. In: *Catalysis Communications*. January 5, 2012. vol. 17, pp. 118–125. doi: 10.1016/J.CATCOM.2011.10.030.
172. CHMIELARZ, L., WĘGRZYN, A., WOJCIECHOWSKA, M., WITKOWSKI, S. and MICHALIK, M. (2011). Selective Catalytic Oxidation (SCO) of Ammonia to Nitrogen over Hydrotalcite Originated Mg-Cu-Fe Mixed Metal Oxides. In: *Catalysis Letters*. 2011, vol. 141, No. 9, pp. 1345–1354. doi: 10.1007/s10562-011-0653-8.
173. POLATO, C.M.S., HENRIQUES, C.A., RODRIGUES, A.C.C. and MONTEIRO, J.L.F. (2008). De-SO_x Additives Based on Mixed Oxides Derived from Mg, Al-Hydrotalcite-like Compounds Containing Fe, Cu, Co or Cr. In: *Catalysis Today*. 2008, vol. 133–135, No. 1–4, pp. 534–540. doi: 10.1016/j.cattod.
174. LI, C., WEI, M., EVANS, D.G. and DUAN, X. (2014). Layered Double Hydroxide-Based Nanomaterials as Highly Efficient Catalysts and Adsorbents. In: *Nano Small Micro*. 2014, vol. 10, No. 22, pp. 4469–4486. doi: 10.1002/smll.201401464.
175. NICHITUS, S., CALIN, G., BURLUI, A., STADOLEANU, C. and BURLUI, V. (2015). Layered Double Hydroxides (LDHs) Type Materials Used in Water Treatment. In: *Engineering Materials*. 2015, vol. 660, pp. 273–278. doi: 10.4028/www.scientific.net/KEM.660.273
176. BENIGNO, B., PÁRAMO, R., BLANCO, E. and CASANOVA, C. (2014). Thermal Conductivity and Specific Heat Capacity Measurements of CuO Nanofluids. In: *Journal of Thermal Analysis and Calorimetry*. 2014, vol. 115, No. 2, pp. 1883–1891.
177. XU, Z.P. and ZENG, H.C. (2001). Decomposition Pathways of Hydrotalcite-like Compounds Mg_1-$xAl_x(OH)_2(NO_3)x \cdot nH_2O$ as a Continuous Function of Nitrate Anions. In: *Chemistry of Materials*. 2001, vol. 13, No. 12, pp. 4564–4572. doi: 10.1021/cm010347g.
178. BIRJEGA, R., MATEIA, A., MITU, B., IONITA, M.D., FILIPESCU, M., STOKKER-CHEREGI, F., LUCULESCU, C., DINESCU, M., ZAVOIANU, R., PAVEL, O.D. and COROBE, M.C. (2013). Layered Double Hydroxides/Polymer Thin Films Grown by Matrix Assisted Pulsed Laser Evaporation. In: *Thin Solid Films*. 2013, vol. 543, No. 30, pp. 63–68. doi: 10.1016/j.tsf.2013.02.120.
179. MODESTO-LÓPEZA, L.B., CHIMENTÃO, R.J., ÁLVAREZA, M.G.J., ROSELL-LLOMPARTA, M. and FRANCISCO, L. (2014). Direct Growth of Hydrotalcite Nanolayers on Carbon Fibers by Electrospinning. In: *Applied Clay Science*. 2014, vol. 101, pp. 461–467. doi: 10.1016/j.clay.2014.07.037.
180. WANGA, Y., ZHANGA, D., LVAB, D. and SUN, Y. (2015). Mg-Al Mixed Metal Oxide Film Derived from Layered Double Hydroxide Precursor Film: Fabrication and Antibacterial Properties. In: *Journal of the Taiwan Institute of*

Chemical Engineers. 2015, vol. 57, pp. 160–166. doi: 10.1016/j.jtice.2015.05.017.
181. ZHANG, F., ZHANG, CH., SONG, L., ZENG, R., LIU, Z. and CUI, H. Corrosion of In-Situ Grown MgAl-LDH Coating on Aluminum Alloy. In: *Transactions of Nonferrous Metals Society of China*. 2015, vol. 25, No. 10, pp. 3498–3504. doi: 10.1016/S1003-6326(15)63987-5.
182. TSUJI, T. *et al*. (2014). *Copper-Based Catalyst Precursor, Method for Manufacturing same, and Hydrogenation Method*. Inventors: Tomoaki TSUJI, Keiichi TABATA, Toshihiro SUGAYA, Akio NAKASHIMA. PCT/JP2013/073378. Canadian Patent, 2883573 A1. March 06, 2014. Available from: Canadian Patents Database.
183. MOHANTY, P., KABIRAJ, D., MANDAL, R.K., KULRIYA, P.K., SINHA, A.S.K. and RATH, CH. (2014). Evidence of Room Temperature Ferromagnetism in Argon/Oxygen Annealed TiO_2 Thin Films Deposited by Electron Beam Evaporation Technique. In: *Journal of Magnetism and Magnetic Materials*. 2014, vol. 355, pp. 240–245. doi: 10.1016/j.jmmm.2013.12.025.
184. SEDLAČEK, M., PODGORNIK, B. and VIŽINTIN, J. (2014). Correlation between Standard Roughness Parameters Skewness and Kurtosis and Tribological Behaviour of Contact Surfaces. In: *Tribology International*. 2014, vol. 48, pp. 102–112. doi: 10.1016/j.triboint.2011.11.008.
185. WANGA, W., ZHOUA, J., ACHARIB, G., YUC, J. and CAI, W. (2014). Cr(VI) Removal from Aqueous Solutions by Hydrothermal Synthetic Layered Double Hydroxides: Adsorption Performance, Coexisting Anions and Regeneration Studies. In: *Colloids and Surfaces A: Physicochemical and Engineering Aspects*. 2014, vol. 457, No. 5, pp. 33–40. doi: 10.1016/j.colsurfa.2014.05.034.
186. ZHAO, L., LI, X. and ZHAO, JI. (2013). Correlation of Structural and Chemical Characteristics with Catalytic Performance of Hydrotalcite-Based CuNiAl Mixed Oxides for SO_2 Abatement. In: *Chemical Engineering Journal*. 2013, vol. 223, No. 1, pp. 164–171. doi: 10.1016/j.cej.2013.02.103.
187. XUE, W., WANG, CH., CHEN, R. and DENG, Z. (2002). Structure and Properties Characterization of Ceramic Coatings Produced on Ti–6Al–4V Alloy by Microarc Oxidation in Aluminate Solution. In: *Materials Letters*. 2002, vol. 52, No. 6, pp. 435–441. doi: 10.1016/S0167-577X(01)00440-2.
188. OLAKANMI, E.O., COCHRAN, R.F. and DALGARNO, K.W. (2015). A Review on Selective Laser Sintering/Melting (SLS/SLM) of Aluminium Alloy Powders: Processing, Microstructure, and Properties. In: *Progress in Materials Science*. 2015, vol. 74, pp. 401–477. doi: 10.1016/j.pmatsci.
189. SAKALIUNIENE, J., ABAKEVICIENE, B., SLAPIKAS, K. and TAMULEVICIUS, S. (2015). Influence of Magnetron Sputtering Deposition Conditions and Thermal Treatment on Properties of Platinum Thin Films for Positive Electrode-Electrolyte-Negative Electrode Structure. In: *Thin Solid Films*. 2015, vol. 594, pp. 101–108. doi: 10.1016/j.tsf.2015.10.016.

List of Scientific Publications on the Theme of the Dissertation

Publications in Journals Included into the *Institute for Scientific Information* (ISI) Database

1. **ZADAVIČIŪTĖ, S.**, BALTAKYS, K., EISINAS, A. (2015). Adsorption Kinetic Parameters of Fe^{3+} and Ni^{2+} Ions by Gyrolite // *Materials Science = Medžiagotyra*. Kaunas: KTU. ISSN: 1392-1320. 2015, vol. 21, No. 1, pp. 117–122.
2. BANKAUSKAITĖ, A., EISINAS, A., BALTAKYS, K., **ZADAVIČIŪTĖ, S**. (2015). A Study on the Intercalation of Heavy Metal Ions in a Wastewater by Synthetic Layered Inorganic Adsorbents // *Desalination and Water Treatment*. Philadelphia, PA: Taylor & Francis. ISSN: 1944-3994. 2015, vol. 56, iss. 6, pp. 1576–1586.
3. **ZADAVIČIŪTĖ, S.,** BALTAKYS, K., BANKAUSKAITĖ, A. (2017). The Effect of Microwave and Hydrothermal Treatments on the Properties of Hydrotalcite: a Comparative Study // *Journal of Thermal Analysis and Calorimetry*. Dordrecht: Springer. ISSN: 1388-6150. 2017, vol. 127, iss. 1, pp. 189–196.
4. **ZADAVIČIŪTĖ, S.,** BALTAKYS, K., EISINAS, A., BANKAUSKAITĖ, A. (2017). Simultaneous Adsorption at 25 °C and the Peculiarities of Gyrolite Substituted with Heavy Metals // *Journal of Thermal Analysis and Calorimetry*. Dordrecht: Springer. ISSN: 1388-6150. 2017, vol. 127, iss. 1, pp. 335–343.
5. **ZADAVIČIŪTĖ, S.,** BANKAUSKAITĖ, A., BALTAKYS, K., EISINAS, A. (2018). The Study of C_p Determination of Hydrotalcite Intercalated with Heavy Metal Ions // *Journal of Thermal Analysis and Calorimetry*. Dordrecht: Springer. ISSN: 1388-6150. 2018, vol. 131, iss. 1, pp. 521–527.

Publications of International Scientific Conferences

1. **ZADAVIČIŪTĖ, S.,** BALTAKYS, K. (2015). The Adsorption Capacity of Gyrolite for Mn^{2+} Ions // *Chemistry and Chemical Technology 2015*: Programme and Proceedings of the International Conference, Vilnius, Lithuania, January 23, 2015 / Vilnius University, Lithuanian Academy of Sciences, Kaunas University of Technology, Center for Physical Sciences and Technology. [S.l.: s.n, 2015], ISBN: 9786094594618. pp. 162–165.
2. BALTAKYS, K., **ZADAVIČIŪTĖ, S.,** BANKAUSKAITĖ, A. (2015). The Effect of Microwave and Hydrothermal Treatments on the Properties of Hydrotalcite: a Comparative Study // *3rd Central and Eastern European Conference on Thermal Analysis and Calorimetry, CEEC-TAC 3*: August 25–28, 2015, Ljubljana, Slovenia: book of abstracts / Editors: Andrei Rotaru, Romana Cerc Korošec; Central and Eastern European Committee for Thermal

Analysis and Calorimetry. Rostock: Greifswald, 2015, ISBN: 9783940237347. p. 294.

3. BALTAKYS, K., **ZADAVIČIŪTĖ, S.,** BANKAUSKAITĖ, A. (2015). The Effect of Mechanochemical Treatment Conditions on Hydrotalcite Particle Size Distribution // *Advanced Materials and Technologies*: book of abstracts of the 17th international conference-school, August 27–31, 2015, Palanga, Lithuania. Kaunas: Kaunas University of Technology. ISSN: 1822-7759. 2015, p. 155.
4. **ZADAVIČIŪTĖ, S.,** BANKAUSKAITĖ, A., BALTAKYS, K., NIŪNIAVAITĖ, D., JEFIMOVAITĖ, L. (2016). A Comparative Study of α-C_2SH and Hydrotalcite Adsorption Capacities // *BaltSilica 2016*: book of abstracts of the 7th Baltic conference on silicate materials, May 26–27, 2016, Kaunas, Lithuania / Kaunas University of Technology, Riga Technical University, Adam Mickiewicz University in Poznan. Kaunas: Kaunas University of Technology. ISSN: 2243-6057. 2016, p. 78.
5. **ZADAVIČIŪTĖ, S.,** SAKALIŪNIENĖ, J., BANKAUSKAITĖ, A., ABAKEVIČIENĖ, B., BALTAKYS, K. (2016). The Roughness Parameters of Thin Films Prepared from Different Targets Based on Gyrolite // *Advanced Materials and Technologies*: book of abstracts of the 18th international conference-school, August 27–31, 2016, Palanga, Lithuania. Kaunas: Kaunas University of Technology. ISSN: 1822-7759. 2016, p. 53.
6. JEFIMOVAITĖ, L., BANKAUSKAITĖ, A., **ZADAVIČIŪTĖ, S.,** BALTAKYS, K. (2016). The Simultaneous Adsorption Capacity of Hydrotalcite for Co^{2+}, Cr^{3+}, Cu^{2+} Ions // *Chemistry and Chemical Technology*: international conference of the Lithuanian Society of Chemistry: Lithuanian Academy of Science, Kaunas University of Tehnology, Vilnius, Lithuania, April 28–29, 2016: book of abstracts / Fizinių ir technologijos mokslų centras, Vilniaus universitetas, Lietuvos mokslų akademija, Kauno technologijos universitetas. [S.l.: s.n, 2016], ISBN: 9786099551135. p. 216.
7. RINGYTĖ, V., **ZADAVIČIŪTĖ, S.,** BALTAKYS, K. (2016). Effect of Partial Water Vapour on Hydrotalcite Sample Structure // *Chemistry and Chemical Technology*: international conference of the Lithuanian Society of Chemistry: Lithuanian Academy of Science, Kaunas University of Technology, Vilnius, Lithuania, April 28–29, 2016: book of abstracts / Fizinių ir technologijos mokslų centras, Vilniaus universitetas, Lietuvos mokslų akademija, Kauno technologijos universitetas. [S.l.: s.n, 2016], ISBN: 9786099551135. p. 217.
8. **ZADAVIČIŪTĖ, S.,** BANKAUSKAITĖ, A., BALTAKYS, K., EISINAS, A. (2016). The Study of C_p Determination of Hydrotalcite Intercalated with Heavy Metal Ions // *Proceedings of International Conference of Thermal Analysis and Calorimetry in Russia (RTAC-2016),* September 16–23, 2016, Saint-Petersburg, Russia, vol. 1. Saint-Petersburg: Peter the Great St.

Petersburg Polytechnic University, 2016, ISBN: 9785742254478. pp. 224–227.
9. **ZADAVIČIŪTĖ, S.,** BANKAUSKAITĖ, A., BALTAKYS, K. The Kinetic Parameters of Simultaneous Adsorption of Hydrotalcite for Co^{2+}, Cu^{2+} and Cr^{3+} Ions // *Chemistry and Chemical Technology 2017*: proceedings of the international conference, April 28, 2017, Kaunas. Kaunas: Kaunas University of Technology. ISSN: 2538-7359. 2017, p. 83.

Acknowledgments

I would like to gratefully acknowledge the enthusiastic and encouraging supervision of professor **Kestutis Baltakys** who has provided me with invaluable counseling on the thesis and has also systematically and persistently shown confidence in me.

I also owe special thanks to dr. A. Bankauskaitė for their support, professional comments and valuable remarks.

I am grateful to all of my friends and colleagues from the Department of Silicate Technology for their support and friendship. They all contributed to the success of this project in very different ways. Finally, I would like to thank my family who, throughout my childhood and academic career years, have always been encouraging and supporting me in whatever direction my studies and research took me.

SL344. 2018-04-12, 13,5 leidyb. apsk. l. Tiražas 12 egz. Užsakymas 166.
Išleido Kauno technologijos universitetas, K. Donelaičio g. 73, 44249 Kaunas
Spausdino leidyklos „Technologija“ spaustuvė, Studentų g. 54, 51424 Kaunas